UQAR

Université du Québec
à Rimouski

CARACTÉRISATION DE LA TAILLE ET COMPOSITION DES PARTICULES EN SUSPENSION DANS L'ESTUAIRE DU SAINT-LAURENT

Mémoire présenté

dans le cadre du programme de maîtrise en Océanographie

en vue de l'obtention du grade de maître ès sciences

PAR

© ANNE-SOPHIE FABRIS

Novembre 2020

Composition du jury :

Jean-Pierre Gagné, président du jury, UQAR-ISMER

Pierre Larouche, directeur de recherche, Institut Maurice-Lamontagne

Jean-Carlos Montero-Serrano, codirecteur de recherche, UQAR-ISMER

Brent Law, examinateur externe, Institut océanographique de Bedford

Dépôt initial le 2 août 2020   Dépôt final le 23 novembre 2020

UNIVERSITÉ DU QUÉBEC À RIMOUSKI
Service de la bibliothèque

Avertissement

REMERCIEMENTS

Premièrement, je tiens à remercier mon directeur de recherche Pierre Larouche d'avoir accepté de me diriger suite à mon intérêt face à ce projet. Merci pour le temps accordé à nos rencontres et à l'évolution du projet jusqu'au produit final. Je remercie aussi mon co-directeur Jean-Carlos Montero-Serrano de s'être joint à l'idée originale et d'avoir apporté un nouvel aspect au projet qui m'aura permis de gagner de l'expérience sur le terrain et en laboratoire. Merci d'avoir toujours eu ta porte ouverte aux discussions et à mes questionnements. Une mention spéciale à tous ceux que j'ai pu côtoyer pendant mes sorties en mer et dans les laboratoires qui me font encore plus apprécier les moments de travail. Mes remerciements au soutien de Marie-Pier St-Onge pour l'organisation des sorties en mer et de Claude Belzile en laboratoire. Un grand merci à Christiane Dufresne et Gesche Winkler de m'avoir donné l'opportunité de participer aux missions sur le Lampsilis.

J'ai eu la chance de créer plusieurs liens d'amitié au fil de mes deux années qui m'ont permis d'aimer la vie à Rimouski. Les nombreux *potlucks,* les soirées films, la piscine, l'escalade et nos multiples pauses dans le local de maîtrise pour discuter sont des activités qui me manquent déjà et qui ont été écourtées trop vite.

Finalement, merci à ma famille de m'avoir supporté dans ce projet. À distance, puis à l'imprévu de manière très rapprochée où vous avez su vous adapter à mon horaire de travail bien différent du vôtre.

Merci à vous tous de prendre le temps de lire ces mots et ce qui s'ensuit.

AVANT-PROPOS

Ce mémoire de maîtrise est présenté en trois parties : une introduction générale rédigée en français, un chapitre principal rédigé en anglais sous la forme d'un article scientifique en prévision d'être soumis pour publication à la revue internationale « *Regional Studies in Marine Science* » et une brève conclusion générale rédigée en français.

L'article présenté dans ce mémoire de maîtrise : Fabris, A.-S., Larouche, P., Montero-Serrano, J.C. *Characterization of the St. Lawrence Estuary's suspended matter size and composition,* a été rédigé par moi-même avec la supervision de Pierre Larouche (IML) et Jean-Carlos Montero-Serrano (UQAR-ISMER). En tant que premier auteur, ma contribution à ce travail fut la réalisation des analyses de composition minéralogique et géochimique élémentaire avec l'assistance de Claude Belzile, le traitement des données de tailles des particules, la création des graphiques et la rédaction de l'article. Pierre Larouche et Jean-Carlos Montero-Serrano ont fourni l'idée originale, l'implémentation du développement de la méthode, la formation nécessaire pour réaliser les analyses de données et de laboratoire et ont contribué à la rédaction et révision de l'article. De plus, Mehmet Yayla (IML), Michel Gosselin (UQAR-ISMER) et Jade Paradis-Hautcoeur (UQAR-ISMER) ont effectué les analyses de chlorophylle. Gesche Winkler (UQAR-ISMER) et Dominique Lavallée (UQAR-ISMER) ont effectué les analyses de concentrations de la matière en suspension (organique et inorganique) pour les échantillons d'hiver 2019. Pierre Larouche a effectué ces mêmes analyses pour les échantillons de 2010.

x

RÉSUMÉ

L'estuaire du Saint-Laurent (ESL) est un large système estuarien couvert de glace en hiver. La dynamique de la matière particulaire en suspension (MPS) dans cet estuaire est fortement influencée par la circulation induite par les vents, les marées et le ruissellement des rivières. Bien qu'il existe de l'information concernant la composition et la dynamique de la MPS dans l'ESL, celle-ci est manquante en hiver. Par ailleurs, il existe peu d'information sur la distribution des tailles des particules (PSD), paramètre important pour déterminer la sédimentation de la matière dans la colonne d'eau. Cette étude tente donc de caractériser (1) la PSD et (2) la composition des particules détritiques en suspension dans l'ESL en conditions printanières et hivernales. La PSD a été mesurée avec un diffractomètre laser dans la colonne d'eau au printemps 2010 et en laboratoire à l'aide d'échantillons d'eau prélevés à des profondeurs discrètes à l'hiver 2019. La diffraction des rayons X et la spectroscopie aux rayons X à dispersion d'énergie ont été utilisées pour la caractérisation de la composition minéralogique et géochimique des particules en hiver.

Les résultats n'ont montré presque aucune variation de la structure verticale de la PSD dans l'estuaire supérieur au printemps et dans la zone de turbidité maximale en hiver en raison du mélange vertical. Des particules grossières (>63 µm) au printemps et des particules de taille moyenne (4-63 µm) en hiver étaient plus présentes en amont qu'en aval. Cela peut être dû à une sédimentation plus élevée dans les eaux calmes de l'estuaire maritime. Dans l'estuaire maritime, les particules grossières étaient plus présentes en hiver qu'en été près de la surface. Elles sont probablement des flocs formés de particules ayant été apportées par la glace ou provenant du rejet d'eau douce des rivières utilisées pour l'hydroélectricité. La composition minéralogique et géochimique de la MPS hivernale était similaire aux études antérieures sur les sédiments indiquant une origine principale du Bouclier canadien et secondaire des Appalaches. Dans l'ensemble, bien qu'elles soient toutes deux présentes, la variabilité saisonnière était plus importante que la variabilité spatiale pour la PSD, tandis que la composition géochimique et minéralogique était constante à travers l'ESL. Cette étude a fourni de nouvelles informations importantes sur la dynamique de la MPS dans un environnement estuarien subarctique.

Mots clés : Estuaire du Saint-Laurent, taille des particules, matière particulaire en suspension, composition des particules, minéralogie, géochimie élémentaire, dynamique sédimentaire.

ABSTRACT

The St. Lawrence Estuary (SLE) in eastern Canada is a large seasonally ice-covered estuarine system. The suspended particulate matter (SPM) dynamics in this estuary is strongly influenced by wind-induced circulation, tides and river runoff. Although information exists concerning the composition and the SPM dynamics in the SLE, it is missing in winter. Furthermore, there is little information on the particle size distribution (PSD), an important parameter for determining the sedimentation of matter in the water column. This study therefore attempts to characterize (1) the PSD and (2) the composition of the detrital particles in suspension in the SLE in spring and winter conditions. The PSD was measured with a laser diffractometer in the water column for spring 2010 and in the laboratory using water samples taken at discrete depths for winter 2019. X-ray diffraction and energy-dispersive X-ray spectroscopy were used for the characterization of the particles' mineralogical and geochemical composition in winter.

Results showed very little variations in the vertical structure of the PSD in the Upper Estuary in spring and in the maximum turbidity zone in winter due to vertical mixing. Larger particles (>63 µm) in spring and medium size particles (4-63 µm) in winter were more present upstream than downstream. This may be due to higher sedimentation in the calmer waters of the Lower Estuary. In the Lower Estuary, larger particles were more present in winter than summer near the surface. They were probably flocs of particles either brought by the ice or coming from the discharge of freshwater from rivers used for hydroelectricity. The mineralogical and geochemical composition of winter SPM was similar to previous sediment studies indicating a main origin from the Canadian Shield and a secondary source from the Appalachians. Overall, although both were present, seasonal variability was more important than spatial variability in the PSD, while the chemical and mineralogical composition were constant throughout the SLE. This study provided valuable new information on SPM dynamics in a sub-Arctic estuarine environment.

Keywords: St. Lawrence Estuary, particle sizes, suspended particulate matter, particle composition, mineralogy, elemental geochemistry, sediment dynamics.

TABLE DES MATIÈRES

LISTE DES FIGURES

Fig. 7. Spring vertical distribution of (A, F, K) normalized volume concentration (V[D], ppm), (B, G, L) volume concentration density at small size class (<4 μm) medium size class (4-63 μm) and large size class (>63 μm), (C, H, M) $c_p(670)$ and D_V^{50}, (D, I, N) temperature and salinity, (E, J, O) Wetstar measured chlorophyll fluorescence (Chl fluorescence) and discrete Chl-*a* samples measured by fluorescence

xx

LISTE DES ABRÉVIATIONS, DES SIGLES ET DES ACRONYMES

$b_{bp}(\lambda)$ Coefficient de rétrodiffusion.

$a(\lambda)$ Coefficient d'absorption.

C.C.G.S.   *Canadian Coast Guard Ship*.

Chl-*a*   Chlorophylle-*a*, *Chlorophyll-a*.

Chl fluorescence   *Chlorophyll fluorescence from WetStar fluorometer, µg L^{-1}.*

c_p   *Particulate beam attenuation coefficient measured by LISST, m^{-1}.*

CV   *Coefficient of variation*

D_V^{50}   *Median particle diameter of the volume distribution.*

DOF   *Degree-of-fit.*

ESL   Estuaire du Saint-Laurent.

Fluo Chl-*a*   *Chlorophyll-a concentration measured by fluorescence method, µg L^{-1}.*

LISST   *Sequoia LISST-100X type B*

MIP   Matière inorganique particulaire.

MOP   Matière organique particulaire.

MPS   Matière particulaire en suspension.

N.G.C.C.   Navire de la Garde Côtière Canadienne.

N(D)   *Particle number concentration at size class D, m^{-3}.*

N'(D)   *Particle number density at size class D, m^{-3} µm^{-1}.*

PIM   *Particulate inorganic matter, g m^{-3}.*

POM   *Particulate organic matter, g m^{-3}.*

PSD   Distribution de taille des particules, *Particle size distribution*.

SLE   *St. Lawrence Estuary*.

SPM   *Suspended particulate matter*.

Stn.   *Station*.

UCC *Upper continental crust.*

V(D) *Volume concentration at size class D, ppm.*

V'(D) *Volume concentration density at size class D, ppm μm^{-1}.*

V'(D)$_{SMALL}$ *Volume concentration density at small size classes (<4 μm), ppm μm^{-1}.*

V'(D)$_{MEDIUM}$ *Volume concentration density at medium size classes (4-63 μm), ppm μm^{-1}.*

V'(D)$_{LARGE}$ *Volume concentration density at large size classes (>63 μm), ppm μm^{-1}.*

Wt.% *Weight percent.*

LISTE DES SYMBOLES

ξ *Junge slope of the particle size distribution (PSD).*

λ *Wavelength, nm.*

INTRODUCTION GÉNÉRALE

CONTEXTE RÉGIONAL

L'estuaire du Saint-Laurent (ESL) couvre une superficie de 12 820 km^2 depuis la ville de Québec jusqu'à Pointe-des-Monts (D'Anglejan, 1990). Il est caractérisé par de grandes variations horizontales dans ses propriétés physico-chimiques, dont les matières dissoutes et particulaires en suspension, les courants de marée et la production primaire (D'Anglejan & Smith, 1973; D'Anglejan, 1990). La circulation estuarienne amène dans l'ESL de l'eau douce en surface depuis les rivières vers le golfe et de l'eau salée en profondeur circulant en sens inverse (Koutitonsky & Bugden, 1991). Les sources principales d'eau douce dans l'estuaire sont le fleuve Saint-Laurent (12 000 m^3 s^{-1}), la rivière Saguenay (2 100 m^3 s^{-1}) et trois grandes rivières sur la Côte-Nord (1 600 m^3 s^{-1} total) : Betsiamites, aux Outardes et Manicouagan (Pinet et al., 2011). Avec un débit annuel moyen combiné de 159 m^3 s^{-1}, les rivières situées sur la Côte-Sud de l'estuaire maritime ont une moindre influence sur le système estuarien du Saint-Laurent (St. Lawrence Center, 1996).

L'ESL est généralement divisé en deux sous-régions selon sa productivité biologique et sa bathymétrie (Levasseur et al., 1984) : l'estuaire moyen (Québec au fjord du Saguenay) qui est partiellement mélangé et l'estuaire maritime (fjord du Saguenay à Pointe-des-Monts) avec intrusion d'eau salée en profondeur (Montes-Hugo et al., 2012). L'estuaire moyen est relativement peu profond avec des profondeurs d'environ 60 m (D'Anglejan, 1990). La présence de plusieurs hauts fonds et îles influence l'intensité des courants (Mertz & Gratton, 1990). La circulation moyenne qui y est présente va de l'amont vers l'aval (Ingram & El-Sabh, 1990) et est contrôlée par l'écoulement du fleuve et les marées semi-

diurnes (D'Anglejan & Smith, 1973). L'effet des marées y est important dû au rétrécissement de l'estuaire et la remontée de la topographie vers l'amont. Les courants de marée sont responsables de plus de 90% des variations de courants qu'on y retrouve (Saucier & Chassé, 2000). Un fort gradient de salinité est présent de l'amont vers l'aval dû au grand apport d'eau douce à Québec ce qui augmente la stratification et diminue la circulation verticale en aval (Nieke et al., 1997).

À cause de ses grandes dimensions, l'estuaire maritime possède plus de caractéristiques océaniques et est plus exposé aux vagues et courants tidaux. Avec la présence du chenal Laurentien, l'estuaire maritime peut atteindre des profondeurs variant entre 250 et 400 m (El-Sabh & Silverberg, 1990). En été, trois couches distinctes y sont présentes : la couche de surface, la couche intermédiaire froide et la couche profonde. La couche de surface s'écoule généralement vers l'aval. Elle est principalement issue des apports d'eau douce et varie entre 10 et 30 m de profondeur. La circulation dans la couche de surface est complexe (Saucier et al., 2009). En juin, lors d'importants apports d'eau par le fleuve et la rivière Saguenay, un gyre cyclonique entre Pointe-au-Père et Baie-Comeau et un gyre anticyclonique entre Baie-Comeau et le début du golfe se forment. En août, lorsque le débit des rivières a diminué, les eaux du golfe entrent dans l'estuaire par la côte nord ce qui inverse la direction des gyres (El-Sabh et al., 1982; Mertz et al., 1989). Des courants transversaux sont présents entre les gyres (El-Sabh, 1988). Le ruissellement des eaux douces contrôle donc en grande partie la circulation à la surface (Plourde et al., 2002). Le vent affecte aussi la circulation et le mélange des eaux. Cet effet est réduit en hiver avec la présence des glaces de décembre à mars. En contrepartie, la glace ajoute une couche qui augmente l'effet de friction et produit plus de mélanges turbulents (El-Sabh, 1988).

La température et salinité de la couche de surface dans l'ESL fluctuent le plus par rapport aux autres couches (Galbraith et al., 2019). En hiver, la couche de surface se refroidit, devient plus dense, et se joint à la couche intermédiaire froide ce qui augmente la circulation verticale (Gilbert & Pettigrew, 1997). Au printemps et en été, une nouvelle couche de surface plus chaude est créée par le réchauffement atmosphérique et l'apport

d'un plus grand volume d'eau douce moins dense. Il y a alors, en été, une couche intermédiaire froide qui s'écoule en moyenne vers l'amont.

La couche profonde, qui résulte d'un mélange entre le courant du Labrador et le Gulf Stream, circule de l'aval vers l'amont. Aux plus grandes profondeurs (>250 m) les eaux sont hypoxiques due à la stratification toujours présente et la circulation lente vers la tête du chenal Laurentien (Lefort et al., 2012). À la tête du chenal Laurentien, les marées internes et la topographie permettent la remontée et le mélange des eaux profondes riches en éléments nutritifs près de la surface (Therriault & Lacroix, 1976; Therriault & Levasseur, 1985). Cela constitue une pompe à nutriments importante qui permet une forte production primaire (MPO, 2007). Au printemps, la stratification plus importante qui se forme, conjuguée à une augmentation de l'intensité lumineuse dans la couche de surface, favorise la présence de floraisons phytoplanctoniques à travers l'estuaire maritime (Levasseur et al., 1984). À l'automne, le mélange des eaux intermédiaires riches en nutriments par les vents peut générer de nouveau la floraison des phytoplanctons (Blais et al., 2018).

Un des principaux tributaires de l'estuaire, le fjord du Saguenay, fait 110 km de long et comprend trois bassins (Belzile et al., 2016). Le premier bassin près de l'embouchure du fjord atteint 240 m de profondeur et est séparé de l'estuaire par un seuil d'une profondeur de 20 m. Ce seuil limite les échanges avec l'estuaire de sorte que seulement l'eau dense de l'estuaire peut y entrer grâce aux processus de marées (Belzile et al., 2016). Les deuxième et troisième bassins ont des profondeurs maximales de 270 m (Locat & Levesque, 2009). Le fjord est fortement stratifié et la couche de surface peu profonde s'écoule en direction de l'aval. Plusieurs couches sont présentes en profondeurs avec des courants ayant des directions opposées (Galbraith et al., 2018).

L'IMPORTANCE DE LA MATIÈRE PARTICULAIRE EN SUSPENSION

Dans les environnements côtiers, tels les estuaires, la variabilité spatiale et temporelle de la matière particulaire en suspension (MPS) est généralement très élevée (Doxaran et al., 2002; Montes-Hugo & Mohammadpour, 2012). Il est donc important de bien connaitre cette variabilité puisque les particules en suspension sont liées à plusieurs phénomènes physiques, géochimiques et biologiques telles les floraisons de phytoplanctons ainsi que l'agrégation et la remise en suspension des sédiments (Wang et al., 2013a; Eleveld et al., 2014). La MPS peut aussi adsorber et accumuler des polluants inorganiques et organiques tels que les pesticides organochlorés (Ramalhosa et al., 2005; Leadprathom et al., 2009) et les métaux traces (Hart, 1982; Ramalhosa et al., 2005).

Les années où il y a un grand apport d'eau douce dans l'estuaire du Saint-Laurent, les concentrations de MPS y sont plus élevées au printemps puisque cela élève le niveau marin et amène une plus grande érosion des berges (Montes-Hugo et al., 2012). Cette augmentation en MPS est aussi due aux floraisons de phytoplanctons principalement présentes dans les zones de remontée topographique de l'estuaire maritime où les nutriments sont amenés en surface. Les années où le débit des rivières durant l'été est faible, les concentrations de MPS sont plus élevées à l'automne dû à la diminution du niveau d'eau (Montes-Hugo et al., 2012). Cela permet aux vagues générées par les vents et aux gradients de densité de causer la remise en suspension des sédiments dans les régions peu profondes (Coulombier et al., 2012). En cas de pluies automnales, les concentrations en MPS peuvent également augmenter dû à des débits des rivières plus élevés (Ministère du Développement durable, 2016).

L'estuaire moyen est caractérisé par la zone de turbidité maximale qui s'étend sur 100 km en aval de l'Île d'Orléans. La marée cause de grandes variations dans le gradient vertical des concentrations de MPS dans cette région (Silverberg & Sundby, 1978; Lebeuf et al., 2019). Les concentrations de MPS sont plus faibles dans l'estuaire maritime puisque les courants y sont moins forts permettant une plus grande sédimentation (Gobeil, 2006).

Le taux de sédimentation est particulièrement élevé dans le chenal Laurentien, atteignant plus de 0.7 cm an^{-1} (Smith & Schafer, 1999). Il faut toutefois noter que le bilan et les caractéristiques des MPS sont mal connus dans l'ESL (Lebeuf et al., 2019).

Dionne (1969, 1984) a étudié l'apport de sédiments fins depuis les côtes par la glace dans l'estuaire moyen en hiver, mais l'importance de cet apport n'a pas encore été bien documentée. Lebeuf et al. (2019) supposent aussi un apport important de MPS par les glaces pour combler la balance sédimentaire de l'ESL qui présente de plus hauts taux de sédimentation que les apports mesurés en saison estivale. Fait intéressant, une diminution de 39% du budget de la MPS et de 36% de celui de matière particulaire inorganique entre la période 1997-2001 et la période 2014-2016 a été notée sans pouvoir en expliquer la cause ni si cette diminution est apparue soudainement ou est une tendance lente (Lebeuf et al., 2019). Comme cette diminution peut avoir un impact important sur les processus biogéochimiques présents dans l'ESL, une meilleure résolution temporelle des variations de la MPS dans l'ESL serait grandement utile.

LA COMPOSITION DE LA MATIÈRE EN SUSPENSION DANS L'ESTUAIRE DU SAINT-LAURENT

La MPS qui est présente dans l'ESL est principalement issue du transport par les rivières de matière ayant été érodée et provenant de l'altération des roches. La matière inorganique particulaire (MIP) contribuait de 60 à 90% à la MPS dans l'estuaire moyen à l'été 1971 (D'Anglejan & Smith, 1973). Dans l'estuaire maritime, la matière organique particulaire (MOP) est plus importante. Elle représentait de 29 à 49% de la MPS entre avril et octobre de 1998 à 2001 (Larouche & Boyer-Villemaire, 2010). Aux printemps 2000 et 2001 de 11 à 54% de la MPS dans tout l'estuaire était d'origine organique dont en moyenne 26.5% de la MOP était du phytoplancton (Montes-Hugo & Mohammadpour, 2012).

Les sédiments issus de la MPS proviennent principalement de roches métamorphiques et ignées du Bouclier canadien affleurant sur la Côte Nord et de roches

6

sédimentaires de la chaine des Appalaches, composées de schistes argileux, affleurant sur la Côte Sud (Dolgopolova & Isupova, 2011; Jaegle, 2015; Casse et al., 2017). La minéralogie du Bouclier canadien est principalement représentée par les amphiboles, feldspaths potassiques, feldspaths plagioclases et des couches d'un mélange d'illites et de smectite (Jaegle, 2015; Casse et al., 2017). La chaine des Appalaches a plutôt comme principales composantes le quartz et les phyllosilicates (Jaegle, 2015; Casse et al., 2017). L'origine, la nature et le mode de transport de cette matière vers l'ESL sont très peu documentés (ex. D'Anglejan & Smith, 1973).

L'ÉTUDE DE LA TAILLE DES PARTICULES

La taille de la MPS est une propriété importante à étudier puisque la vitesse de chute des particules est affectée par leur taille (Ahn, 2012) ce qui affecte à son tour les flux verticaux et horizontaux dans la colonne d'eau (Reynolds et al., 2008). De plus, la taille des particules influence la pénétration, la diffusion et l'atténuation de la lumière dans la colonne d'eau (Babin et al., 2003). La connaissance de la distribution de taille des particules (PSD) est essentielle pour comprendre l'écologie et la biochimie des estuaires incluant la dynamique des particules et le cycle du carbone (Loisel et al., 2006). Dans les environnements côtiers et estuariens, la PSD est affectée par des processus tels les vents, les courants, les marées et les vagues en plus de l'activité biologique et des changements de climats avec les saisons (Jonasz, 1983; Renosh et al., 2014). Les particules en suspension présentes dans ce type d'environnement sont souvent sous forme de flocs et d'agrégats (Eisma et al., 1990). La MPS est composée de matière organique et inorganique incluant des sédiments en suspension et du phytoplancton. La taille des particules en suspension est donc liée aux concentrations de chlorophylle-a (Chl-a) et de MPS (Kostadinov et al., 2009; Lyu et al., 2017).

LES MÉTHODES UTILISÉES POUR MESURER LA TAILLE DES PARTICULES

Plusieurs techniques sont disponibles pour mesurer la taille des particules. Cela inclut le compteur Coulter (Sheldon et al., 1972; Milligan & Kranck, 1991), le microscope électronique à transmission (Harris, 1977), les systèmes d'imagerie des particules tel la FlowCam (Reynolds et al., 2010), la méthode de diffraction par laser (Agrawal & Pottsmith, 2000; Slade & Boss, 2006; Reynolds et al., 2010), la cytométrie en flux (Yentsch et al., 1983) et la télédétection (Wang et al., 2016). La taille des particules *in situ* est la configuration dans laquelle la MPS est transportée (Kranck & Milligan, 1991). À l'exception de la diffraction par laser, les méthodes *in situ* demandent beaucoup de temps et de nombreux échantillons afin de bien caractériser la taille des MPS. La prise d'échantillons étant essentielle, des fixatifs chimiques sont aussi nécessaires pour préserver les échantillons jusqu'à leur analyse, ce qui a le potentiel de compromettre leur intégrité (Reynolds et al., 2008).

Le LISST-100X est un diffractomètre laser qui permet de mesurer des particules allant de quelques microns à plus d'une centaine de microns (Sun et al., 2016). Il a été démontré que cet instrument donne de bons résultats non seulement en milieu océanique, mais aussi en environnements côtiers (Ahn & Grant, 2007; Reynolds et al., 2008, 2010; Boss et al., 2018). La particularité de cet appareil est qu'il peut être déployé directement dans la colonne d'eau, ce qui permet d'avoir une plus grande résolution verticale tout en n'affectant pas les particules mesurées. Le LISST-100X peut aussi être utilisé en mode laboratoire. Reynolds et al. (2010) ont déterminé que les résultats en mode laboratoire sont similaires à ceux obtenus *in situ*, mais pourraient différer dans des environnements avec de gros agrégats.

L'utilisation de la télédétection est un autre moyen pour mesurer la taille de la MPS à la surface de l'eau. Les particules en suspension ont un grand impact sur les propriétés optiques des eaux (Figure 1). La diffusion de la lumière par les particules dépend de leurs forme, de leurs taille et de leurs indice de réfraction et donc de leurs composition (Loisel et

al., 2006). La distribution des tailles des particules influence l'atténuation (affaiblissement) de la lumière, le coefficient de rétrodiffusion des eaux (portion de la lumière diffusée dans la direction d'origine) et donc la radiance (puissance du rayonnement) reçue par les capteurs satellitaires (Zhou & Cao, 2008; Shi et al., 2014). Depuis les valeurs de radiance obtenues par les capteurs satellitaires, il est possible d'obtenir les valeurs de propriétés optiques inhérentes telles la rétrodiffusion, $b_{bp}(\lambda)$ et l'absorption, $a(\lambda)$ à des longueurs d'onde spécifiques. De là, il est ensuite possible d'obtenir la distribution des tailles des particules (Figure 2; ex. Ciotti & Bricaud, 2006; Devred et al., 2006; Loisel et al., 2006; Hirata et al., 2008; Kostadinov et al., 2009; Slade & Boss, 2015; Shi & Wang, 2019).
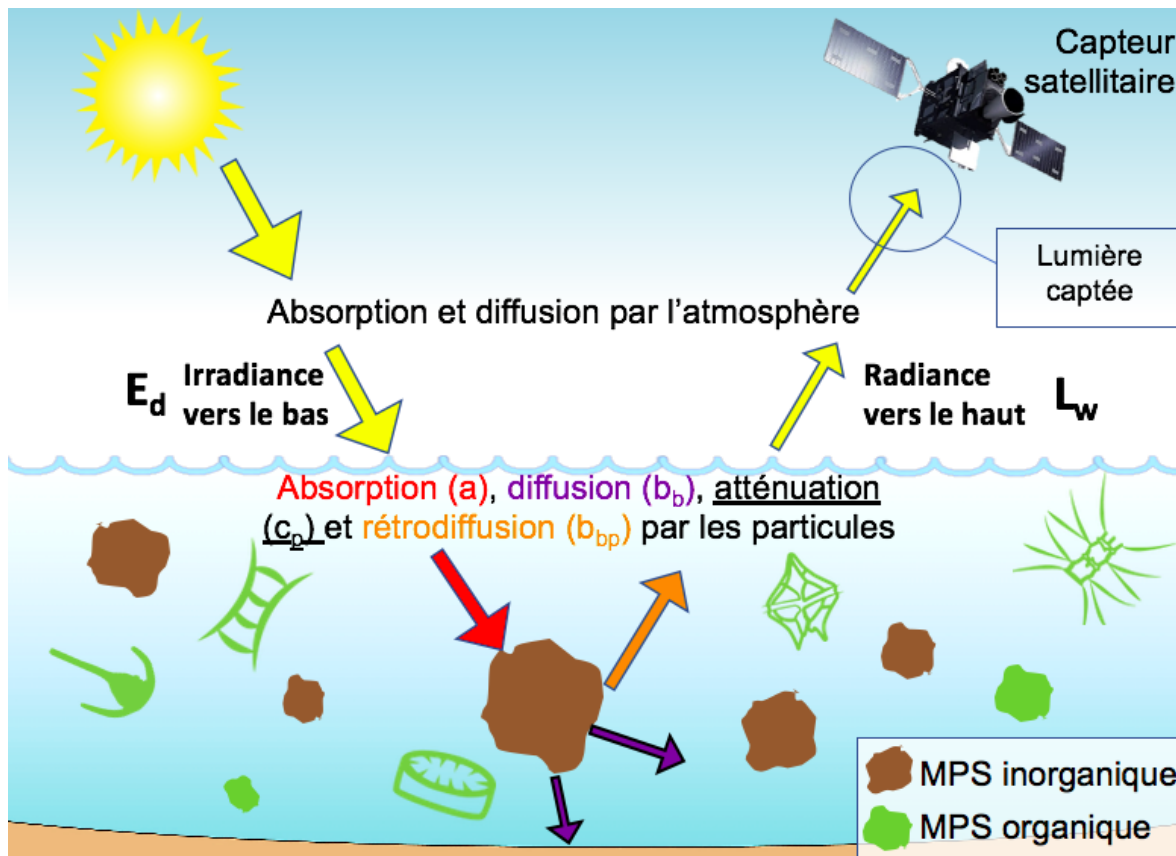
Figure 1. Facteurs influençant la lumière captée par les capteurs satellitaires (modifiée depuis Laanen, 2007)
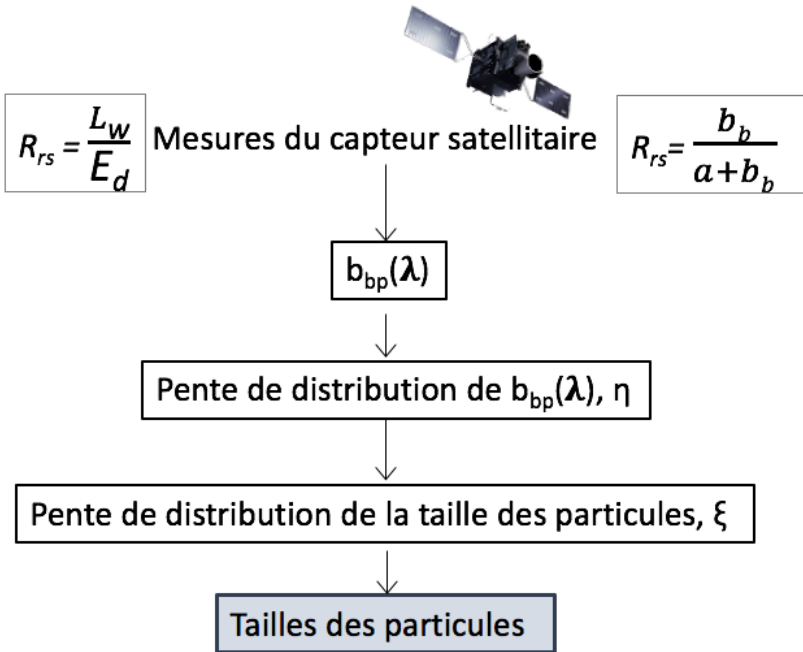
Figure 2. Organigramme des étapes depuis les capteurs satellitaires jusqu'à la taille des particules (modifié depuis Kostadinov et al., 2009) où R_{rs} est la réflectance de télédétection, L_w est la radiance vers le haut, E_d est l'irradiance vers le bas, b_b est la diffusion, a est l'absorption et b_{bp} est la rétrodiffusion

Ces méthodes permettent d'utiliser les données de télédétection pour obtenir les valeurs de taille et d'autres processus associés liés tels la production primaire et le transport des sédiments. Cela a pour avantage d'avoir une meilleure résolution spatiale et temporelle en plus de prendre moins de temps et de diminuer les coûts (Lei et al., 2018).

Afin d'utiliser les algorithmes de télédétection, il est toutefois nécessaire que ceux-ci soient applicables aux eaux de l'écosystème étudié. En effet, les propriétés optiques des eaux varient en fonction du type d'eau présent. Deux catégories ont été déterminées, les eaux de Cas-1 et de Cas-2 (Prieur & Sathyendranath, 1981; IOCCG, 2000). Les eaux de Cas-1 sont principalement caractéristiques des eaux océaniques où la concentration en Chl-*a* a le plus d'impact sur les variations dans les propriétés optiques. Dans les eaux de Cas-2, comme l'ESL, ce sont plutôt les concentrations en matière en suspension et la coloration des matières organiques dissoutes qui ont la plus grande incidence (Mobley, 1994). La

présence de plus de constituants augmente la complexité des eaux de l'ESL d'un point de vue de télédétection. Il a déjà été montré que les algorithmes OC4v4, EOF, GSM01 et GIOP pour obtenir les valeurs de Chl-*a* ne sont pas applicable à l'ESL (Yayla, 2009; Laliberté et al., 2018). Il est donc probable que les algorithmes pour mesurer la taille des MPS ne donnent pas de bons résultats dans l'ESL. Des algorithmes adaptés doivent alors être développés afin de tenir compte du type de particules présent. Il est donc nécessaire d'en apprendre davantage sur ces particules.

TRAVAUX PRÉCÉDENTS SUR LA TAILLE DES PARTICULES

Des travaux récents ont été effectués dans d'autres zones côtières et estuariennes concernant la distribution des tailles des particules (ex. Barone et al., 2015; Huang et al., 2016; Qiu et al., 2016; Shi & Wang, 2019). Il a été déterminé que la MPS provient principalement de sédiments remis en suspension et que la taille des particules est plus grossière près des côtes et diminue vers le large (Park et al., 2001; Xi et al., 2014).

Par le passé, les études sur la taille des particules dans l'ESL ont utilisé l'analyse par composante principale sur les spectres de tailles obtenus à l'aide d'un compteur Coulter afin de décrire la PSD (Chanut & Poulet, 1979; Poulet et al., 1986a; Poulet et al., 1986b). Les travaux plus récents utilisent plutôt des paramètres telles la pente de la distribution du nombre de particules par unité de volume en rapport à la gamme de taille (ex. Buonassissi & Dierssen, 2010; Reynolds et al., 2010; Xi et al., 2014) ou encore la taille médiane (ex. Qiu et al., 2016; Sun et al., 2016) qui peuvent être obtenus depuis les valeurs d'un LISST-100X.

La taille des particules a précédemment été étudiée dans l'ESL (D'Anglejan & Smith, 1973; Silverberg & Sundby, 1978; Chanut & Poulet, 1979; Kranck, 1979; Chanut & Poulet, 1982; Poulet et al., 1986a; Poulet et al., 1986b). D'Anglejan & Smith (1973) ont mesuré à l'été 1971, dans l'estuaire moyen, la taille des particules entre 3.9 et 62.5 µm à l'aide d'un

microscope. La plupart des particules mesuraient moins de 7 μm. Poulet et al. (1986a) ont obtenu des spectres de tailles des particules de 1.26 à 180 μm à l'aide d'un compteur Coulter pour l'estuaire et le golfe du Saint-Laurent au printemps et à l'automne 1974. La forme de ces spectres variait selon la salinité des eaux et donc selon la région de l'estuaire. En juin 2013, la taille des particules à la surface (0-2 m) a été caractérisée pour les différentes régions de l'estuaire avec le LISST-100X utilisé en mode laboratoire (Mohammadpour et al., 2017). Des particules relativement larges (>10 μm) étaient présentes dans l'estuaire moyen et une grande proportion de particules <0.4 μm étaient présentes dans l'estuaire maritime. Il y avait corrélation entre la pente de distribution et les propriétés optiques inhérentes.

Même si ces travaux ont jeté les bases des connaissances des tailles des particules dans l'ESL, il reste encore de nombreuses questions à répondre sur ce sujet puisqu'il n'existe encore aucune caractérisation de la distribution spatiale et verticale des tailles des particules dans l'ESL ni aucune mesure en période hivernale.

OBJECTIFS DE RECHERCHE

L'objectif général de ce projet est de caractériser la taille et la composition de la matière particulaire en suspension présentes dans la colonne d'eau de l'ESL en saison printanière (mai 2010) et hivernale (février 2019). Deux objectifs spécifiques ont été définis :

Objectif spécifique 1 : Déterminer la distribution verticale et horizontale des tailles des particules en suspension dans l'ESL. Les concentrations de MIP, MOP et Chl-*a* seront comparées aux données de tailles pour inférer le type de particules présentes. Cet objectif permettra de répondre aux questions suivantes :

(1) Quelle est la variation spatiale et verticale de la distribution des tailles des particules le long de l'ESL ?

(2) Quelle est la différence dans la distribution selon la saison ?

(3) Quelle est la relation entre la distribution et les paramètres biogéochimiques (MIP, MOP, Chl-*a*) ?

Objectif spécifique 2 : Déterminer la composition minéralogique et géochimique des particules détritiques présentes dans les eaux de surface de l'ESL à l'hiver. La détermination de la signature minéralogique et chimique de la MPS permettra de documenter la nature et l'origine des particules détritiques en suspension et de mieux comprendre la dynamique sédimentaire dans l'ESL. Cet objectif permettra de répondre aux questions suivantes :

(1) Quelles sont la nature et l'origine des particules détritiques de l'ESL en saison hivernale ?

(2) Est-ce que les particules détritiques en suspension sont principalement dérivées de l'érosion des roches du Bouclier canadien ou des Appalaches, ou d'un mélange des deux ?

AUTRES RÉALISATIONS

Au cours de ma maîtrise, j'ai eu l'opportunité de présenter les principaux résultats de mon projet de recherche lors de divers congrès nationaux et internationaux :

Fabris, A.-S., Larouche, P., Montero-Serrano, J.-C. (2020). Characterization of the St. Lawrence Estuary's suspended matter size and composition. European Geosciences Union (EGU): Sharing Geoscience Online (session GM3.7), May 4-8, Online.

Fabris, A.-S., Larouche, P., Montero-Serrano, J.-C. (2020). Caractérisation de la taille et composition de la matière particulaire en suspension dans l'estuaire du Saint-Laurent. Réunion scientifique annuelle de Québec-Océan, 9-11 mars, Château Mont-Sainte-Anne, Beaupré, Canada.

Fabris, A.-S., Larouche, P., Montero-Serrano, J.-C. (2019). The St. Lawrence estuary's suspended matter size and composition in winter. ArcticNet Annual Scientific Meeting, December 2-5, Halifax, Canada.

Fabris, A.-S., Larouche, P., Montero-Serrano, J.-C. (2019). Particle size distribution in the St. Lawrence Estuary and their sedimentological properties. Congrès des étudiant.e.s du GEOTOP, 22-24 mars, Centre de villégiature Jouvence, Orford, Canada.

Fabris, A.-S., Larouche, P., Montero-Serrano, J.-C. (2018). Propriétés optiques de la matière en suspension dans les eaux de l'estuaire du Saint-Laurent : distribution des tailles des particules. Réunion scientifique annuelle de Québec-Océan, 5-6 novembre, Rivière-du-Loup, Canada.

J'ai également eu l'opportunité d'embarquer deux fois à bord du N.G.C.C. Amundsen, soit à l'hiver 2019 et à l'hiver 2020 dans le cadre de la mission hivernale Odyssée Saint-Laurent dans l'estuaire et le golfe du Saint-Laurent. Ces missions ont permis de recueillir une partie des échantillons qui sont étudiés dans le cadre de ce mémoire de maîtrise. À l'été 2019, j'ai pu participer à la mission estivale d'Odyssée Saint-Laurent à bord du Lampsilis afin d'aider aux opérations d'échantillonnage, de mesures de la taille des particules et de filtrations dans l'estuaire fluvial et moyen.

CHAPITRE 1
CARACTÉRISATION DE LA TAILLE ET COMPOSITION DE LA MATIÈRE EN SUSPENSION DANS L'ESTUAIRE DU SAINT-LAURENT

1.1 RÉSUMÉ EN FRANÇAIS

La distribution des tailles des particules (PSD) est une propriété importante de la matière en suspension qui permet de décrire les flux de particules dans la colonne d'eau. La composition minéralogique et géochimique des particules détritiques fournit des indices sur leur origine et la dynamique sédimentaire. L'estuaire du Saint-Laurent, dans l'est du Canada, est un environnement côtier dynamique où aucune description récente de la composition des particules et de la PSD dans la colonne d'eau n'a été réalisée. Dans cette étude, nous caractérisons la PSD tant verticalement qu'horizontalement et sa variabilité entre la saison printanière de 2010 et la saison hivernale de 2019 à partir de données obtenues avec un diffractomètre laser LISST-100X. Les résultats ont montré l'importance de la sédimentation en aval, car les particules grossières, soit plus grandes que 63 µm, en mai et les particules entre 4 et 63 µm en février étaient moins présentes qu'en amont. Dans cette même section de l'estuaire, les particules grossières avaient des concentrations plus élevées en hiver qu'en été, probablement en raison de la formation de flocs, du transport par la glace et de la charge plus élevée en matière en suspension des rivières régularisées. En amont, aucune variabilité verticale importante n'est présente au printemps et dans la zone de turbidité maximale en hiver en raison du mélange vertical. La composition minéralogique et élémentaire des particules détritiques en suspension en hiver a été déterminée avec un diffractomètre à rayons X et un microscope électronique à balayage couplé à un spectromètre à rayons X à dispersion d'énergie. La composition était similaire dans tout l'estuaire et indiquait une origine principale depuis le Bouclier canadien avec la

province des Appalaches comme source secondaire. Pour la PSD, la variabilité saisonnière était plus importante que la variabilité spatiale. Ce n'était pas le cas pour la composition minéralogique et élémentaire qui était presque constante autant spatialement qu'entre deux différentes saisons. Ces résultats amènent de nouvelles informations sur la dynamique de la matière en suspension au printemps et en hiver pour un environnement estuarien large et subarctique.

Characterization of the St. Lawrence Estuary's suspended matter size and composition

Anne-Sophie Fabris[1], Pierre Larouche[2], Jean-Carlos Montero-Serrano[1]

[1] Institut des sciences de la mer de Rimouski, Université du Québec à Rimouski, 310 allée des Ursulines, C.P. 3300, Rimouski, QC, G5M 1L7, Canada

[2] Fisheries and Oceans Canada, Maurice-Lamontagne Institute, 850 route de la Mer, Mont-Joli, QC, G5H 3Z4, Canada

1.2   ABSTRACT

Particle Size Distribution (PSD) is an important property of suspended matter that allows describing the flow of particles in the water column. The mineralogical and geochemical composition of detrital particles provides clues to their origin and the sedimentary dynamic. The St. Lawrence Estuary, in eastern Canada, is a dynamic coastal environment where no recent description of the composition of particles and the PSD has been completed. In this study, we characterize the PSD both vertically and horizontally and its variability between the spring 2010 and winter 2019 seasons from data obtained with a LISST-100X laser diffractometer. The results showed the importance of downstream sedimentation as coarse particles, larger than 63 μm, in May and particles between 4 and 63 μm in February were less present than upstream. In this same section of the estuary, coarse particles had higher concentrations in winter than in summer, possibly due to flocculation, ice transport and the higher suspended matter load of regulated rivers. In the upstream section, no substantial vertical variability is present in spring and in the zone of maximum turbidity in winter due to vertical mixing. The mineralogical and elemental composition of the suspended detrital particles in winter was determined with an X-ray diffractometer and a scanning electron microscope coupled with an energy-dispersive X-ray spectrometer. The composition was similar throughout the estuary and indicated a primary origin from the Canadian Shield with the Appalachian province as a secondary source. For

the PSD, the seasonal variability was greater than the spatial variability. This was not the case for the mineralogical and elemental composition which was similar both spatially and between two different seasons. These results provide new information on the dynamics of suspended matter in spring and winter for a large estuarine and subarctic environment.

1.3 INTRODUCTION

Over the last few decades, marine and terrestrial environments of arctic and subarctic regions were strongly influenced by recent climate change (IPCC, 2019). As a result, the ice cover has reduced (Comiso et al., 2017), the sea level has risen (Barnett et al., 2017; Kemp et al., 2018), coastal erosion has increased (Asselman et al., 2003) and the frequency and intensity of floods have multiplied (Dahlke et al., 2012). These environmental changes also generate regional variations of suspended particulate matter (SPM) concentrations in marine environments (Gagnon et al., 1997).

The SPM present in waters is composed of organic and inorganic matter having various physical and chemical properties (Sholkovitz, 1976). One of these properties is the particle size distribution (PSD) which is affected by phytoplankton blooms (Li & Logan, 1995), sediment provenance (Pye & Blott, 2004; Itamiya et al., 2019), sedimentation and resuspension of particles (Mikkelsen & Pejrup, 2001; Ahn, 2012). Apart from individual particles, composite particles known as aggregates may be present and coming from the erosion of soils or the compaction of flocs (Woodward et al., 2002; Tao et al., 2018). They retain their larger size during transport. Single particles and aggregates can flocculate through physical, chemical and biological mechanisms to form larger particles called flocs (Droppo et al., 1998). Flocs can eventually break up due to stress caused, for example, by sampling (Eisma, 1986; Woodward et al., 2002). SPM is an important parameter to characterize as it contributes to pollutant dispersion (Ramalhosa et al., 2005; Ma et al., 2009). A high concentration of SPM also affects light attenuation in the water column (Devlin et al., 2008) and the heat budget through a higher light absorption (Morel & Antoine, 1994; Löptien & Meier, 2011). A few studies have been done in the St. Lawrence

Estuary (SLE; Eastern Canada) to characterize the size and composition of SPM either spatially or vertically (Loring & Nota, 1973; Chanut & Poulet, 1982; Poulet et al., 1986a; Mohammadpour et al., 2017), but none have been done in winter conditions.

The SLE is a dynamic coastal environment affected by winds, tides, river runoffs and ice which generate large variations of its sedimentological, biological and chemical properties and consequently the dynamic of its particles (Sinclair, 1978; Drapeau, 1992; Larouche & Boyer-Villemaire, 2010; Jaegle, 2015). The SPM's sources in the SLE during winter are still relatively unknown. The SLE is characterized by two main geological provinces having different mineralogical and chemical signatures (Loring & Nota, 1973; Jaegle, 2015; Casse et al., 2017): (1) the Canadian Shield on the North Shore, characterized by metamorphic and igneous rocks and (2) the Appalachian Region on the South Shore, composed of sedimentary rocks leading to distinctive mineralogical and elemental geochemical signatures. The metamorphic rocks of the Canadian Shield are characterized by amphibole, pyroxene, plagioclase feldspar and potassium (K) feldspar while the sedimentary rocks of the Appalachian Region are mainly composed of quartz, clays and phyllosilicates (Loring & Nota, 1973; Jaegle, 2015). The mineralogical and elemental geochemical signatures of the SPM could allow for estimation of the relative contribution of these two sources to the SLE. This knowledge is necessary to determine the principal origin of terrigenous contributions and for better understanding of the sedimentary dynamic and coastal erosion processes operating in the SLE.

Considering the large size of the SLE, the use of remote sensing would be a suitable way to follow the PSD variations in this dynamic environment. There exist a few algorithms to measure particle sizes from remote sensing applicable to ocean-like environments. One of them is through the use of satellite-derived chlorophyll-*a* (Chl-*a*) concentrations (Uitz et al., 2006; Uitz et al., 2010; Hirata et al., 2011). Satellite-derived inherent optical properties can also be used, such as the absorption distribution (Ciotti & Bricaud, 2006; Devred et al., 2006; Hirata et al., 2008; Organelli et al., 2013), the backscattering distribution (Loisel et al., 2006; Kostadinov et al., 2009) and the use of

both (Neukermans et al., 2016). Unfortunately, the complex optical properties of the SLE (Nieke et al., 1997; Yayla, 2009; Montes-Hugo et al., 2012) brings difficulty in using the algorithms already developed (Mélin & Vantrepotte, 2015; Mohammadpour et al., 2017; Laliberté et al., 2018). In order to validate and improve the PSD algorithms for the SLE, the size distribution and the composition of the particles *in situ* need to be better characterized through different seasons. These two factors influence the optical parameters of the remote sensing algorithms (Loisel et al., 2006; Neukermans et al., 2012) as well as sediment flow and the phytoplankton dynamic in the SLE (Loisel et al., 2006; Larouche & Boyer-Villemaire, 2010; Neukermans et al., 2012).

In this context, we aimed to (1) provide new insights on the spatial and vertical PSD in the SLE for the spring 2010 and winter 2019, and (2) characterize the mineralogical and geochemical composition of SPM present in the surface waters of the SLE during winter 2019 to assess the contributions from specific sediment sources during winter times. This study provides an opportunity to improve the regional knowledge on the PSD and composition of SPM in the SLE.

1.4   MATERIALS AND METHODS

1.4.1   Study Area and Sampling

The SLE is among the largest estuaries in the world (El-Sabh & Silverberg, 1990). It is divided (Fig. 3) in two zones with different bathymetry, circulation and biological productivity (Levasseur et al., 1984). The Upper Estuary (3,470 km^2) from Quebec City to the Saguenay Fjord is greatly influenced by tides due to its bathymetry and its funnel shape. It includes a maximum turbidity zone in the upstream section (Saucier & Chassé, 2000). The Lower Estuary (9,350 km^2) from the Saguenay Fjord to the Gulf of St. Lawrence (Levasseur et al., 1984; D'Anglejan, 1990) has a complex circulation due to its large dimension and topography. Various upwellings, gyres and mixing zones are present (DFO,

2012). The transverse currents in the Lower Estuary produce in general a flow of water toward the southern shore at the surface while the deeper waters move in the direction of the North Shore (Neu, 1970). Most of the SPM present in the SLE find their origin from upstream, the Saguenay River as well as North and South Shore rivers (Garrels & Mackenzie, 1971; Loring & Nota, 1973; Jaegle, 2015; Casse et al., 2017).

A first sampling episode was done in the spring 2010 (19-23 May) on board the C.C.G.S. Martha L. Black. Water samples for the analysis of Chl-*a* and of the SPM were taken at 20 stations (Stns. S-14 to S-45 and S-S3) along the estuary (Fig. 3). The water samples were collected with a rosette comprised of Niskin type bottles, a Seabird 911 CTD sensor and a Wetstar fluorometer. The fluorometer was uncalibrated and only used to characterize the vertical chlorophyll structure. After the rosette cast was done, a profiling optical cage including a Sequoia LISST-100X Type-B (hereafter called LISST) was used to continuously measure the particle size spectra in the water column. A second sampling in the SLE was done during the Odyssée Saint-Laurent 2019 winter expedition (3-13 February) on board the C.C.G.S. Amundsen. 10 stations (Stns. W-1 to W-12) between Quebec City and East of Pointe-des-Monts were sampled (Fig. 3). During this mission, the same type of rosette sampling was done than in 2010. Due to the presence of ice (up to 80% coverage) and cold temperatures, the use of an optical profiler was impossible and was replaced by the acquisition of water samples (~0.5 L) taken at discrete depths in the water column. Particle size analysis was performed using the LISST in benchtop mode. The samples were first gently inverted twice for homogenization. A syringe was then used to slowly insert the sample in the chamber through a tube to avoid bubble formation. The chamber was mounted between the optic components of the LISST and a magnetic stir bar was present to avoid sinking of the particles. A piece of aluminum foil was used to cover the chamber to minimize contamination by ambient light. A single water sample (~30-60 L) was also collected at 10 m depth, filtered on 0.8 µm membranes (Isopore, polycarbonate) and preserved at 4°C for analysis of the SPM mineralogical and geochemical composition.

22
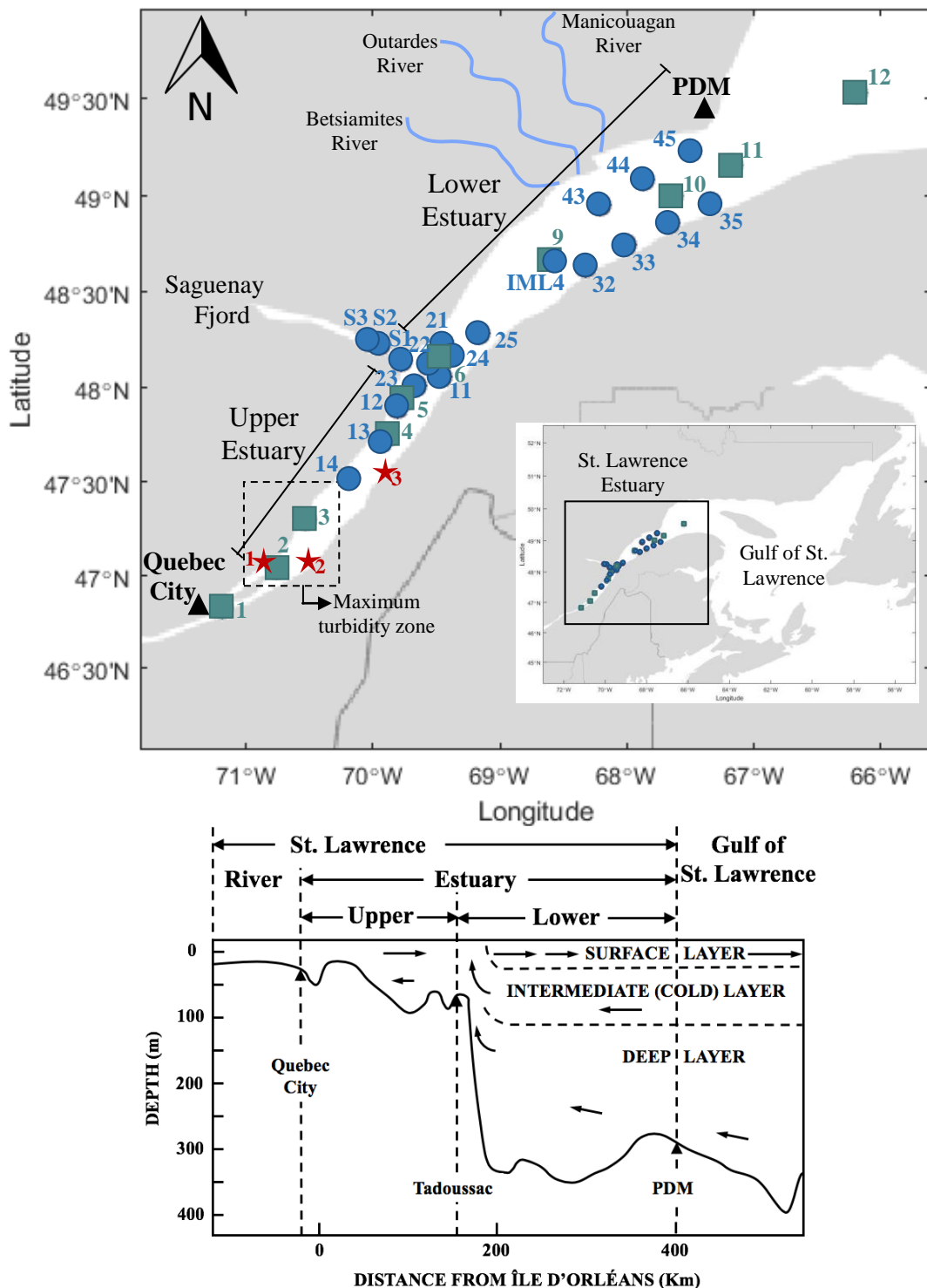
Fig. 3. A) Location of stations sampled in spring 2010 (blue circles) and winter 2019 (green squares). The red stars represent tidal marshes (1: Cap Tourmente, 2: Montmagny, 3: Kamouraska), B) Water masses of the SLE and basic state of motion (modified from Koutitonsky & Bugden, 1991). Notes: PDM=Pointe-des-Monts. The cold intermediate layer disappears in winter (Gilbert & Pettigrew, 1997)

For the summer and winter samples, Chl-*a* concentration measurements were analyzed using the fluorescence method (Parsons et al., 1984) to complete the data from the profiling fluorometer. To determine the SPM concentration, the water samples were filtered onto pre-weighed 21 or 25 mm glass fiber filters (Whatman, GF/F), rinsed with Milli-Q water and kept frozen until lyophilized or dried at 100°C for at least 3 hours. From the weighed SPM samples, particulate inorganic matter (PIM) and particulate organic matter (POM) measurements were determined by burning the filters at 450 degrees for 5 hours. The vertical profiles obtained from the WetStar fluorometer were binned to 1 m intervals. To evaluate the accuracy of the measurements, SPM and Chl-*a* blanks were done every day in 2010 while duplicates at each depth were performed in 2019. The mean coefficient of variation (CV) of SPM samples was 11% for both years, the mean CV of PIM were 3% (2010) and 13% (2019), the mean CV of POM were 26% (2010) and 9% (2019), while Chl-*a* had a mean CV of 5% (2010) or 7% (2019).

1.4.2   PSD Measurements

The LISST measures the scattered light and uses an inversion model based on Mie theory to obtain the particle volume concentration (V[D]) at 32 size classes placed logarithmically from a diameter (D) of 1.25 to 250 μm (Agrawal & Pottsmith, 2000). Data for the PSD was processed using the manufacturer provided software LISST-SOP (LISST-100X Particle Size Analyzer, 2015) and analyzed with MATLAB®. The 2010 data were median-binned to 1 m intervals. For the 2019 data, the median was calculated using measurements taken over 60 seconds (at 1 Hz sampling rate) at discrete depths. Median-binned data associated with an optical transmission higher than 99.5% were discarded as too clear water, indicating a too low signal to noise ratio (LISST-100X Particle Size Analyzer, 2015). The particle number concentration (N[D]) was calculated from:

$$N(D) = 6\ V(D)\ /\ \pi D^3$$

through assumption of spherical particles using the midpoint of each size class as the volume-equivalent diameter, D (Reynolds et al., 2010; Sun et al., 2016; Runyan et al., 2020). The average particle number for a given size class of width ΔD represents the particle number density (N'[D]). It is obtained from the equation:

$$N'(D) = N(D) / \Delta D$$

The volume concentration density V'(D) can be expressed as:

$$V'(D) = V(D) / \Delta D$$

The SLE is very dynamic and vertical profiles are often different over short distances. Three stations were selected to represent the various sections of the estuary. Closely located stations from spring and winter were selected to better compare between seasons. Stns. S-12 and W-5 were chosen to represent the Upper Estuary downstream of the maximum turbidity zone. Stns. S-IML4 and W-9 were selected as representative of the Lower Estuary as this is the position of a long-term monitoring program that measures various oceanographic data (Galbraith et al., 2019). Due to strong currents, only the top 40 m of Stn. S-12 and the top 50 m of Stn. S-IML4 were sampled with the LISST. Only the top 200 m of Stn. W-9 were sampled due to a sampling problem. Stn. S-S2 is one of three stations in the Saguenay River measured in spring for which the top 152 m were sampled. Stn. W-1 is the most upstream station sampled in winter and is representative of the St. Lawrence river input into the estuary. Other key stations are presented in the supplementary material (Fig. S1).

Preliminary data analysis showed unimodal and bimodal V'(D) spectra. There was a visible maximum in the smallest size class followed by a minimum in the other small size classes (Fig. 4B,C,E) that could be from an artifact created by the LISST. This shape is often seen in LISST data and may result from particles in suspension smaller than what can be measured by the instrument or the presence of non-spherical particles which create scattering patterns that are not taken into account by the LISST's inversion

algorithm (Agrawal & Traykovski, 2001; Agrawal et al., 2008; Buonassissi & Dierssen, 2010; Neukermans et al., 2012; Slade & Boss, 2015).
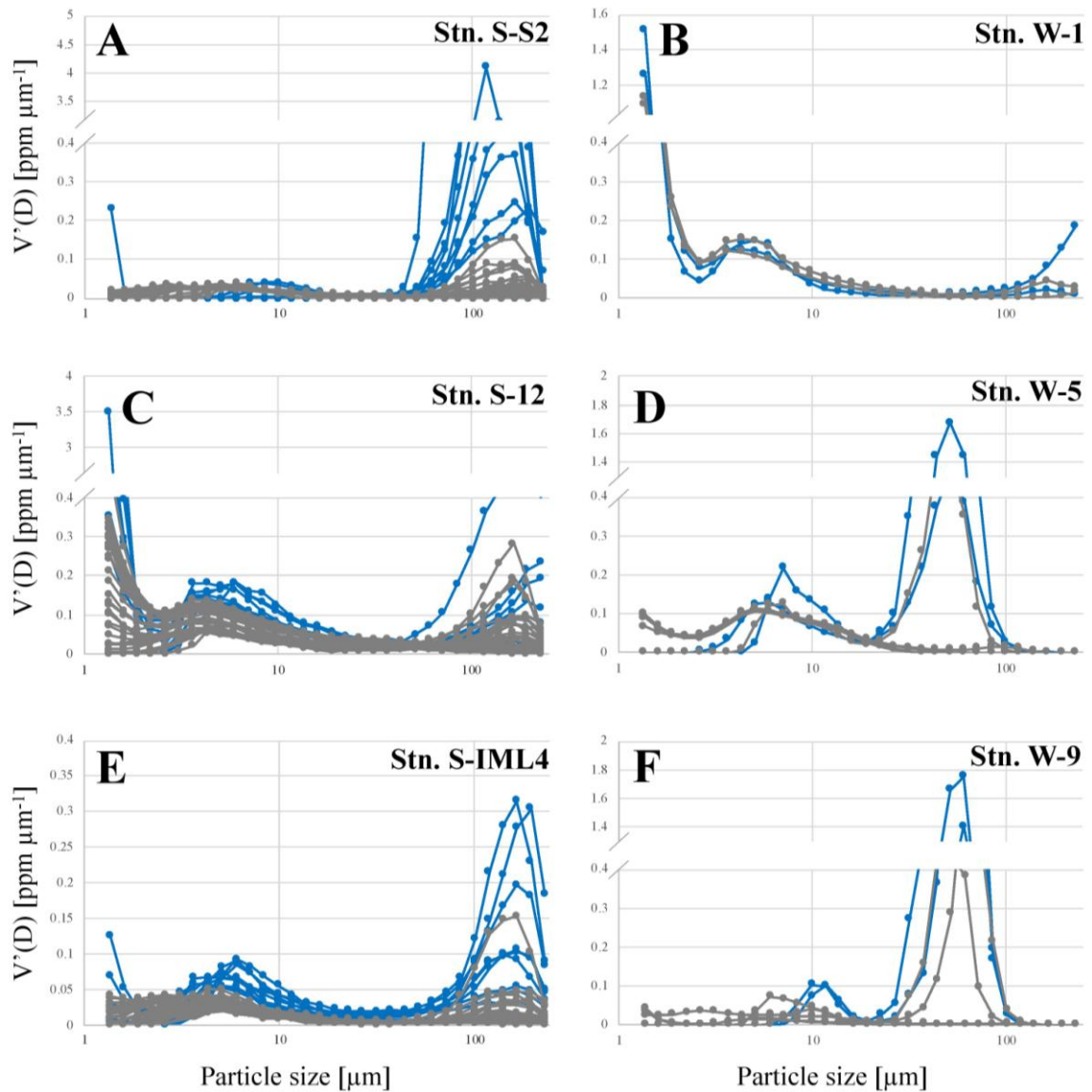
Fig. 4. Volume concentration density V'(D) at various depths in spring 2010 (A, C, E) and winter 2019 (B, D, F) for representative stations (A: Stn. S-S2, B: Stn. W-1, C: Stn. S-12, D: Stn. W-5, E: Stn. S-IML4, F: Stn-W-9). Blue lines correspond to surface depths (between 1 and 10 m)

The median particle diameter of the volume distribution $D_V{}^{50}$ corresponding to the 50th percentile diameter with a half of accumulated volume concentration was also calculated to estimate the relative concentration of small to large particles (e.g. Qiu et al., 2016; Lei et al., 2018).

As the PSD data generally followed a power law model (Fig. 5), the PSD slope (ξ, *Junge)* was calculated with D representing the median of each size classes over the range 6.03 to 165 µm using the function:

$$N'(D) = N'(D_0) \left(\frac{D}{D0}\right)^{-\xi},$$

where D_0 is the reference diameter set at 31.6 µm which was the midpoint of the logarithmic size range. That size range was chosen to minimize the effect of the rising tail at smaller sizes and the low values at the largest size classes (Fig. 5) that are partially due to particle sinking in benchtop mode (Reynolds et al., 2010). Least square minimization on the log-transformed data of each distribution was used for calculations as performed in previous studies (Vidondo et al., 1997; Buonassissi & Dierssen, 2010; Reynolds et al., 2010). For 2010, at the exception of Stn. S-21 the average fit gave good regression statistics with a determination coefficient R^2 between 0.82 and 0.99. For 2019, at the exception of Stns. W-9 and W-12, the R^2 was good (0.83 to 0.99). The other stations had a R^2 that ranged between 0.64 and 0.75.
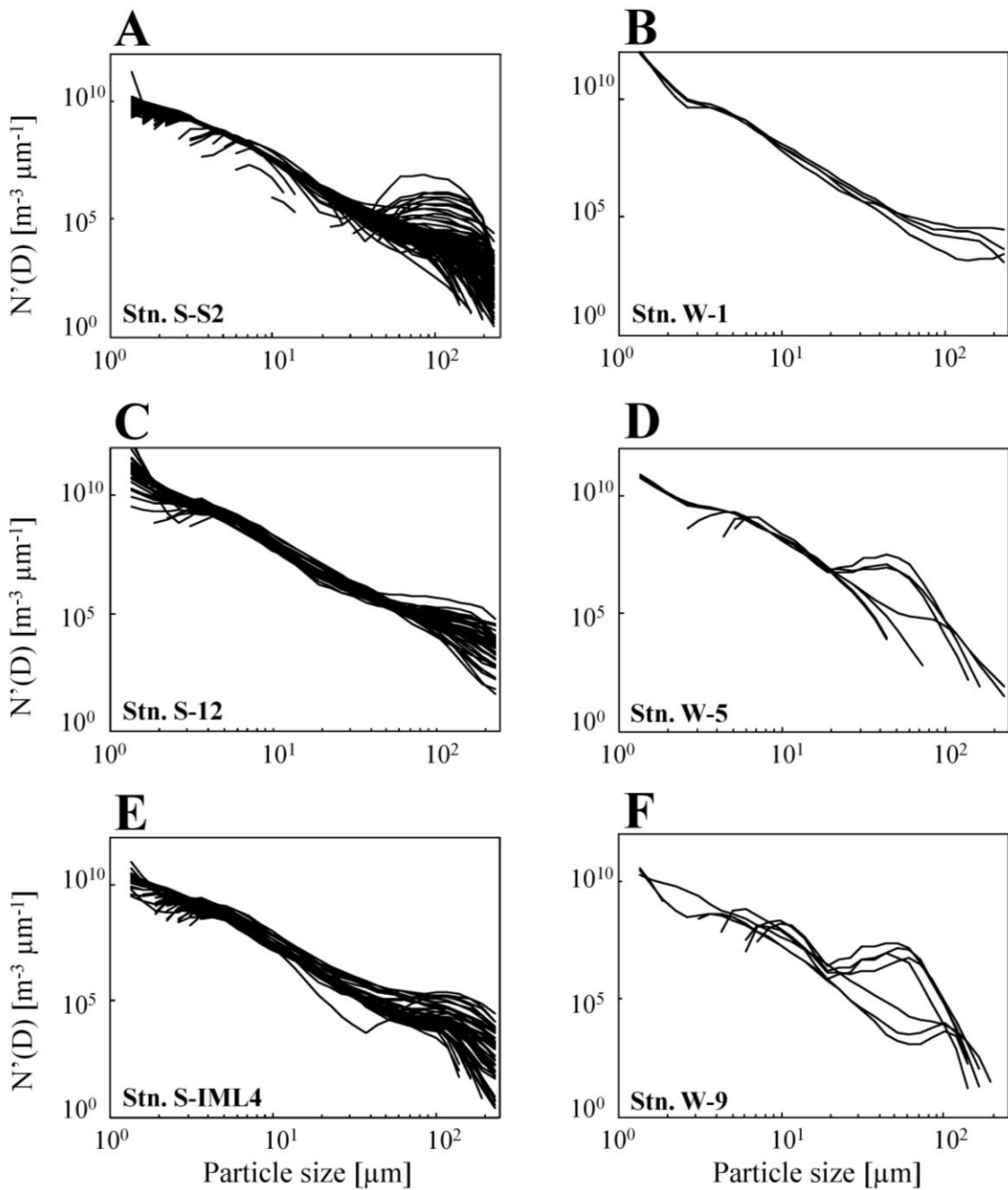
Fig. 5. Particle number density N'(D) in spring 2010 (A, C, E) and winter 2019 (B, D, F) at various depths for representative stations (A: Stn. S-S2, B: Stn. W-1, C: Stn. S-12, D: Stn. W-5, E: Stn. S-IML4, F: Stn-W-9)

1.4.3 Geochemical and mineralogical composition analysis

The filters with the SPMs sampled at 10 m were placed in a beaker and covered with demineralized water. The beakers were then placed in an ultrasonic bath cleaner for a period of 1 to 3 hours to separate the particulate matter from the filters. The beakers containing the SPM were decanted and air dried in a clean hood for several days. SPM samples were transferred into 50 mL Falcon tubes and pretreated with 5 mL of hydrogen peroxide (H_2O_2; 30 %) and 5 ml of hydrochloric acid (HCl; 0.5 M) for at least 24 hours to oxidize the organic matter and remove biogenic carbonates. Next, samples were mixed with demineralized water and centrifuged at 3500 rpm for 45 minutes. This rinsing process was repeated three times. SPM slurries were oven-dried overnight at approximately 60°C and then homogenized with an agate mortar. This process follows previous methodology to treat filter samples to obtain fine particles (e.g., Jaegle, 2015; Desiage et al., 2018; Caron et al., 2020). The aliquots of these SPM samples were used for geochemical and mineralogical analysis.

Prior to elemental composition analysis, aliquots of SPM samples were placed onto 12 mm carbon adhesive tabs (Electron Microscopy Sciences). The elemental analysis was done by using an INCA X-sight energy-dispersive X-ray spectrometer (Oxford Instruments) coupled to a JEOL 6460LV scanning electron microscope. X-ray spectra were measured from 40 detrital particles manually and randomly selected at various positions over the sample using the microscope (Fig. S2B). This also avoided measurements of empty spaces on the tabs. Each spectrum was acquired for 60 seconds of live time at an accelerating voltage of 20 kV. System optimization was done using copper as standard. From these results, outliers (data point more than 1.5 interquartile ranges below the 1st quartile or above the 3rd quartile) were removed (Aczel & Sounderpandian, 2008). This represented between 2 and 8 % of the data points per station. Major elemental ratios were used to determinate the geochemical classification and mineralogical maturity (Fe/K vs Si/Al, expressed as oxides). Ratios were also used to discriminate sediment provenance (Si/Ca vs Al/Ca) in the SPM samples by comparing with data obtained in bedload samples

taken at the mouth of rivers from Tadoussac to Sept-Îles on the North Shore and between Trois-Pistoles and Mont-Saint-Pierre on the South Shore (Table S1; Jaegle, 2015; Casse, 2018). Al and Si concentrations are preferential in clay and quartz minerals respectively indicating an Appalachian source, while Ca is associated with the plagioclase enriched metamorphic rocks of the Canadian Shield (Ramesh & D'Anglejan, 1995; Jaegle, 2015; Casse, 2018).

In addition, aliquots of SPM samples were pipetted with ethanol on glass slides. Samples were then air-dried and analyzed by quantitative X-ray diffraction (qXRD) using a PANalytical X'Pert Powder diffractometer. This instrument is fitted with a copper tube (Cu K-alpha=1.54178 Å), operating at 45 kV and 40 mA, and a post diffraction graphite monochromator. The samples were analyzed from 5 to 65° 2θ with a counting time of 2 seconds per step. Bulk mineral associations were analyzed following the qXRD method developed by Eberl (2003) and Eberl & Smith (2009) and used in other marine geology studies that deal with sediment mineralogy (e.g., Andrews & Vogt, 2014; Andrews et al., 2015; Andrews et al., 2016; Deschamps et al., 2018; Desiage et al., 2018; Caron et al., 2020). For the quantification of the major mineralogical components, the XRD scans obtained were converted into mineral weight percent (wt.%) using the standardless option of the Excel macro-program Rockjock v11 (Eberl, 2003; Eberl & Smith, 2009). This program uses a full-pattern fitting method that permits the quantification of whole-sediment mineralogy with a precision of ±3 wt.% (Eberl, 2003). To verify the quality of this fitting procedure, a degree-of-fit (DOF = minimum absolute difference) statistic was calculated between the measured and simulated XRD patterns. The DOF values obtained with our samples were satisfying as they were close to 0.100 (Eberl & Smith, 2009). They were within a range of 0.096 to 0.130 with an average of 0.116. The calculated total mineral wt.% was normalized to a sum of 100%. Note that the polytypes of illites, smectite, plagioclase feldspar, and K-feldspar are reported as a total amount (e.g., Andrews & Vogt, 2014; Desiage et al., 2018). We present the wt.% data for 7 minerals (Table S2), but we focus on quartz, K-feldspar, plagioclase, and clays (kaolinite, smectite, illites, chlorite+biotite) and the clays/(plagioclase+K-feldspar) ratio to document changes in

sediment provenance and transport in the SLE (e.g., Jaegle, 2015; Casse et al., 2017). The clays/(plagioclase+K-feldspar) ratio allows discriminating the sediments from the Appalachian domain (Palaeozoic sedimentary rocks) from those from the Canadian Shield (Grenvillian metamorphic rocks) and thus, document changes in sediment transport in the SLE (Casse et al., 2017).

1.5 RESULTS

1.5.1 Vertical particle size distribution

1.5.1.1 Spring 2010

Fig. 6 shows the vertical distribution of N(D) against 32 particle size classes for the three representative stations along the estuary in spring 2010. The particle number concentration varied from 90.45 to 5.33×10^{11} m^{-3} (Fig. 6). The Saguenay River (Stn. S-2) followed by the Upper Estuary (Stn. S-12) had the highest concentration of fine particles compared to the Lower Estuary (Stn. S-IML4). There was no important vertical variation in the number concentration for particles sizes up to 80 μm at the three stations while higher numbers of large particles where only observed in the surface layer.
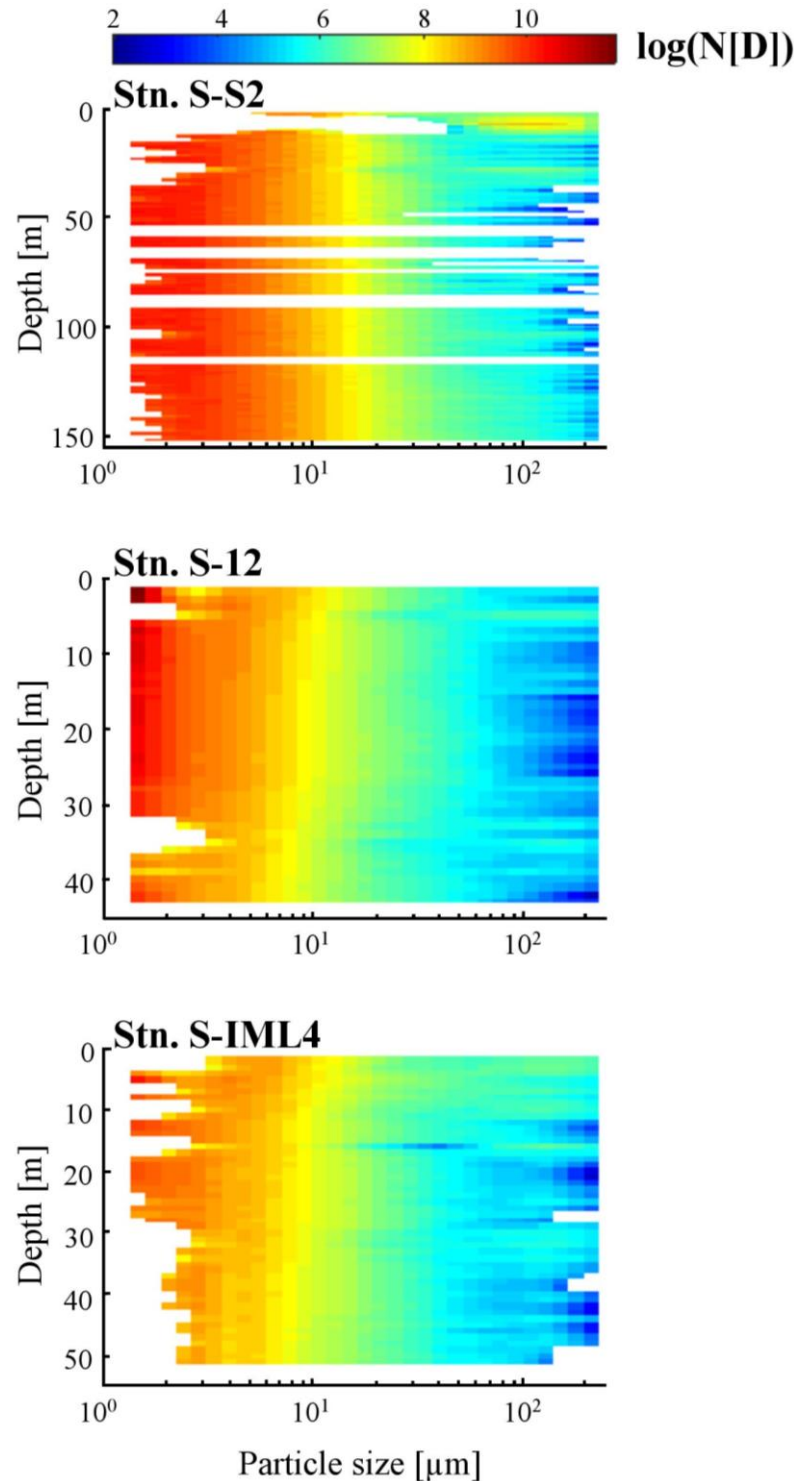
Fig. 6. Vertical distribution of normalized particle number concentration (N[D], m^{-3}) at three representative stations in spring 2010 (top: Stn. S-S2, middle: Stn. S-12, bottom: Stn. S-IML4). Notes: N(D) is log-transformed for better visualization. Blank areas are where no data were returned by the LISST

Fig. 7 shows spring vertical profiles of V(D) against particle size classes, the PSD slope, D_V^{50}, the particulate beam attenuation coefficient (c_p), temperature, salinity and Chl-*a*. The size classes of V'(D) are : small (<4 μm), medium (4-63 μm) and large (>63 μm) particles. For the inorganic portion of the suspended matter these classes are representative of clay, silt and sand, while organic particles occupy a wide range of sizes (USGS, 2006). Particles in the medium and large size classes can also be microflocs (36-133 μm) formed from single grains or macroflocs (> 133 μm) composed of small particles and microflocs (Eisma, 1986).

The Saguenay River (Fig. 7A-E) had larger particles around 10 m corresponding to an important pycnocline and a higher extracted Chl-*a* concentration (>0.6 μg L^{-1}) near the surface. The rest of the vertical structure was near constant with a higher mean PSD slope than at the surface. The average D_V^{50} of the water column down to 152 m was 85 μm with a lower median between 36 and 70 m.

In the Upper Estuary (Fig. 7F-J), there was a dominance of smaller particles (D_V^{50} < 100 μm) at 10 m that corresponds to the pycnocline and between 15 and 25 m. There is a peak of large particles at 5 m that reflects through increases in V'(D)$_{LARGE}$, c_p(670) and D_V^{50}. The PSD slope did not show much variation indicating a nearly constant size distribution throughout the sampled water column. The average D_V^{50} of the water column down to 43 m was 101 μm. The Chl-*a* had relatively low concentrations with no distinguishable vertical structure.

The Lower Estuary (Fig. 7K-O) was more oligotrophic with an important vertical temperature and salinity gradient as well as an important surface extracted Chl-*a* concentration (up to 6 μg L^{-1}). Note that there was a discrepancy between the two Chl-*a* measurement methods. The extracted values were considered more precise than the fluorometer ones. The average D_V^{50} of the water column down to 51 m was 98 μm. A change in the vertical structure of the PSD slope happens around 20 m. The higher values below 20 m denote the presence of relatively fewer large particles.

In general, $c_p(670)$ closely followed the shape of V'(D)$_{LARGE}$ since these particles increased the total volume concentration and particle concentration has the highest impact on attenuation (Qiu et al., 2016). V'(D)$_{SMALL}$ and V'(D)$_{MEDIUM}$ still had an influence in increasing the attenuation, but their variation was more constant with depth and did not translate with peaks in c_p values. Both D_V^{50} and the PSD slope are highly correlated to $c_p(670)$ and V'(D)$_{LARGE}$. There was no correlation between $c_p(670)$ and Chl-*a* at any station which indicates that it does not affect attenuation at that wavelength.
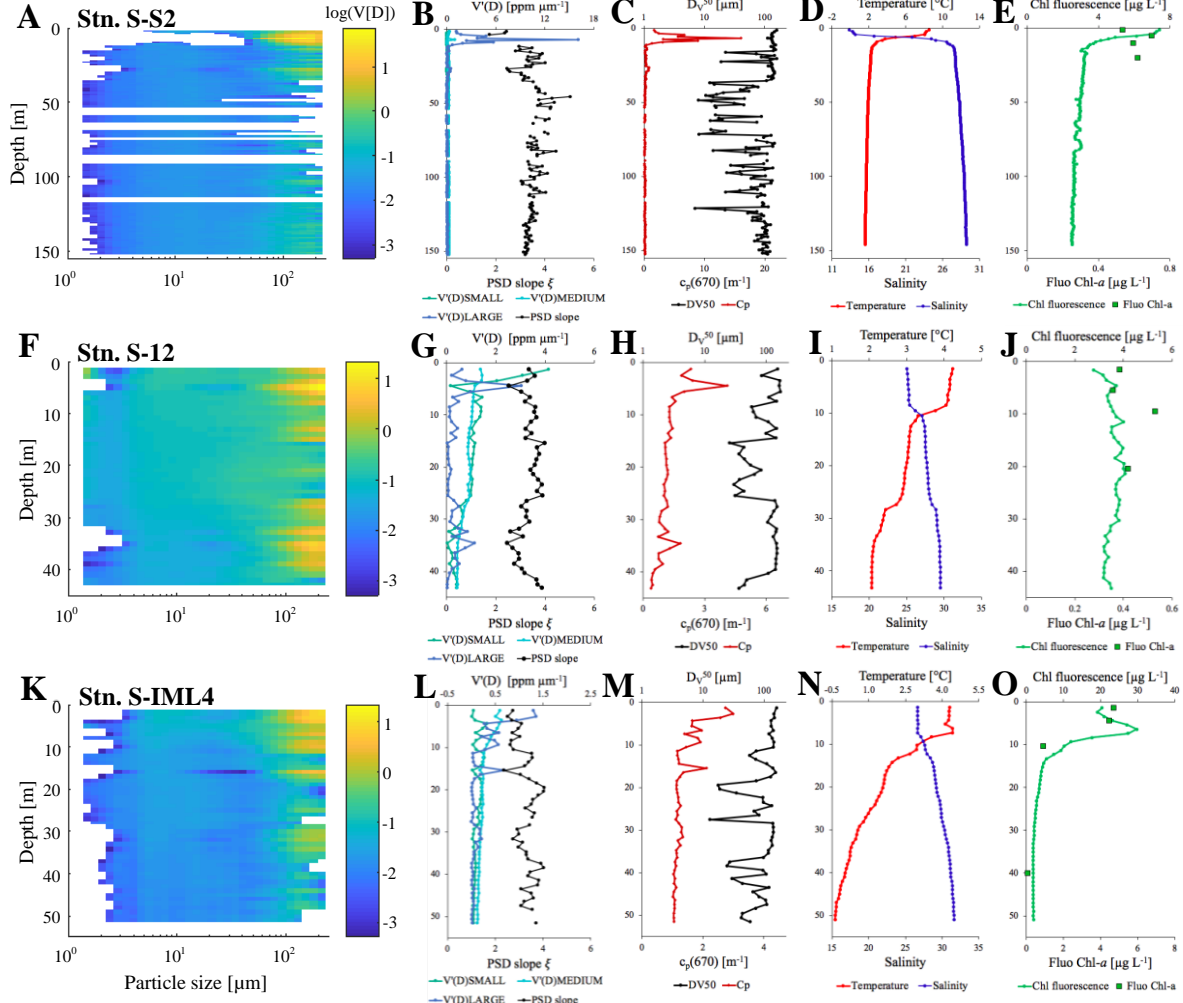
Fig. 7. Spring vertical distribution of (A, F, K) normalized volume concentration (V[D], ppm), (B, G, L) volume concentration density at small size class (<4 µm) medium size class (4-63 µm) and large size class (>63 µm) and PSD slopes, (C, H, M) $c_p(670)$ and D_V^{50}, (D, I, N) temperature and salinity, (E, J, O) Wetstar measured chlorophyll fluorescence (Chl fluorescence) and discrete Chl-*a* samples measured by fluorescence method (Fluo Chl-*a*) at three representative stations (top: Stn. S-S2, middle: Stn. S-12, bottom: Stn. S-IML4). Notes: V(D) is log-transformed for better visualization. Blank areas are where no data were returned by the LISST. The horizontal scale for the biogeochemical parameters isn't the same for each station

1.5.1.2   Winter 2019

Fig. 8 presents the vertical N(D) distribution of the three winter representative stations. Contrary to spring 2010, the water column was sampled from top to bottom but

only at specific depths due to the presence of ice, not allowing resolving the SPM's fine vertical structure. There is not much vertical structure observed at Stn. W-1 (Québec City) for small- and medium-sized particles while relatively more large particles are observed at 10 and 45 m. Station W-5 (Upper Estuary) had a higher concentration of 30-70 µm particles in the surface layer (0-25 m). Station W-9 (Lower Estuary) showed a similar vertical pattern with more 40-80 µm particles down to 50 m. These peaks in medium to large size particles disappeared at deeper depths.
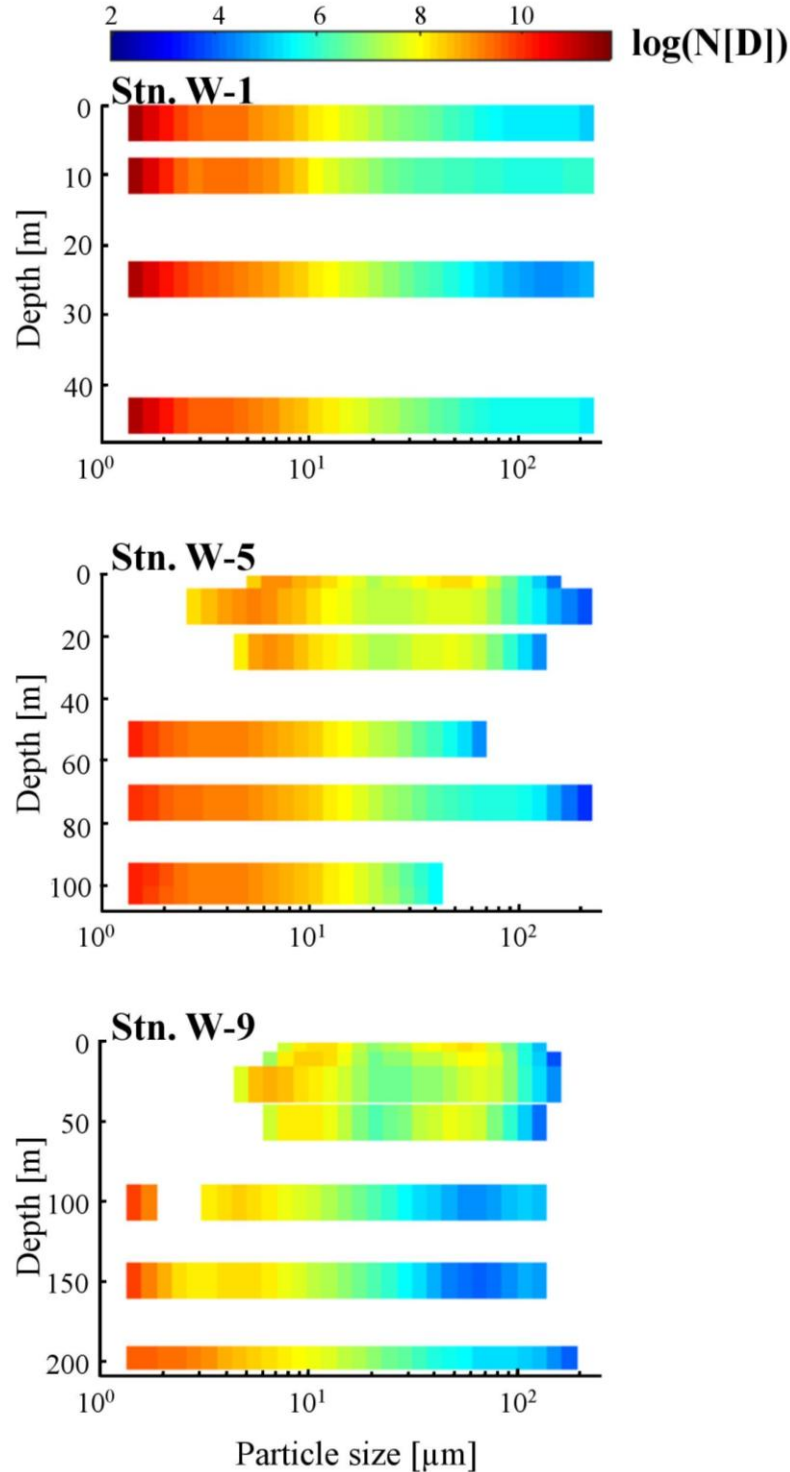
Fig. 8. Vertical distribution of normalized particle number concentration (N[D], m⁻³) at three representative stations for winter (top: Stn. W-1, middle: Stn. W-5, bottom: Stn. W-9). Notes: N(D) is log-transformed for better visualization. Blank areas are where no data were returned by the LISST

Fig. 9 shows V(D) against particle size classes and various vertical profiles of biogeochemical data of selected winter stations. At Quebec City (Fig. 9A-E), there was a presence of large particles at 10 and 45 m, that does not correspond to any other biophysical parameter (Chl-*a* or stratification). The average D_V^{50} over the entire water column was 102 µm.

In the Upper Estuary (Fig. 9F-J), there was a strong stratification with a pycnocline at around 20 m. Despite very low concentrations, the vertical structure of Chl-*a* appears to be linked to the water column stratification. There was a higher number of 30-70 µm size particles down to 25 m (Fig. 9F) as also indicated by V'(D)$_{MEDIUM}$ (Fig. 9G). Under 50 m there were only small particles in low concentration (Fig. 9F). The average D_V^{50} down to 43 m was 43 µm while it was of 28 µm over the entire water column reflecting the decrease of medium size particles concentration with depth. C_p was well correlated to V'(D)$_{MEDIUM}$. Values for all parameters remained almost constant under 50 m.

In the Lower Estuary (Fig. 9K-O), the V(D) distribution at station W-9 (Fig. 9K) was similar to the one in the Upper Estuary. The water column was well mixed down to 25 m as a result of winter convection. There was a slightly stronger Chl-*a* fluorescence vertical gradient (Fig. 9O) than in the Upper Estuary, but concentrations remained overall very small. Medium to large size classes (40-80 µm) dominated down to 50 m (Fig. 9K). The large size class (Fig. 9L) was slightly more important than in the Upper Estuary and coincided with higher Chl-*a* concentrations down to 25 m. From 100 to 200 m, low particle concentrations were observed. The average D_V^{50} of the water column down to 51 m was 56 µm.
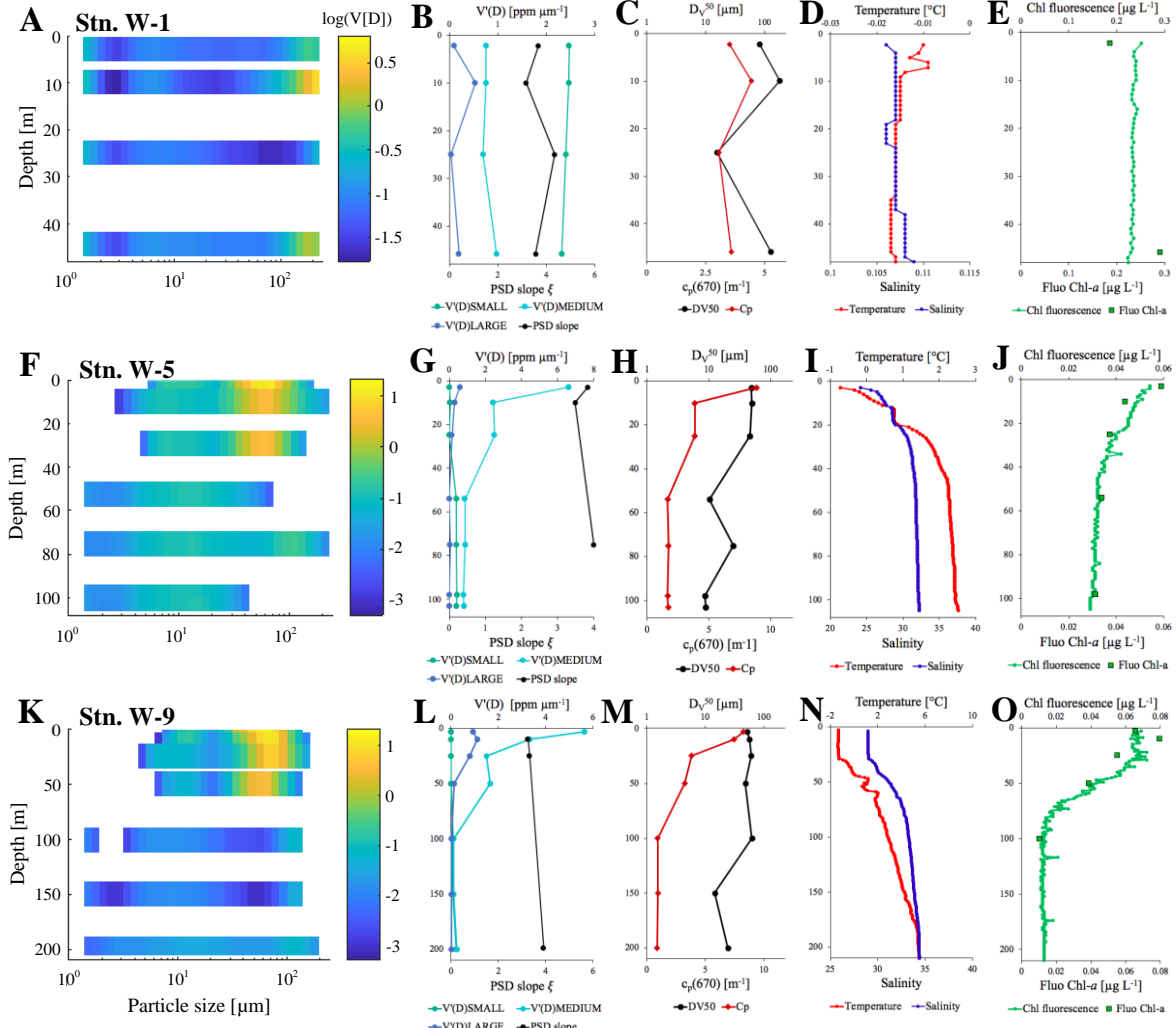
Fig. 9. Winter vertical distribution of (A, F, K) normalized volume concentration (V[D], ppm), (B, G, L) volume concentration density at small size class (<4 µm) medium size class (4-63 µm) and large size class (>63 µm) and PSD slopes, (C, H, M) $c_p(670)$ and D_V^{50}, (D, I, N) temperature and salinity, (E, J, O) Wetstar measured chlorophyll fluorescence (Chl fluorescence) and discrete Chl-*a* samples measured by fluorescence method (Fluo Chl-*a*) at three representative stations (top: Stn. W-1, middle: Stn. W-5, bottom: Stn. W-9). Notes: V(D) is log-transformed for better visualization. Blank areas are where no data were returned by the LISST. The horizontal scale for the biogeochemical parameters isn't the same for each station

1.5.2   PSD spatial variability

Figs. 10 and 11 show the spatial distribution for the particle number density N'(D) of the three size classes, D_V^{50}, the PSD slope, SPM concentrations, PIM% and Chl-*a* concentrations calculated using data from the first 10 m of the water column.

1.5.2.1   Spring 2010

In spring, there was no strong spatial variation at the surface for the small size class N'(D) at the exception of Stn. S-IML4 and in the Saguenay River where lower number density was observed (Fig. 10A). The medium size class N'(D) was almost constant everywhere except again for lower values in the Saguenay River (Fig. 10B) and slightly higher values in the Upper Estuary. The largest size class N'(D) shows strong spatial variability with higher values in the Upper Estuary, the Saguenay River and at Stn. 21 at the head of the Lower Estuary (Fig. 10C). Globally, larger particles were more present along the South Shore of the Lower Estuary than the North Shore (Fig. 10D) and agrees with the low slope values (Fig. 10E). D_V^{50} varied between 80-137 µm in the Upper Estuary, 72-146 µm in the Lower Estuary and was ~140 µm in the Saguenay River (Table S3). The SPM concentration was low everywhere (1-3 mg L^{-1}) except in the Upper Estuary where the influence of the maximum turbidity zone can be seen (Fig. 10F). The particulate inorganic matter proportion varied between 78 to 84% in the Upper Estuary, 51 to 56% in the Saguenay River and 33 to 78% in the Lower Estuary (Fig. 10G). Accordingly, Chl-*a* concentrations were low (<0.5 µg L^{-1}) in the Upper Estuary and higher (up to 6 µg L^{-1}) in the Lower Estuary (Fig. 10H). A correlation analysis showed that there was no relationship between the PSD slopes and any of the biogeochemical parameters (Chl-*a*, PIM, POM) in spring as R^2 ranged between 0 and 0.26 (Fig. S3).
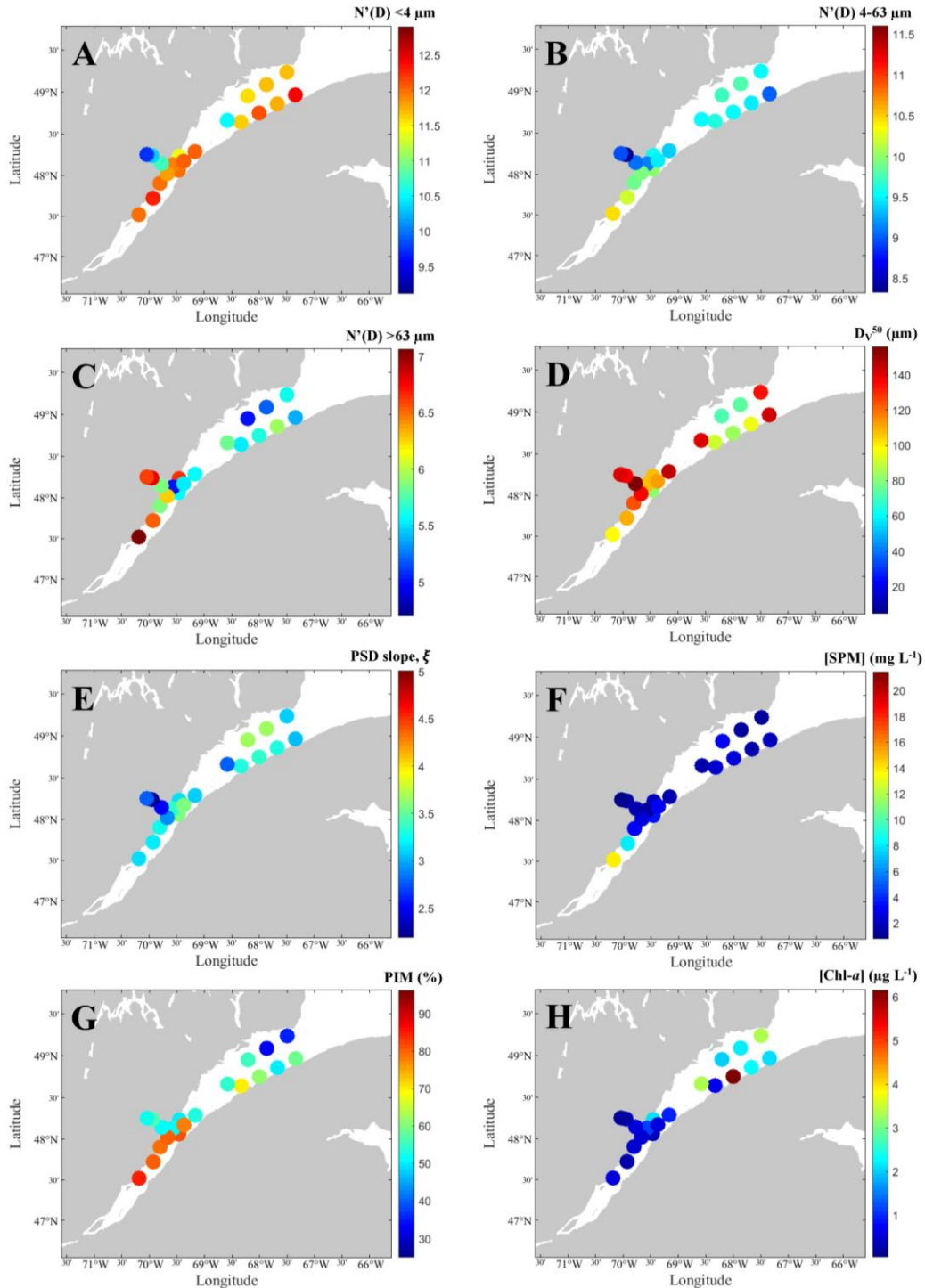
Fig. 10. Map of spring spatial distribution of total particle number density for (A) small size class (<4 μm), (B) medium size class (4-63 μm) and (C) large size class (>63 μm) (unit: $m^{-3}\mu m^{-1}$) and spatial distribution of (D) D_V^{50}, (E) PSD slope, (F) SPM concentration, (G) percentage of PIM and (H) Chl-*a* concentration for the surface layer (1-10 m). The values of N'(D) are the 10-based logarithm exponent

1.5.2.2   Winter 2019

In winter, there were decreasing number density of small and medium size classes from the Upper Estuary to the Lower Estuary (Fig. 11A-B) while larger size class particles tended to be more important in the Lower Estuary (Fig. 11C). In the maximum turbidity zone of the Upper Estuary (Stns. W-2 and W-3), small and medium size classes dominate with the highest N'(D) measured. This reflects in the lowest D_V^{50} and highest PSD slope values at these stations (Fig. 11D-E). Small single grain particles (<4 μm) were absent at stations W-9 and W-12 (Lower Estuary) and present in low concentration at Stn. W-5 (Upper Estuary). Overall, the D_V^{50} values were low, ranging between 11 and 50 μm in the Upper Estuary and 47 to 63 μm in the Lower Estuary (Fig. 11D). SPM concentration decreased downstream of the maximum turbidity zone. At the representative stations of the Upper and Lower Estuary, they were of 9 mg L-1 at Stn. W-5 and 2 mg L-1 at Stn. W-9 (Fig. 11F). Particulate inorganic matter accounted for 71 to 77% of the SPM present in the Lower Estuary and 79 to 87% in the Upper Estuary (Fig. 11G). As can be expected, there were extremely low Chl-*a* concentrations (<0.3 μg L-1) measured in winter with the exception of the maximum turbidity zone where values were between 0.4 and 0.8 μg L-1 (Fig. 11H). As in the spring, the PSD slope had no relationships with any of the biogeochemical parameters (Chl-*a*, PIM, POM) for the Upper Estuary region. The highest correlation was with Chl-*a* (R^2=0.57, N=11), but was not significant (p<0.01). The relationship with PIM/TSM (R^2=0.66, N=6) and between Chl-*a* and POM (R^2= 0.72, N=7) had slightly higher correlation values, but the sample number was too low to draw a conclusion. In the Lower Estuary, the small number of samples available did not allow testing the relationships (Fig. S4).
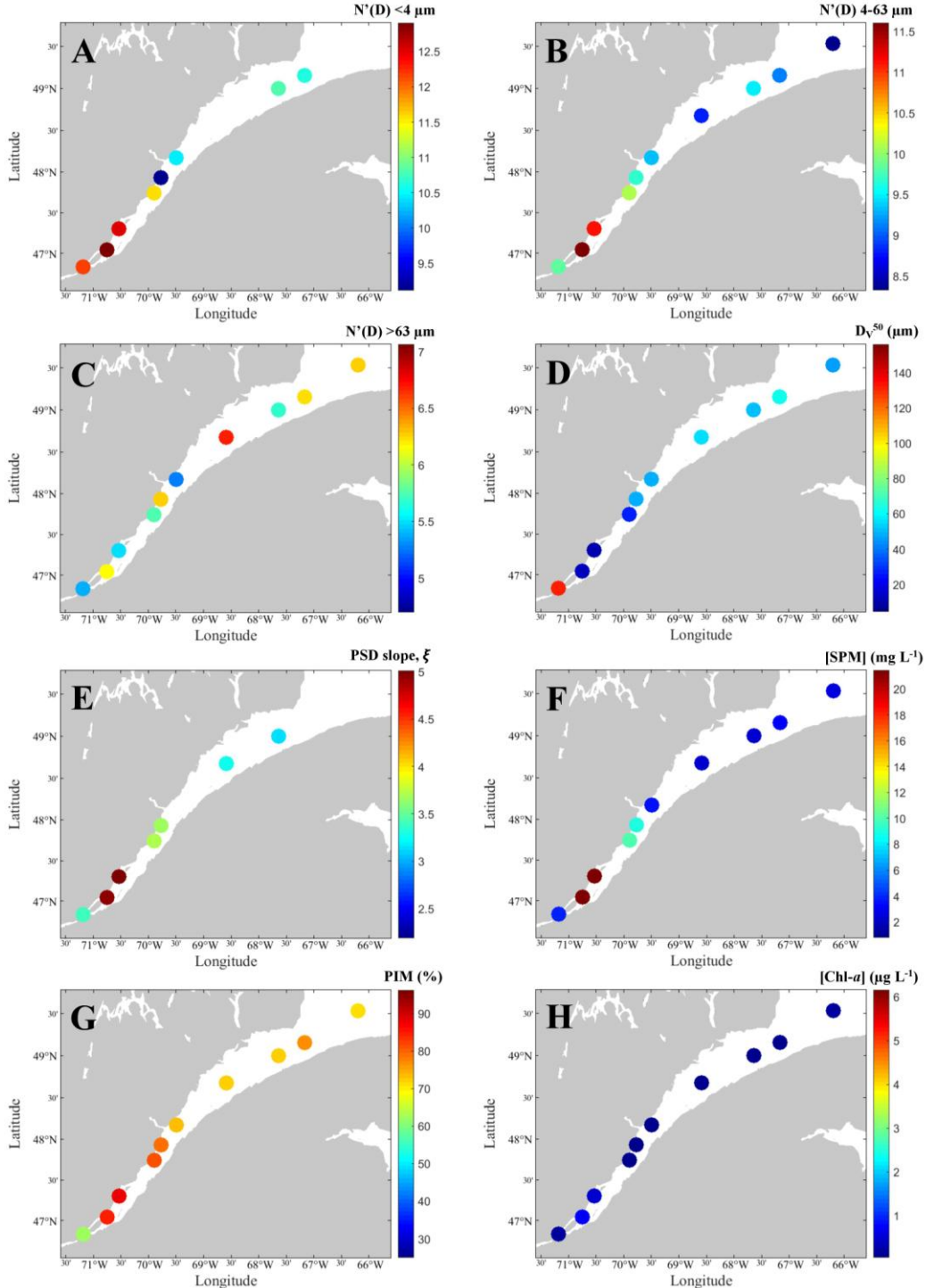
Fig. 11. Map of winter spatial distribution of total particle number density for (A) small size class (<4 μm), (B) medium size class (4-63 μm), and (C) large size class (>63 μm) (unit: m^{-3} μm^{-1}) and spatial distribution of (D) D$_V^{50}$, (E) PSD slope, (F) SPM concentration, (G) percentage of PIM and (H) Chl-*a* concentration for the surface layer (1-10 m). The values of N'(D) are the 10-based logarithm exponent

1.5.3   Winter composition of surface SPM

The log(SiO_2/Al_2O_3) versus log(Fe_2O_3/K_2O) classification diagram (Herron, 1988) illustrates that the SLE's SPM are geochemically classified as shale and wacke similarly to summer values and to bedload sediment samples from the Canadian Shield and the Appalachian domain (Fig. 12A). The SPM samples normalized to upper continental crust (UCC) values (McLennan, 2001) diagram shows a similar elemental geochemical composition between winter and summer values (Fig. 12B). It suggests an enrichment in K_2O and in Fe_2O_3 for the Upper Estuary and the depletion of Na_2O for the Upper Estuary in winter compared to summer data. There were lower concentrations of Fe_2O_3 in the Lower Estuary than in the Upper Estuary which agrees with the summer results. Contrary to summer, Na_2O concentrations were higher in the Lower Estuary.
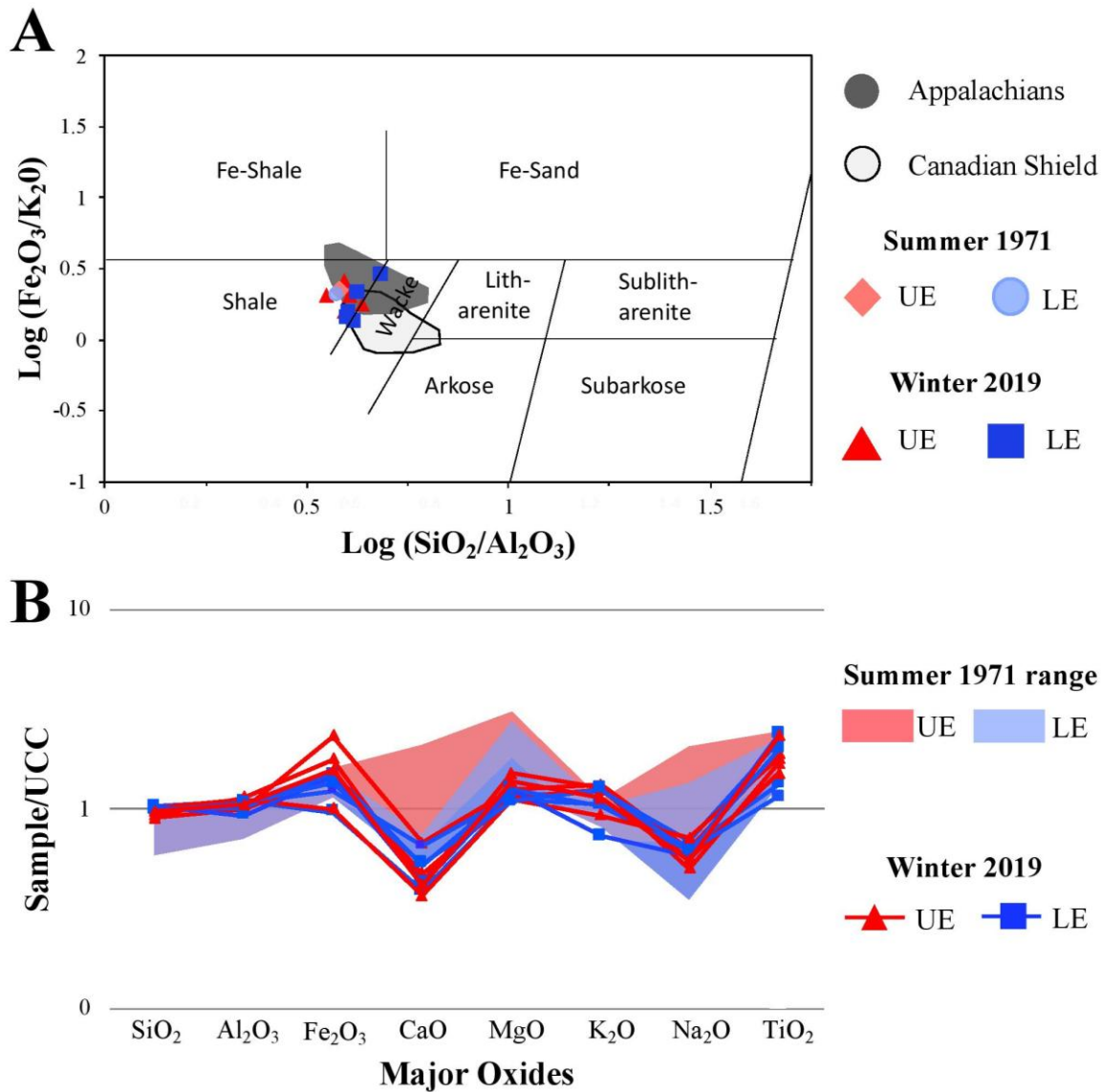
Fig. 12. A) Herron (1988) geochemical classification diagram and B) UCC-normalized spider diagrams for major oxides from surface SPM in the Upper Estuary (UE) and Lower Estuary (LE) compared to values from summer 1971 (D'Anglejan & Smith, 1973) and bedload samples from the Canadian Shield and the Appalachian domain (Casse, 2018).

Fig. 13 shows the most abundant crystalline minerals in the SPM at 10 m. Total feldspars represented by K-feldspar (11-15 %) and plagioclase (13-26 %) was the most

important, followed by high percentages of clays (15-35 %) and quartz (2-14 %). Amorphous silica (mainly biogenic silica) was also detected in the qXRD analysis of all SPM samples (8-44 %; Table S2).
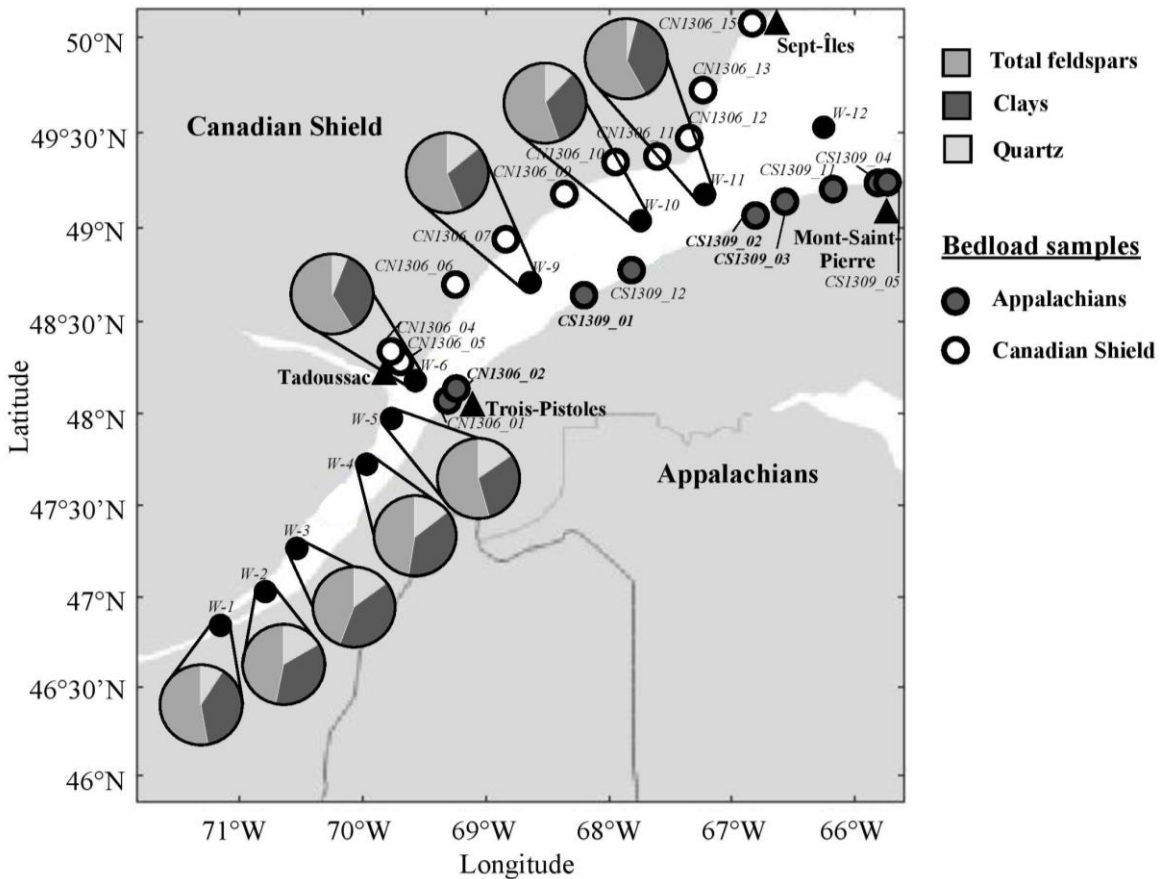
Fig. 13. Pie chart distribution of crystalline minerals (total feldspars [K-feldspar+plagioclase], clays and quartz) in the SPM at 10 m depth of the St. Lawrence Estuary in winter and localisation of bedload samples

Fig. 14 shows a comparison of the chemical ratios Si/Ca and Al/Ca for the SPM samples at 10 m and bedload sediment sources samples collected in the SLE (Jaegle, 2015; Casse, 2018). SPM samples show low Si/Ca (<30) and Al/Ca (<8) ratios as do bedload sediment derived from the Canadian Shield. Low ratios are also present for four samples (CN1306_02, CS1309_01, CS1309_02 and CS1309_03) collected at riverbanks on the South Shore while samples closer to

the mouth of the estuary on the Appalachian side had higher ratios. The qXRD analysis showed relatively similar mineralogical composition between all the stations along the estuary with the clays/total feldspars ratio varying between 0.53 and 0.92, and maximum values (0.78-0.92) observed in the maximum turbidity zone.
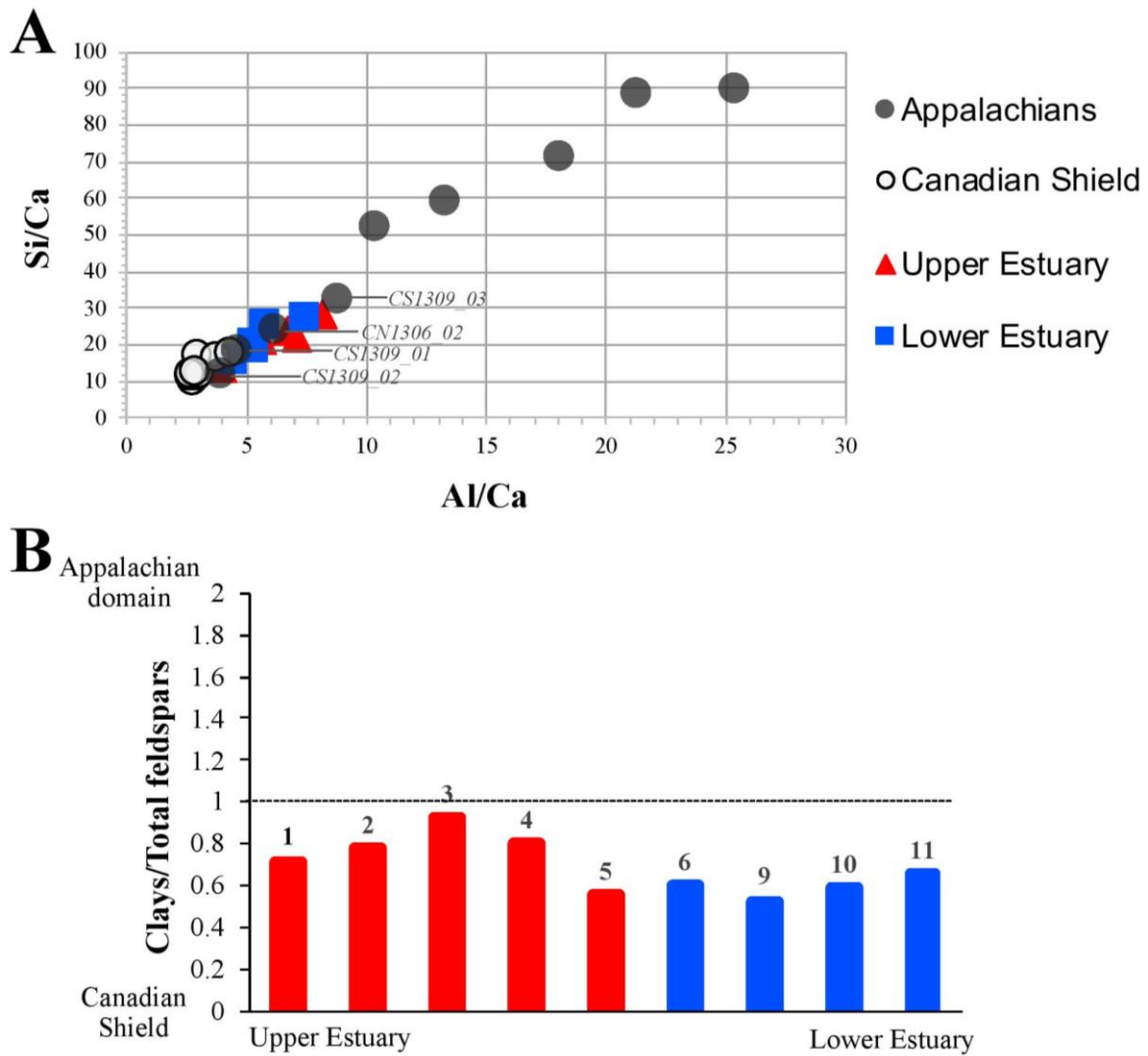
Fig. 14. Distribution of surface SPM samples and sediment samples from the Canadian Shield and the Appalachian domain in A) Si/Ca vs Al/Ca and B) Clays/Total feldspars diagrams. Note: The variability of Appalachians samples in A) is due to the heterogeneity of the sedimentary rocks present (Jaegle, 2015; Casse et al., 2017; Casse et al., 2019)

1.6   DISCUSSION

1.6.1   Upper Estuary

Stn. W-1 provides information about the winter PSD and input in the estuary from the St. Lawrence River. The homogeneity of the water column reflects the vertical mixing present (Fig. 9A-E). There are relatively more large particles and organic matter (Fig. 11D,E,G) than what is found downstream probably due to the presence of benthic diatoms from adjacent marsh sediments (Gearing et al., 1994) as indicated by a high proportion of amorphous silica (mainly biogenic) in its mineralogical composition (Table S2).

In the maximum turbidity zone, the SPM concentration increases. The increase is present for the inorganic fraction and for all size classes, but it is most important for medium size particles, lowering the median size (Fig. 11). As salinity and SPM concentrations rise in this zone, so does flocculation which increases the settling velocity of larger particles (Jago et al., 2006; Ralston & Geyer, 2017; Tao et al., 2018). The deposition may be temporarily as the water column is well mixed (Fig. S1) due to the presence of strong tidal currents that help retain the particles in this zone (Gobeil, 2006). The high concentrations are also caused by the erosion of sediments from tidal flats at Cap Tourmente on the North Shore and various zones on the South Shore such as Montmagny (Fig. 3). It is thought that the foraging of food by the Great Snow Geese in the fall destabilizes the summer mud deposits and increases the release of particles (Lucotte & D'Anglejan, 1986; Drapeau, 1990). The sediment export continues in winter from shore erosion by the ice (Lucotte & D'Anglejan, 1986; St. Lawrence Center, 1996).

The Canadian Shield acts as a primary source of detrital SPM as indicated by the higher proportion of total feldspars (Fig. 13). The importance of the clay-size class is relatively more important in the Upper Estuary (Fig. 11A). This is also seen in the mineralogy content with an increase in total clays relative to the other stations (Fig. 14B),

likely suggesting a noticeable secondary contribution from the Appalachian domain. We hypothesize that the recurrent incorporation of fine-grained intertidal sediments from the Kamouraska region (Fig. 3) into the landfast ice during winter (Neumeier & Cheng, 2015), and the subsequent offshore transport, contributes to increasing the sedimentary contribution from the Appalachians in the maximum turbidity zone. Alternatively, the higher proportion of clays than downstream stations may also indicate a tertiary source from upstream. The St. Lawrence Lowlands is mostly composed of clay deposited on the Champlain Sea which the St. Lawrence River can erode and transport (Elson, 2010; Gouvernement du Québec, 2012). The clay fraction in winter 2019 in the Upper Estuary was dominated by illites and chlorite (Table S2) similarly to summer 1971 results (D'Anglejan & Smith, 1973).

Downstream of the maximum turbidity zone, the average spring PSD slope near the surface (Fig. 10E) was similar to results obtained in summer 2013 (Mohammadpour et al., 2017). Nearly no change in the PSD slope was present between 1-10 m (Fig. 10E) and 25-50 m (Fig. S5E) showing that there was a similar mixture of particles between the two layers for all stations in the Upper Estuary in spring and reflecting the presence of vertical mixing (Neu, 1970). While resuspension is present in the maximum turbidity zone, the SPM in the downstream area of the Upper Estuary is mostly affected by advection over the tidal cycles (D'Anglejan & Ingram, 1976).

Stations S-12 and W-5 were located near each other allowing comparison of the vertical distribution in the Upper Estuary between seasons downstream of the maximum turbidity zone. The N(D) vertical profiles showed the dominance of fine particles (Figs. 6 and 8). These observations are consistent with previous measurements in the Upper Estuary made in the spring of 1971 that showed a higher frequency for particles between 5 and 7 µm (D'Anglejan & Smith, 1973). However, an important number of 30-70 µm size particles were present in the first 25 m in winter compared to summer results. These particles could be aggregates formed in the maximum turbidity zone from compaction of finer particles through tidal movement and/or flocs formed prior to sampling that have a

lower effective density and can remain longer near the surface (Dyer & Manning, 1999; Tao et al., 2018). The low temperatures (Fig. 9I) and the high SPM (Fig. 11F) concentration facilitates the flocculation process in surface waters (Woodward et al., 2002). In spring, the high concentration of particles in the largest size classes (>100 µm) near the surface (Fig. 6B) may be macroflocs that are more porous, have a smaller settling velocity and that can stay a longer time in the surface layer than microflocs (Wang et al., 2013b). Macroflocs may be less present in winter results as they are easily destroyed during sampling (Eisma, 1986).

SPM concentrations and the concentration of small size class particles were higher in the Upper Estuary for both seasons and decreased downstream. Concentrations are typically higher in the well-mixed zone and decrease as a two-layer circulation develops (Silverberg & Sundby, 1978). The SPM concentration was higher in winter than in spring possibly resulting from erosion by the ice (Dolgopolova & Isupova, 2011; Lebeuf et al., 2019) or by the higher monthly mean freshwater flow at Quebec City which was of 12,520 m^3/s in January 2019 preceding the sampling period and of 10,635 m^3/s in May of 2010 (DFO, 2020).

The medium size class in winter was more important in the Upper Estuary than in the Lower Estuary (Fig. 11B). In spring, similar results were obtained but with less of a difference between regions (Fig. 10B) while Chanut & Poulet (1982) found a higher proportion (10-30 µm) in the Lower Estuary around the same period in 1974. The largest size class (>63 µm) was more present in spring in the Upper Estuary than in the Lower Estuary (Fig. 10C). This finding is similar to results from Mohammadpour et al. (2017) in June 2013 where particles >10 µm had a higher contribution to the SPM of the Upper Estuary. The large size class also had a higher number density in the spring than in the winter which increases the median size (Figs. 10 and 11). The maximum turbidity zone is a high source of large particles in spring as is the St. Lawrence River (Troude & Sérodes, 1990). This also supports the concept of a deposition of larger particles including

biologically aggregated terrigenous particles in the Lower Estuary because of greater depths and lower currents (D'Anglejan, 1990; Gagné et al., 2009; Lebeuf et al., 2019).

In the more downstream part of the Upper Estuary, the bottom sediment composition (rocks and gravel) indicates a low deposition area (D'Anglejan & Smith, 1973; Loring & Nota, 1973) with the SPM mostly transported downstream to the Lower Estuary.

1.6.2   Lower Estuary

About 14 to 17% of the SPM entering the Upper Estuary will not be retained in the turbidity zone and will move to the Lower Estuary during the ice-free seasons (Lebeuf et al., 2019). The presence of ice in winter may bring particles downstream that would complete the sediment balance. It is estimated that in winter about 50% of the volume of sediments trapped in the ice cover from tidal flats is still present when leaving the turbidity zone and drifting toward the Lower Estuary (Dionne, 1981; Dionne, 2002). The mineralogical and elemental geochemical composition of the SPM over the whole estuary is similar. The low clays/total feldspars, Si/Ca, and Al/Ca ratios (Fig. 14) that characterize the SPM samples indicate that winter suspended detrital sediments in the SLE are a mix of two sources. The SPM originates from the Canadian Shield province through higher proportions of total felspars and Ca, while the Palaeozoic sedimentary rocks of the Appalachian province act as a secondary source. These results confirm previous mineralogical and geochemical interpretations by Jaegle (2015), Casse (2018) and Casse et al. (2019) using bottom sediments from the Lower Estuary. The SPM present in the middle of the Lower Estuary has a lower clays/total feldspars ratio than in the Upper Estuary as the North Shore rivers (Saguenay, Betsiamites, Outardes and Manicouagan; Fig. 3) add Canadian Shield source sediments. In winter, the ice incorporates SPM from the Canadian Shield (Montero-Serrano et al., 2018) and the north-westerly winds combined with the Coriolis force transport it toward the South Shore (Neu, 1970; Fauchot et al., 2008). The tides may have reworked riverbank sediments on the South Shore and incorporated the

transported Canadian Shield sediments which would explain the lower Si/Ca and Al/Ca ratios present in some bedload samples collected in the Appalachian domain.

The elemental geochemical composition of the detrital SPM (Fig. 12) obtained during the winter season was similar to previous results from summer 1971 (D'Anglejan & Smith, 1973). Their geochemical classification suggests that the detrital sediment fractions in the SPM from the SLE are composed of texturally immature and fine-grained particles with limited amounts of alteration from the bedrock sources.

Only slight variations in major oxides could be observed between seasons and location (Fig. 12B). The mineralogical composition in the lower estuary also showed similar composition than during summer time (D'Anglejan, 1970; D'Anglejan & Smith, 1973), with the dominance of plagioclase, K-feldspar, quartz and clays (Fig. 13; Table S2). Contrary to the PSD, these results suggest that seasonal changes in the SLE have little influence on the compositional variability of the detrital SPM.

In the winter, high amorphous silica contents (mostly biogenic silica) in the mineralogical composition of the Lower Estuary's SPM (Table S2) corresponds well with lower PIM percentages in the Lower Estuary than in the Upper Estuary (Fig. 11G). The presence of more small and large size particles (Fig. 10A and C) near the South Shore than near the North Shore in the first 10 m in spring could be explained by the surface currents (Galbraith et al., 2011).

Seasonal variability of particle sizes was also observed in the Lower Estuary. There was a higher number density of small and medium size classes in spring than in winter near the surface while the large size class was more present in winter. (Figs. 10 and 11). These observations are consistent with the hypothesis that the higher number density of larger particles observed during winter in the Lower Estuary may have come from the release of large detrital particles brought by drifting ice (Fig. S6). Alternatively, it can also have found its input from rivers with hydropower dams such as the three main rivers on the North Shore (Betsiamites, Outardes and Manicouagan). Indeed, a high winter demand in

electricity asks for high release of freshwater from behind the dams that can find its way in the SLE (El-Sabh & Silverberg, 1990). This is confirmed by higher SPM load in these rivers in winter than the other seasons for the 2010-2011 period (Jaegler, 2014). The particles released would have flocculated, diminishing the concentration in small size classes and increasing the values in the large size classes. In spring, the dams trap the sediments that would otherwise have been a major input of other organic and inorganic particles (Drapeau, 1990). Larger particles are also more present in winter than in summer in the 25-50 m layer (Figs. S5 and S7) since the surface layer is deeper in winter (Fig. 7, 9 and S2).

Lower inorganic proportion in spring 2010 than in winter 2019 (Figs. 10G and 11G) primarily results from the higher primary productivity (Therriault & Levasseur, 1985) although the lack of a clear correlation between Chl-*a* and POM indicated that Chl-*a* wasn't the major contributor to POM (Fig. S3). The high concentrations of phytoplankton in the Lower Estuary in spring 2010 (Fig. 10H) were typical of the high primary production of this region that starts in May (Zakardjian et al., 2000) when the environmental conditions (stratification, surface light availability and nutrients) are optimal. The St. Lawrence Estuary's phytoplankton can contribute to the medium and large size class particles, particularly in the Lower Estuary since microplankton (20-200 µm) is dominant (Roy et al., 2008; Devine et al., 2017). Diatoms tend to dominate in May, but from 2004 to 2013 there has been an increase in flagellates and dinoflagellates relative to diatoms which are smaller-sized phytoplankton communities (Dufour et al., 2010; Plourde et al., 2014; Devine et al., 2017). The low Chl-*a* concentrations measured in winter indicate that the larger particles present in the Lower Estuary were not phytoplanktonic in nature (Fig. 11H).

The long-term occupation of two stations in the Lower Estuary near the south shore in July and October 1974 respectively showed that the size spectra of particles throughout the water column have random and frequent variations that are not related to the semidiurnal tides present in the SLE (Chanut & Poulet, 1982). These short-term temporal successions of particle size spectra combined with spatial variability help explain the small

differences observed in the PSD vertical structure between stations in the Lower Estuary for a given season (Fig. S1).

Stations S-IML4 and W-9 were located near each other allowing comparison of the vertical distribution between seasons. The average PSD slope was lower in spring than in winter particularly near the surface (Figs. 7L and 9L). This shows the important impact of phytoplankton on the PSD in the SLE during spring. The average surface slope in spring was similar to results from June 2013 (Mohammadpour et al., 2017). The V'(D) spring vertical structure in the Lower Estuary is complex with a higher concentration of large particles in the top 5 m where a high Chl-*a* concentration was measured. Combined to the bimodal V'(D) distribution (Fig. 4E) for surface depths (1-10 m), this higher Chl-*a* concentration suggests the presence of two phytoplankton populations (Reynolds et al., 2008). Despite very small Chl-*a* concentrations in the winter, there is a vertical structure of V(D) that shows the dominance of larger size particles (approx. 70 μm) over the first 25 m that corresponds to the winter surface layer (Fig. 9K). This vertical size distribution is similar to what was present in the Upper Estuary for the respective seasons, indicating the predominance of seasonal over spatial variations. As in the Upper Estuary, these larger particles may be flocs formed from smaller particles. The higher POM proportion in the Lower Estuary helps flocculation as it is highly cohesive (Kranck, 1979; Droppo et al., 1998). This would agree with the fine silt composition of recent sediments in the Laurentian Chanel (Pinet et al., 2011).

1.6.3 Saguenay River

The average surface PSD slope (Fig. 10E) in the Saguenay River was significantly lower (2.49±0.30, N=3 vs 3.42±0.17, N=5; two sample t-test, p<0.02) than summer 2013 measurements (Mohammadpour et al., 2017) indicative of a higher proportion of larger particles. This is, however, the result of our measurements being averaged over the top 10 m of the water column that included a strong peak of larger particles at the pycnocline

(Figs. 6A and 7A-B) where particles tend to accumulate due to a density discontinuity (Fig. 7D) that hinders vertical transport. This discontinuity can cause accumulation and flocculation of terrestrial detritus and phytoplankton debris at the base of the mixed layer (Mann & Lazier, 2006). The higher values of large particles could also be an artefact (Schlieren) often present at the pycnocline and that is induced by different refractive indexes of the two water masses (Mikkelsen et al., 2008). It causes light scattering that generates an increase in beam attenuation and a higher proportion of particles >100 μm (Fig. 7A,C). The average PIM% and Chl-*a* concentrations in the first 10 m were low (Fig. 10G-H). The higher proportion of organic matter may originate from dissolved humic substances that flocculated as it entered the brackish waters in the downstream portion of the Saguenay River (Wollast, 1988; Tremblay & Gagné, 2009). The highest vertical difference of the PSD slope throughout the SLE in spring was observed in the Saguenay River between the first 25 m and the rest of the water column, indicating relatively more large particles in the surface layer than deeper (Fig. 7B). These larger particles have the potential to reach the head of the Lower Estuary due to surface currents (Galbraith et al., 2018). These results are contrary to the observations of higher concentration of particles around 5 μm in the surface layer (1-10 m) and 10 μm in the bottom layer (30-250 m) in spring 1974 (Chanut & Poulet, 1979). This could be caused by missing data for larger size classes in the bottom layer in 2010. In the intermediate layer (25-50 m; Fig. S5), the median size was similar to values at the head of the Lower Estuary indicative of the influence of tidally upwelled and dense estuarine waters on the Saguenay River (Belzile et al., 2016).

1.6.4   Limitations and Uncertainties of the LISST

Other than the Schlieren effect, large particle sinking in benchtop mode, non-spherical particles and particles smaller than the measurable range, the LISST presents other possible artefacts and uncertainties. Since the small rising tail at Stns. S-S2 and S-IML4 were only for the surface depths (Fig. 4A and E) it is possible that this was also caused by stray light contamination that is more important at high scattering angles. This

could be avoided by shading the optical path (Reynolds et al., 2010). The inversion algorithm used in this study assumes a refractive index that can be different from the particles', particularly for small size classes (Andrews et al., 2010). Large flocculated particles composed of a complex assemblage of smaller particles also have variable refractive indexes that would increase the calculated concentration of the smallest measured sizes (Davies et al., 2012). The manipulation of samples for lab measurement in 2019 may have disturbed the aggregates and flocculates and changed their *in situ* states (Traykovski et al., 1999).

For certain size bins and at certain depths, the LISST is missing data. This results in D_V^{50} being an imperfect variable as it takes into account that there are no particles that fit into these size classes. Since no imaging system was used in combination with the LISST, no distinction can be made between medium to large size particles and flocs. Also, the LISST-Type B was limited to particles smaller than 250 µm, which is not representative of the entire size spectra of particles present in the SLE. The use of a digital floc camera could solve both issues. This instrument can see the shape of particles and can measure up to 40 mm (Mikkelsen et al., 2006; Law et al., 2014).

1.7   CONCLUSIONS

Suspended particulate matter dynamics is complex in the St. Lawrence Estuary and cannot be completely understood with the instrument used and spatially and temporally limited data. Combining the unique winter dataset with previous spring measurements, results, however, showed that seasonal variability (winter 2019 vs spring 2010) was more important than spatial variability for the PSD. Winter data showed a high volume of particles between 30 and 80 µm in the upper portion of the water column of the Upper and Lower Estuary that was absent in summer. Results also showed that the presence of large (>63 µm) and mostly inorganic (71 to 77 %), particles in the Lower Estuary in winter support the hypothesis of sediment transport by ice. Lower numbers of large particles in the Lower Estuary than in the Upper Estuary in spring support the idea of vertical mixing in the

56

Upper Estuary as seen in the constant vertical distribution while larger particles can deposit in the Lower Estuary. Geochemical and mineralogical analysis of winter detrital suspended matter composition confirmed that their origin is mainly from the Canadian Shield with a minor contribution from the Appalachians (clays/total feldspars ratio between 0.53 and 0.92). A composition similar to past summer results indicates the lack of seasonal influences.

Despite important results, this study was only a first characterization of particle sizes in winter in the St. Lawrence Estuary. Further study on the spatial and vertical particle size distribution and characterization, especially in winter, is needed to provide a better seasonal understanding of the complex spatial and temporal dynamics of the St. Lawrence Estuary.

CONCLUSION GÉNÉRALE

L'objectif de cette étude était de caractériser la taille et la composition de la matière particulaire en suspension dans l'ESL au printemps et à l'hiver. Les résultats sur la distribution des tailles des particules obtenues avec un LISST-100X étaient généralement similaires aux études précédentes (D'Anglejan & Smith, 1973; Mohammadpour et al., 2017). Les variations observées étaient principalement dues aux différences dans les techniques d'échantillonnage, soit par l'instrument utilisé ou les profondeurs échantillonnées. La Figure 15 est une schématisation des résultats décrits ci-dessous.

Dans l'estuaire moyen, la distribution verticale était relativement homogène au printemps et dans la zone de turbidité maximale en hiver due au mélange vertical présent dans cette zone. Les particules grossières (>63 µm) étaient plus présentes au printemps qu'à l'hiver. Par ailleurs, les concentrations de particules grossières à l'été et de tailles moyennes (4-63 µm) à l'hiver étaient plus élevées dans l'estuaire moyen que l'estuaire maritime et correspondaient principalement à de la matière inorganique. Cela est probablement causé par la sédimentation des particules plus grossières dans l'estuaire maritime alors que dans l'estuaire moyen elles sont activement remises en suspension par le mélange vertical.

Dans l'estuaire maritime, les particules fines (<4 µm) et de tailles moyennes étaient plus nombreuses à la surface au printemps qu'en hiver. Les particules plus grossières étaient pour leur part plus nombreuses à l'hiver. Elles étaient majoritairement inorganiques et pouvaient provenir du transport par les glaces ou d'un plus grand apport par les rivières utilisées pour produire l'hydroélectricité due à une plus grande demande énergétique. Elles peuvent également être représentatives de la floculation de particules plus fines. Les concentrations en matière organique sont plus élevées au printemps principalement à cause de l'importante production primaire présente. Ceci est reflété dans la concentration plus élevée de particules grossières à la surface que dans les eaux de la couche intermédiaire.

À la surface de la rivière Saguenay, la pente de PSD était plus faible que dans l'estuaire due à une grande proportion de particules grossières. La proportion de matière organique y était élevée, mais ne correspondait pas aux concentrations de Chl-*a*. Elle provient probablement de substances humiques ayant floculé.

Des variations spatiales majeures étaient donc présentes dans l'ESL. Toutefois, lorsque la distribution verticale pour l'estuaire moyen et l'estuaire maritime est comparée entre les saisons, la variation temporelle était plus importante (Figure 15). Ces résultats répondent à l'objectif spécifique 1.

La composition géochimique élémentaire et minéralogique de la MPS en hiver était similaire à celle présente en été (D'Anglejan, 1970; D'Anglejan & Smith, 1973) avec dominance des feldspaths (feldspath potassique et plagioclases) puis des argiles et du quartz. Cela témoigne d'une faible influence des saisons sur la composition de la matière détritique. Différents rapports entre les éléments chimiques et minéraux indiquent un apport principal depuis le Bouclier canadien et secondaire par la province des Appalaches dû à l'incorporation et le transport de sédiments par la glace en hiver. Ceci répond à l'objectif spécifique 2.

Ce mémoire a permis de caractériser la taille et la composition des particules en suspension pour la première fois en hiver dans l'ESL. De plus, l'analyse de la taille des particules en suspension dans la colonne d'eau en été n'avait pas été faite depuis les années 1980 (D'Anglejan & Smith, 1973; Chanut & Poulet, 1982; Poulet et al., 1986a; Poulet et al., 1986b). Il est important de se rappeler que les conclusions tirées sont propres au moment de l'échantillonnage et permettent d'avoir un aperçu de la dynamique des particules à ces moments précis. L'utilisation de l'appareil LISST-100X directement dans la colonne d'eau aura permis une plus grande résolution verticale comparée aux années précédentes.

Il serait intéressant d'obtenir une meilleure résolution verticale à l'hiver afin de mieux observer les changements avec la profondeur. Il serait donc préférable en hiver

d'utiliser le LISST-100X en mode continue dans la colonne d'eau. Cela permettrait aussi d'éviter la sédimentation des agrégats dans les bouteilles Niskin et leur fragmentation lors de leur sortie par le fausset. Des données plus en profondeur à l'été seraient aussi intéressantes afin d'avoir une meilleure compréhension de l'entièreté de la colonne d'eau, en plus d'obtenir des données plus récentes afin d'éliminer le facteur interannuel. Un LISST-100X de Type C pourrait être utilisé afin d'obtenir des résultats sur une plus grande gamme de tailles en couvrant jusqu'à 500 µm. La cytométrie en flux pourrait être utilisée pour déterminer les différentes populations de phytoplancton présentes et les classes de taille qu'elles occupent. L'utilisation d'une caméra numérique de silhouette du floc (*digital floc camera*) permettrait à la fois de mesurer les particules jusqu'à 40 mm et de détecter quels types de particules sont présents.

L'obtention de données lors de périodes sans nuages, en continu et sur une plus grande couverture spatiale aideraient à l'amélioration des algorithmes de télédétection permettant l'utilisation de la rétrodiffusion ou de l'absorption perçue par les capteurs satellitaires afin d'obtenir les valeurs de PSD. Cela sera nécessaire afin qu'ils soient adaptés à la complexité optique présente dans l'ESL et puissent ainsi effectuer un meilleur suivi temporel et spatial de la distribution des particules.

Finalement, des mesures de composition des sédiments des basses-terres du Saint-Laurent aideraient à mieux caractériser leurs influences sur la matière en suspension dans l'ESL. Ces améliorations permettront d'effectuer un meilleur suivi de la dynamique des particules en milieu naturel et estuarien.
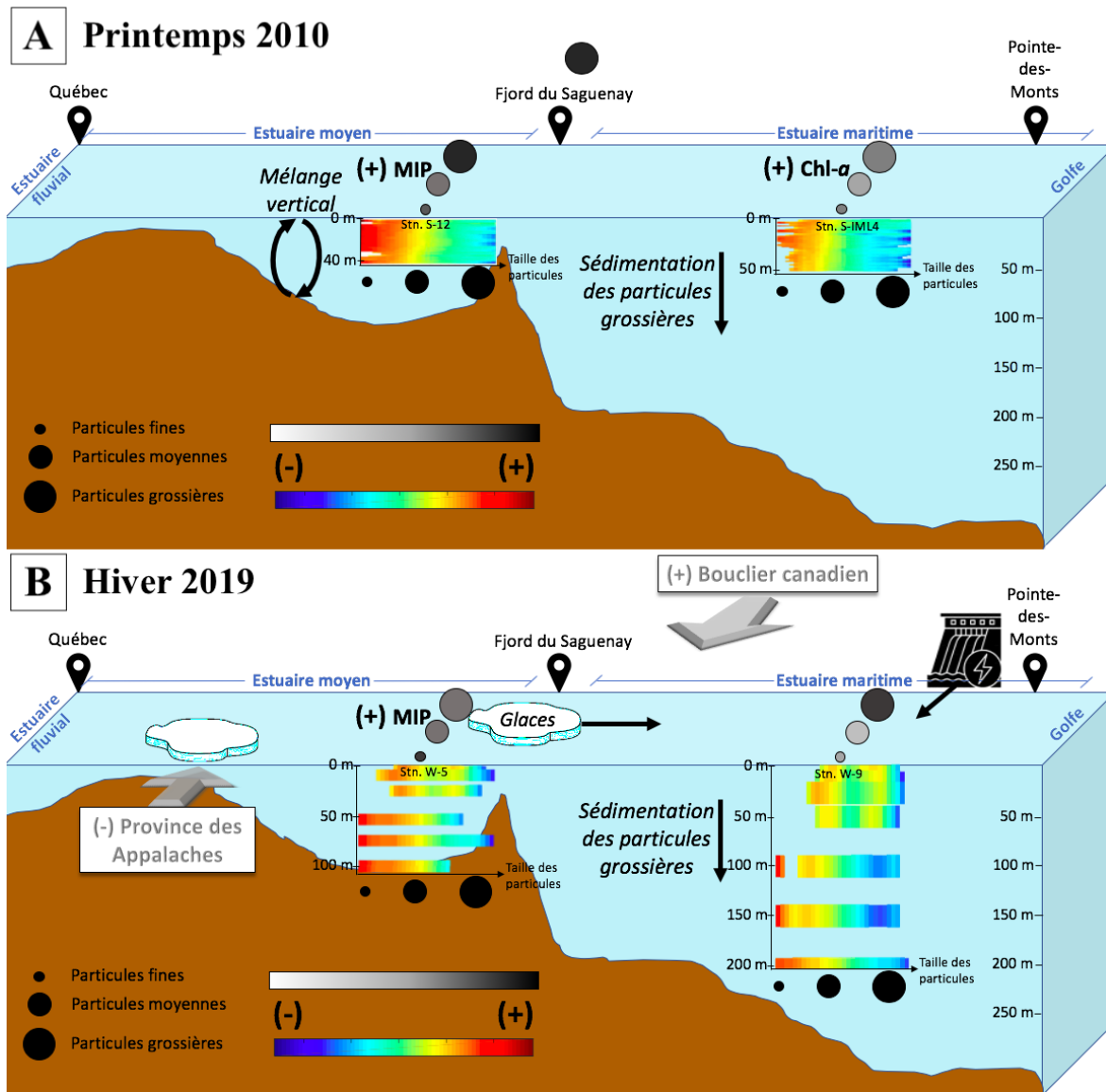
Figure 15. Résumé de la PSD et de la provenance de la MPS A) au printemps 2010 et B) à l'hiver 2019

ANNEXE I

SUPPLEMENTARY MATERIAL
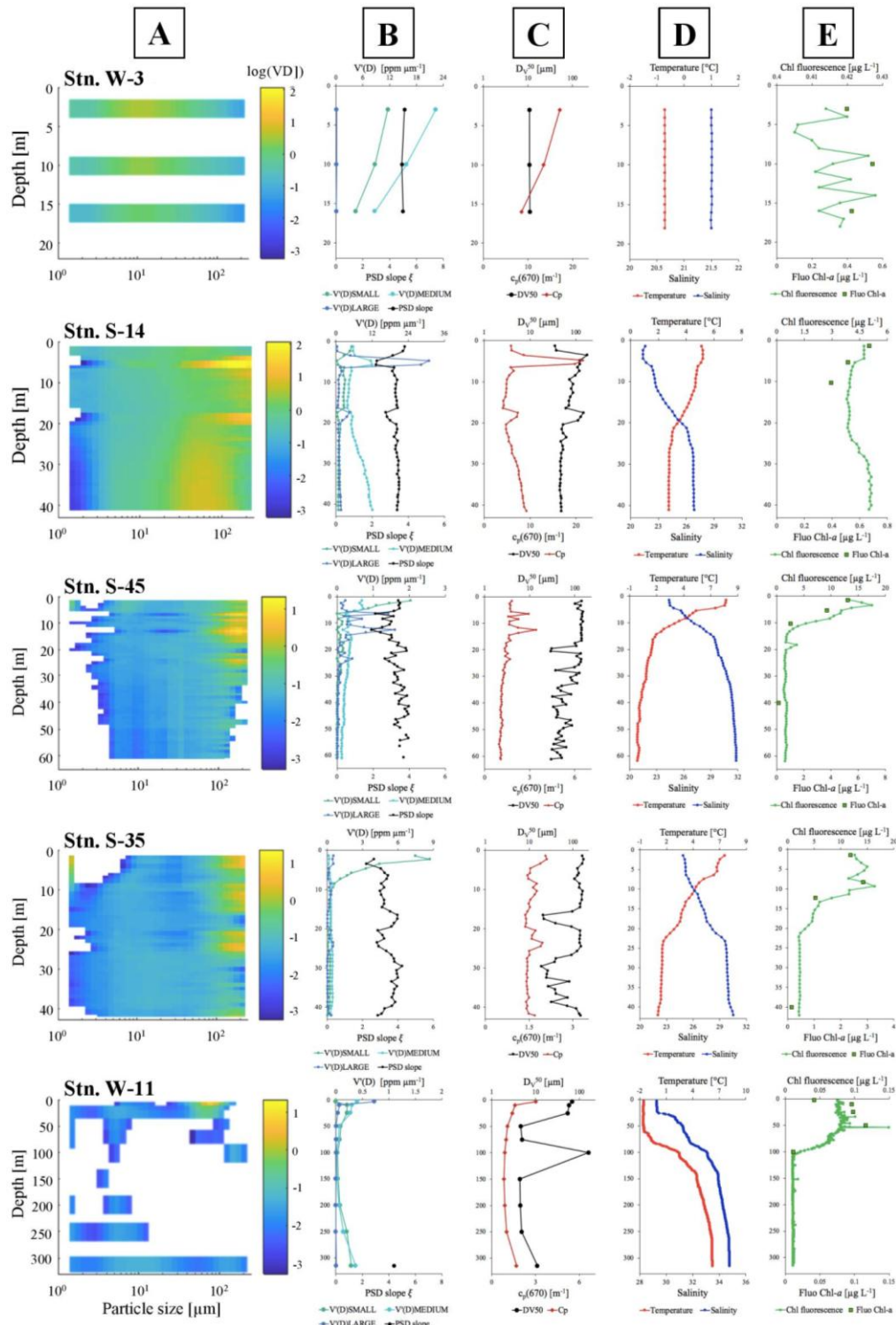
Fig. S1. Vertical distribution profiles of (a) particle volume concentration (V[D], ppm), (b) volume concentration density at small size class (<4 µm) medium size class (4-63 µm)

and large size class (>63 µm), (c) $c_p(670)$ and D_V^{50}, (d) temperature and salinity, (e) Wetstar measured chlorophyll fluorescence (Chl fluorescence) and discrete Chl-*a* samples measured by fluorescence method (fluo Chl-*a*) at supplementary stations with key localisations (from top to bottom: Stn. W-3, Stn. S-14, Stn. S-45, Stn. S-35, Stn. W-11). Notes: V(D) is log-transformed for better visualization. Blank areas are where no data were returned by the LISST. The horizontal scale for the biogeochemical parameters isn't the same for each station
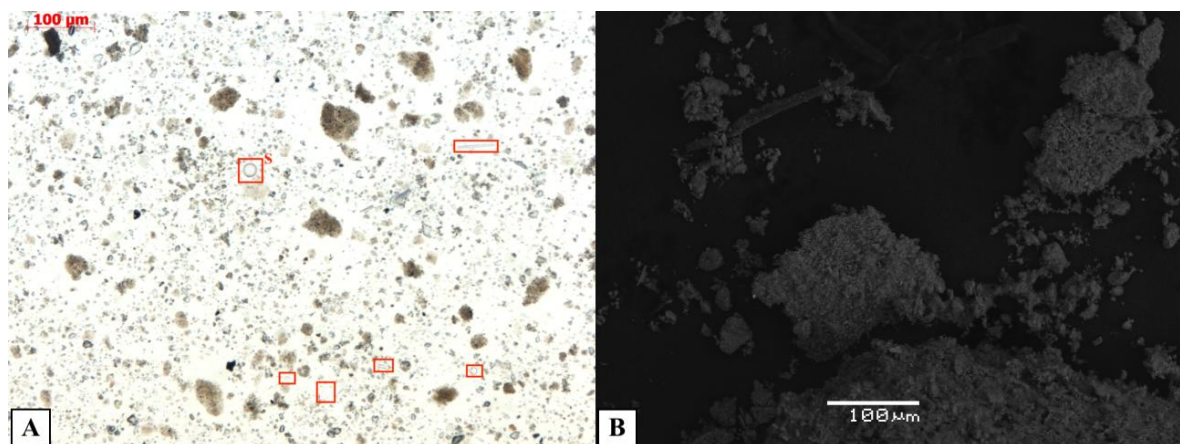
Fig. S2. Two pictures of the composition of matter obtained from 0.8 µm filters at 10 m at Stn. W-9 in winter 2019 taken with : (A) a LSM 700 laser scanning confocal microscope, agglomerations of inorganic matter of different sizes reaching about 80 µm are visible as well as the presence of various diatoms (red squares). A Stephanodiscus sp. ("S") is present in the center of the image and measures approximately 20 µm, and (B) a JEOL 6460LV scanning electron microscope after treatment and homogenization. The action of the mortar broke apart some of the larger particles that had clumped together. Detrital matter dominates the sample.

64
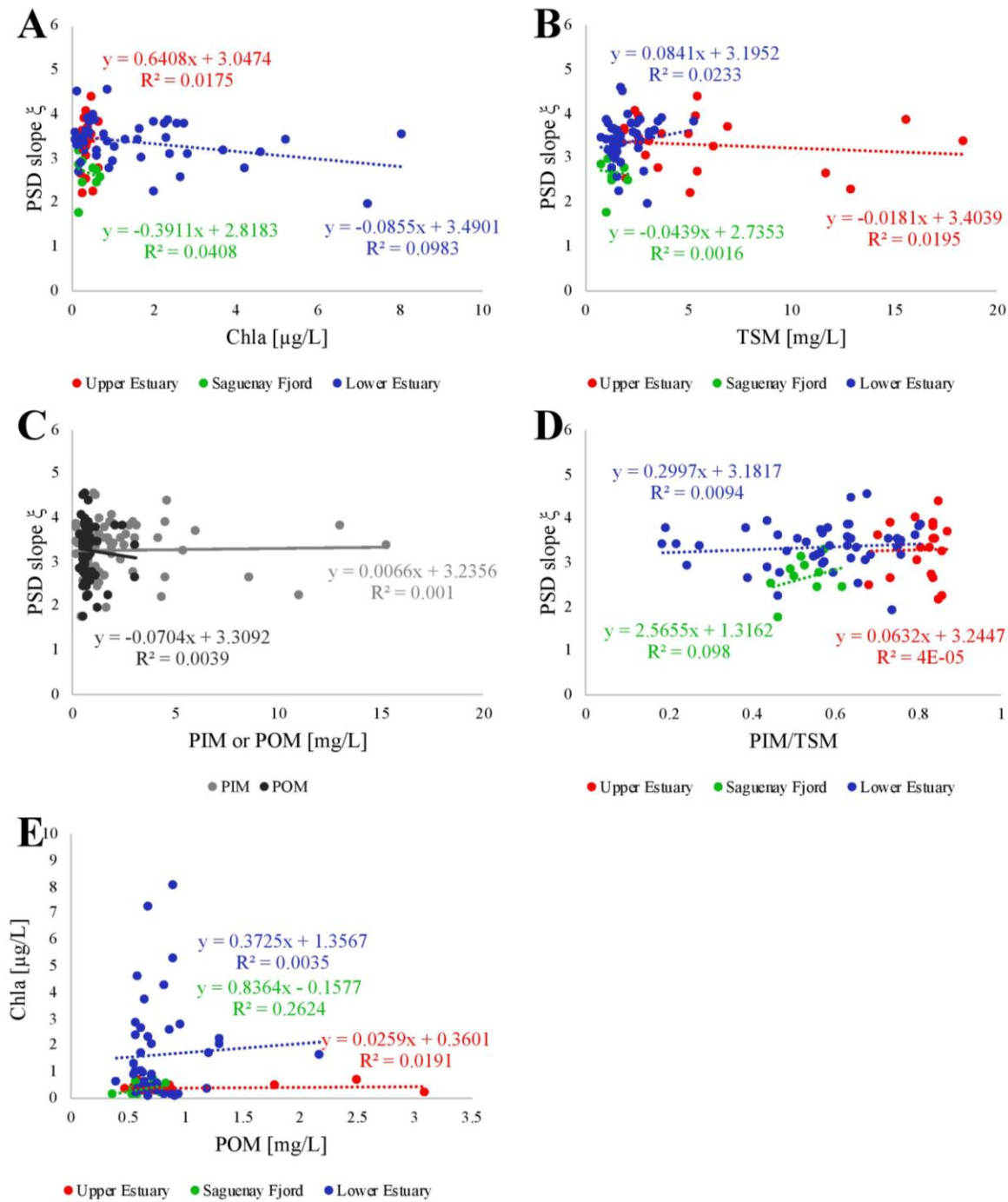
Fig. S3. Scatterplots and regression lines for spring 2010 data of (A) PSD slope versus Chl-*a* (B) PSD slope versus TSM (PIM+POM), (C) PSD slope versus PIM or POM, (D) PSD slope versus PIM/TSM ratio, (E) Chl-*a* versus POM
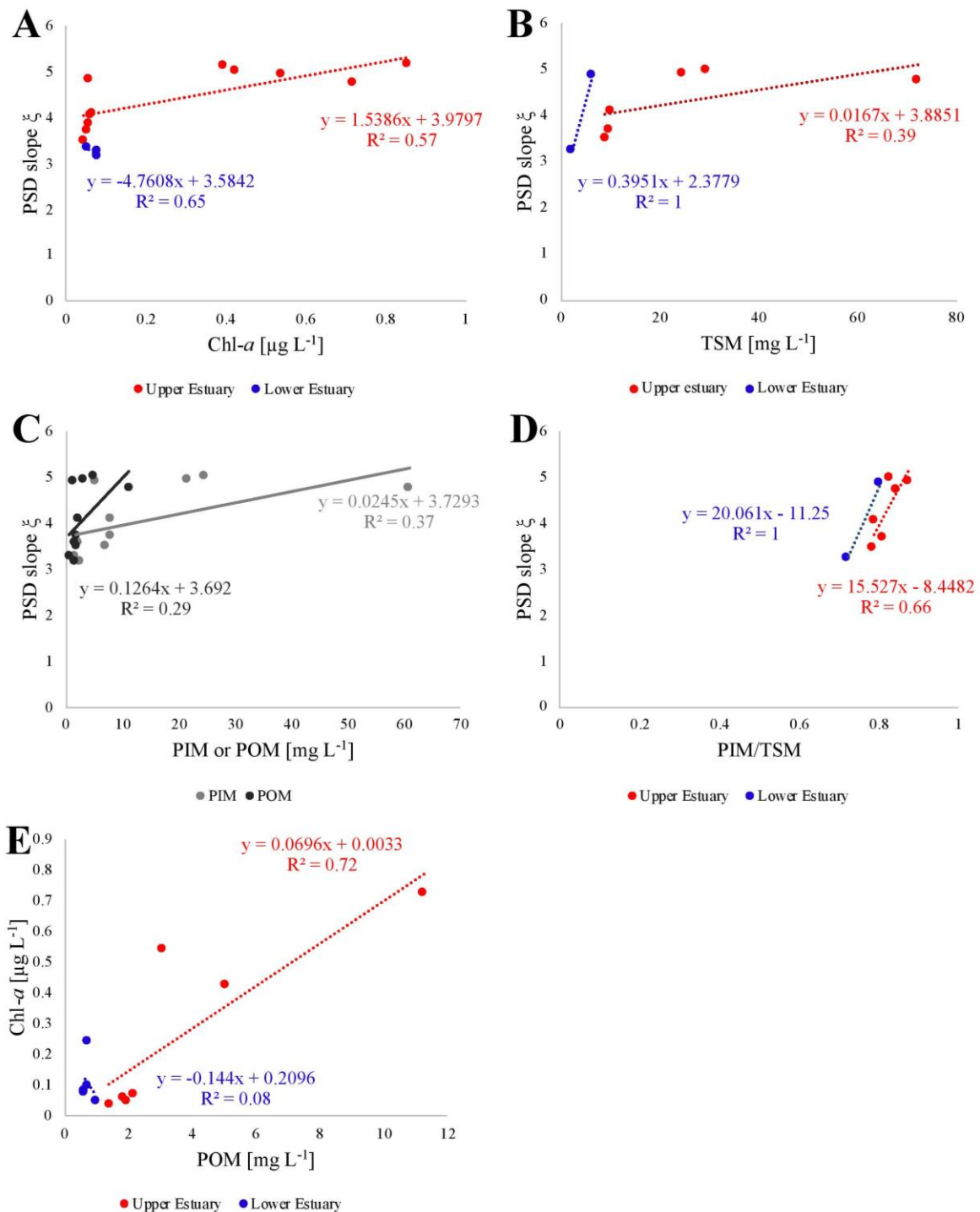
Fig. S4. Scatterplots and regression lines for winter 2019 data of (A) PSD slope versus Chl-*a* (B) PSD slope versus TSM (PIM+POM), (C) PSD slope versus PIM or POM, (D) PSD slope versus PIM/TSM ratio, (E) Chl-*a* versus POM
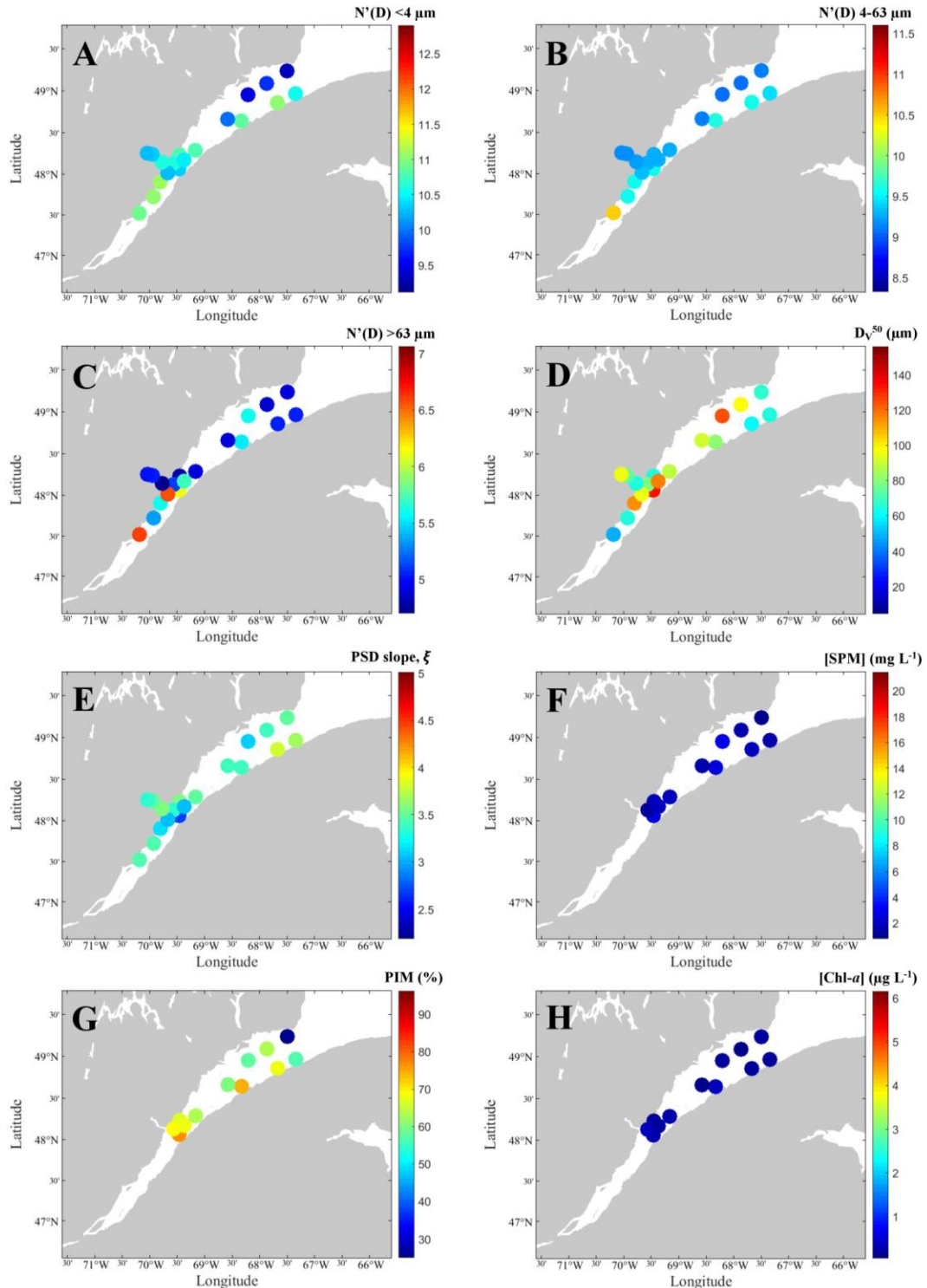
Fig. S5. Map of spring 2010 spatial distribution of total particle number density for (A) small size class (<4 μm), (B) medium size class (4-63 μm), and (C) large size class

(>63 μm) (unit: $m^{-3}\,μm^{-1}$) and spatial distribution of (D) D_V^{50}, (E) PSD slope, (F) SPM concentration, (G) percentage of PIM and (H) Chl-*a* concentration for the water column (25-50 m). The values of N'(D) are the 10-based logarithm exponent
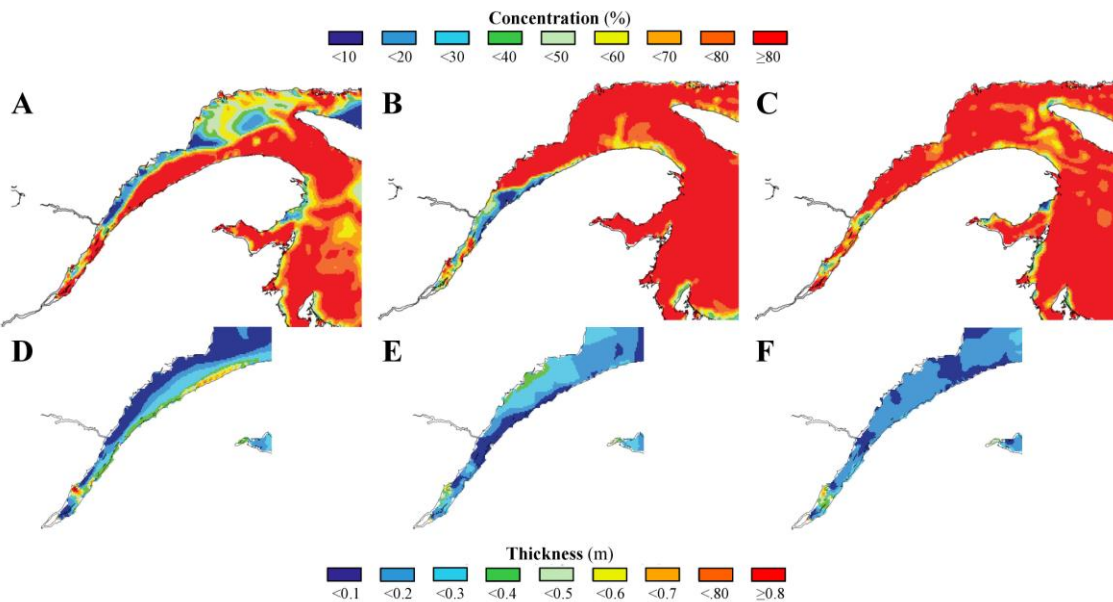
Fig. S6. The evolution of ice concentration (A, B, C) and thickness (D, E, F) through time in winter 2019 for (A, D) February 1st (B, E) February 8th (C, F) February 15th. Source : Observatoire global du Saint-Lauren-OGSL, https://ogsl.ca/ocean, (2020)
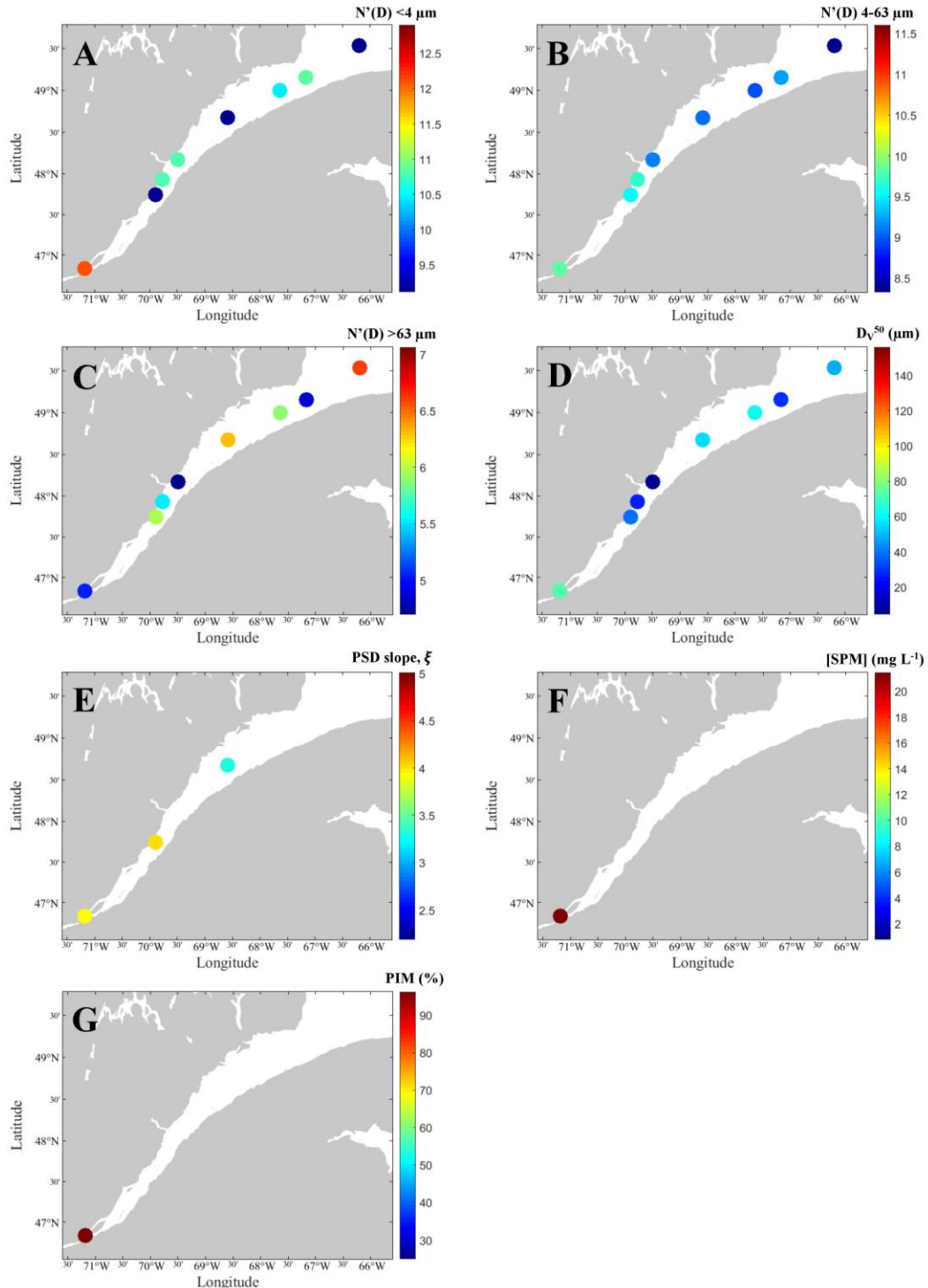
Fig. S7. Map of winter 2019 spatial distribution of total particle number density for (A) small size class (<4 μm), (B) medium size class (4-63 μm), and (C) large size class

(>63 µm) (unit: $m^{-3}\,µm^{-1}$) and spatial distribution of (D) D_V^{50}, (E) PSD slope, (F) SPM concentration, and (G) percentage of PIM for the water column (25-50 m). The values of N'(D) are the 10-based logarithm exponent

Table S1. Concentration of major elements for all SPM and bedload samples analyzed in this study

Station	Area	Latitude	Longitude	%Na$_2$O	%MgO	%Al$_2$O$_3$	%SiO$_2$	%K$_2$O	%CaO	%TiO$_2$	%Fe$_2$O$_3$
W-1	Upper Estuary	46.8312	-71.1828	2.46	2.76	15.14	59.49	4.44	2.83	1.30	11.56
W-2	Upper Estuary	47.0433	-70.7537	2.17	3.01	15.85	63.98	3.83	1.75	1.58	7.84
W-3	Upper Estuary	47.3057	-70.5308	1.96	3.32	17.34	61.28	4.30	1.82	1.16	8.84
W-4	Upper Estuary	47.7428	-69.8959	2.21	2.53	15.05	65.54	4.19	1.99	1.03	7.46
W-5	Upper Estuary	47.9301	-69.7715	2.80	2.48	17.01	66.83	3.11	1.55	1.23	4.99
W-6	Lower Estuary	48.1699	-69.4897	2.50	2.46	16.46	67.66	3.54	1.63	0.91	4.82
W-9	Lower Estuary	48.6769	-68.5923	2.37	2.41	16.22	64.47	4.23	2.24	1.36	6.71
W-10	Lower Estuary	49.0003	-67.6365	2.68	2.57	16.25	63.96	4.17	2.73	1.49	6.16
W-11	Lower Estuary	49.1560	-67.1671	2.42	2.73	15.54	65.39	3.45	2.17	0.79	7.50
W-12	Lower Estuary	49.5295	-66.1956	2.29	2.78	14.08	67.69	2.46	1.78	1.61	7.31
	Upper Estuary mean			2.32	2.82	16.08	63.42	3.98	1.99	1.26	8.14
	Lower Estuary mean			2.45	2.59	15.71	65.84	3.57	2.11	1.23	6.50
CN1306_04	North Shore	48.2413	-69.5980		0.77	16.49	69.91	3.30	4.08	0.84	4.62
CN1306_05	North Shore	48.2291	-69.5537		0.11	12.15	78.36	2.77	3.00	0.52	3.08
CN1306_06	North Shore	48.6435	-69.0987		1.18	17.02	67.83	3.06	4.45	0.96	5.49
CN1306_07	North Shore	48.9442	-68.7111		0.71	16.96	69.69	3.10	4.15	0.72	4.66
CN1306_09	North Shore	49.1580	-68.1869		0.96	15.27	70.92	2.54	4.19	0.75	5.37
CN1306_10	North Shore	49.2918	-67.8949		0.10	16.54	73.07	2.84	4.01	0.48	2.96
CN1306_11	North Shore	49.3208	-67.6371		0.25	14.95	74.70	2.33	4.10	0.52	3.16
CN1306_12	North Shore	49.4183	-67.3060		0.11	15.45	74.90	2.70	3.03	0.65	3.17
CN1306_13	North Shore	49.7584	-67.1771		0.10	16.42	75.54	3.36	2.79	0.25	1.54
CN1306_15	North Shore	50.1475	-66.5847		0.47	15.16	72.71	2.83	3.83	0.66	4.33
CN1306_01	South Shore	48.0948	-69.2149		1.29	13.31	76.60	2.39	0.95	0.57	4.88
CN1306_02	South Shore	48.1318	-69.1847		1.24	16.03	71.66	3.04	1.91	0.87	5.23
CS1309_01	South Shore	48.6254	-68.1297		2.07	15.69	70.64	2.89	2.52	0.67	5.52
CS1309_02	South Shore	49.0983	-66.6769		2.37	17.97	64.37	2.08	3.41	0.97	8.83
CS1309_03	South Shore	49.1224	-66.5004		3.06	16.54	68.44	2.93	1.39	0.82	6.83
CS1309_04	South Shore	49.2237	-65.7968		2.34	17.26	69.32	3.36	0.50	0.82	6.41
CS1309_05	South Shore	49.2296	-65.7360		2.22	15.88	71.21	3.10	0.65	0.79	6.16
CS1309_11	South Shore	49.2069	-66.1697		2.42	15.35	72.24	3.05	0.54	0.66	5.75
CS1309_12	South Shore	48.7556	-67.7951		0.83	14.81	74.72	2.51	0.82	0.55	5.75

Table S2. Main mineralogical composition data of SPM samples (wt. %)

Sample	Area	Latitude	Longitude	Quartz	K-felspar	Plagioclase	Amphibole	Amorphous silica	Chlorite	Illites	Total clays	Total Feldspars
OSL19-01	Upper Estuary	46.8312	-71.1828	5.1	11.2	17.6	8.0	35.8	10.5	6.5	20.6	28.8
OSL19-02	Upper Estuary	47.0433	-70.7537	13.6	12.2	25.8	5.0	12.6	8.0	13.4	29.5	38.0
OSL19-03	Upper Estuary	47.3057	-70.5308	12.9	12.2	25.9	5.6	8.1	7.7	15.0	35.1	38.0
OSL19-04	Upper Estuary	47.7428	-69.8959	11.5	12.2	25.1	6.2	14.2	11.6	14.1	30.0	37.3
OSL19-05	Upper Estuary	47.9301	-69.7715	9.8	13.1	21.6	7.6	25.5	10.7	5.1	19.3	34.7
OSL19-06	Lower Estuary	48.1699	-69.4897	2.6	12.1	13.3	8.6	43.9	10.0	0.8	15.2	25.4
OSL19-09	Lower Estuary	48.6769	-68.5923	8.6	13.1	21.1	7.8	29.2	9.2	5.0	18.0	34.2
OSL19-10	Lower Estuary	49.0003	-67.6365	5.8	13.5	13.1	7.8	40.0	9.9	1.9	15.5	26.5
OSL19-11	Lower Estuary	49.1560	-67.1671	2.0	14.9	14.6	9.1	36.8	11.6	3.1	19.2	29.5

Table S3. Data used for surface distribution maps (1-10 m)

Spring 2010

Station	Longitude	Latitude	log(N'(D) <4 µm [m^{-3} µm^{-1}])	log(N'(D) 4-63 µm [m^{-3} µm^{-1}])	log(N'(D) >63 µm [m^{-3} µm^{-1}])	D$_V$^{50} (µm)	PSD slope	[SPM] (mg L^{-1})	PIM (%)	[Chl-a] (µg L^{-1})
11	-69.4617	48.0593	11.9900	9.9949	5.5699	80.9693	3.5888	3.6510	80.9093	0.4090
12	-69.8025	47.8980	11.9797	9.9112	5.8690	122.8791	3.2748	3.1820	78.4831	0.4251
13	-69.9308	47.7183	12.2860	10.2164	6.5268	109.0710	3.1876	7.9491	79.8300	0.2347
14	-70.1865	47.5217	11.9724	10.4468	7.0651	98.0906	3.1331	13.9773	84.1076	0.5257
21	-69.4498	48.2332	11.3889	9.5799	6.6341	106.5033	3.1264	1.8827	49.5042	2.0595
22	-69.5657	48.1247	11.9372	9.1126	4.9979	107.2390	3.3565	1.1840	51.3074	1.1325
23a	-69.6660	48.0160	11.7872	9.9380	6.2722	136.9698	2.9140	2.5920	80.5556	0.4358
24	-69.3760	48.1708	12.0696	9.4857	5.5337	112.1654	3.5813	3.1160	77.7279	0.6061
25	-69.1690	48.2845	12.0278	9.3602	5.5574	145.7031	3.0907	1.4733	53.4842	0.9025
S1	-69.7768	48.1437	10.7602	9.0453	5.8586	155.9349	2.5020	1.5305	50.6573	0.6106
S2	-69.9493	48.2345	10.3066	8.3286	6.7745	134.9108	2.1877	1.4873	56.1632	0.2360
S3	-70.0387	48.2500	9.7424	8.9931	6.6101	141.0055	2.7905	1.0430	52.7325	0.2025
32	-68.3308	48.6397	11.6477	9.6106	5.5187	90.2108	3.3282	2.3760	69.8653	0.6940
33	-68.0043	48.7467	12.1081	9.5066	5.6574	83.3238	3.3724	2.6958	61.6685	6.1564
34	-67.6677	48.8592	11.7424	9.5025	5.9322	95.0303	3.3017	1.6967	49.7544	2.3133
35	-67.3397	48.9647	12.3979	9.0395	5.3721	142.0320	3.0304	1.9853	58.5964	2.0806
IML4	-68.5813	48.6608	10.5313	9.5277	5.8420	140.0640	2.7878	1.7433	54.1491	3.3747
43	-68.2070	48.9528	11.5893	9.7381	5.0204	72.7085	3.6816	3.3611	55.9008	1.9892
44	-67.8680	49.0863	11.7113	9.7682	5.2012	73.8870	3.6596	1.2180	32.8407	2.2234
45	-67.5017	49.2333	11.6716	9.5446	5.6062	134.2753	3.0848	1.2933	36.0309	3.3177

Winter 2019

Station	Longitude	Latitude	log(N'(D) <4 µm [m^{-3} µm^{-1}])	log(N'(D) 4-63 µm [m^{-3} µm^{-1}])	log(N'(D) >63 µm [m^{-3} µm^{-1}])	D$_V$^{50} (µm)	PSD slope	[SPM] (mg L^{-1})	PIM (%)	[Chl-a] (µg L^{-1})
1	-71.1828	46.8312	12.1442	9.8454	5.3644	131.3863	3.4160	3.9200	62.4150	0.1767
2	-70.7537	47.0433	12.9054	11.6019	6.1701	11.8803	4.9379	72.2195	84.4261	0.7528
3	-70.5308	47.3057	12.4970	11.0914	5.4925	10.8454	5.0097	24.5280	87.4429	0.4486
4	-69.8959	47.7428	11.5958	10.0848	5.7575	27.5898	3.6925	9.8350	81.0269	0.0527
5	-69.7715	47.9301	9.1145	9.6946	6.2864	49.1729	3.6567	9.0400	78.6283	0.0488
6	-69.4897	48.1699	10.4321	9.3024	5.2685	47.1799		3.6163	73.0087	0.0427
9	-68.5923	48.6769		8.8057	6.6670	54.4886	3.2547	2.2193	72.3040	0.0627
10	-67.6365	49.0003	10.8292	9.4987	5.6688	51.4924	3.1553	2.2913	72.7669	0.0760
11	-67.1671	49.1560	10.6196	9.1400	6.2267	62.4170		3.0425	76.9515	0.0655
12	-66.1956	49.5295		8.2702	6.2835	46.1802		2.4374	71.4265	0.2312

RÉFÉRENCES BIBLIOGRAPHIQUES

Aczel, A., & Sounderpandian, J. (2008). *Complete business statistics* (Seventh Edition). McGraw-Hill Higher Education, Boston, USA. 804 p.

Agrawal, Y. C., & Pottsmith, H. C. (2000). Instruments for particle size and settling velocity observations in sediment transport. *Marine Geology*, *168*(1-4), 89-114.

Agrawal, Y. C., & Traykovski, P. (2001). Particles in the bottom boundary layer: Concentration and size dynamics through events. *Journal of Geophysical Research*, *106*(5), 9533-9542. doi: 10.1029/2000JC900160

Agrawal, Y. C., Whitmire, A., Mikkelsen, O. A., & Pottsmith, H. C. (2008). Light scattering by random shaped particles and consequences on measuring suspended sediments by laser diffraction. *Journal of Geophysical Research*, *113*(C4). doi: 10.1029/2007jc004403

Ahn, J. H. (2012). Size distribution and settling velocities of suspended particles in a tidal embayment. *Water Research*, *46*(10), 3219-3228. doi: 10.1016/j.watres.2012.03.038

Ahn, J. H., & Grant, S. B. (2007). Size distribution, sources, and seasonality of suspended particles in southern California marine bathing waters. *Environmental Science & Technology*, *41*(3), 695-702.

Andrews, J. T., Bjork, A. A., Eberl, D. D., Jennings, A. E., & Verplanck, E. P. (2015). Significant differences in late Quaternary bedrock erosion and transport: East versus West Greenland ~70°N - Evidence from the mineralogy of offshore glacial marine sediments. *Journal of Quaternary Science*, *30*(5), 452-463.

Andrews, J. T., Stein, R., Moros, M., & Perner, K. (2016). Late Quaternary changes in sediment composition on the NE Greenland margin (~73°N) with a focus on the fjords and shelf. *Boreas*, *45*(3), 381-397.

Andrews, J. T., & Vogt, C. (2014). Source to sink: Statistical identification of regional variations in the mineralogy of surface sediments in the western Nordic Seas (58°N–75°N; 10°W–40°W). *Marine Geology*, *357*, 151-162. doi: 10.1016/j.margeo.2014.08.005

Andrews, S. W., Nover, D. M., & Schladow, S. G. (2010). Using laser diffraction data to obtain accurate particle size distributions: the role of particle composition. *Limnology and Oceanography: Methods*, *8*(10), 507-526.

Asselman, N. E., Middelkoop, H., & van Dijk, P. M. (2003). The impact of changes in climate and land use on soil erosion, transport and deposition of suspended sediment in the River Rhine. *Hydrological Processes*, *17*(6), 3225-3244. doi: 10.1002/hyp.1384.

Babin, M., Morel, A., Fournier-Sicre, V., Fell, F., & Stramski, D. (2003). Light scattering properties of marine particles in coastal and open ocean waters as related to the particle mass concentration. *Limnology and Oceanography*, *48*(2), 843-859.

Barnett, R. L., Bernatchez, P., Garneau, M., & Juneau, M.-N. (2017). Reconstructing late Holocene relative sea-level changes at the Magdalen Islands (Gulf of St. Lawrence, Canada) using multi-proxy analyses. *Journal of Quaternary Science*, *32*(3), 380-395. doi: 10.1002/jqs.2931

Barone, B., Bidigare, R. R., Church, M. J., Karl, D. M., Letelier, R. M., & White, A. E. (2015). Particle distributions and dynamics in the euphotic zone of the North Pacific Subtropical Gyre. *Journal of Geophysical Research: Oceans*, *120*(5), 3229-3247. doi: 10.1002/2015jc010774

Belzile, M., Galbraith, P. S., & Bourgault, D. (2016). Water renewals in the Saguenay Fjord. *Journal of Geophysical Research: Oceans*, *121*(1), 638-657. doi: 10.1002/2015jc011085

Blais, M., Galbraith, P. S., Plourde, S., Scarratt, M., Devine, L., & Lehouz, C. (2018). Chemical and biological oceanographic conditions in the Estuary and Gulf of St. Lawrence during 2017. DFO Can. Sci. Advis. Sec. Res. Doc. 2017/034. v + 48 p.

Boss, E. S., Haentjens, N., Westberry, T. K., Karp-Boss, L., & Slade, W. H. (2018). Validation of the particle size distribution obtained with the laser in-situ scattering and transmission (LISST) meter in flow-through mode. *Optics Express*, *26*(9), 11125-11136. doi: 10.1364/OE.26.011125

Buonassissi, C. J., & Dierssen, H. M. (2010). A regional comparison of particle size distributions and the power law approximation in oceanic and estuarine surface waters. *Journal of Geophysical Research*, *115*(C10). doi: 10.1029/2010jc006256

Caron, M., Montero-Serrano, J.-C., St-Onge, G., & Rochon, A. (2020). Quantifying provenance and transport pathways of Holocene sediments from the northwestern Greenland margin. *Paleoceanography and Paleoclimatology*, *35*(5), 1-23.

Casse, M. (2018). *Reconstitution de la variabilité naturelle climatique et océanographique dans l'estuaire et le golfe du Saint-Laurent au cours des 10,000 dernières années.* (Thèse). Université du Québec à Rimouski, Institut des sciences de la mer de Rimouski, Rimouski, Canada, 285 p.

Casse, M., Montero-Serrano, J.-C., & St-Onge, G. (2017). Influence of the Laurentide Ice Sheet and relative sea-level changes on sediment dynamics in the Estuary and Gulf of St. Lawrence since the last deglaciation. *Boreas*, *46*(3), 541-561. doi: 10.1111/bor.12230

Casse, M., Montero-Serrano, J.-C., St-Onge, G., & Poirier, A. (2019). REE distribution and Nd isotope composition of estuarine waters and bulk sediment leachates tracing lithogenic inputs in eastern Canada. *Marine Chemistry*, *211*, 117-130. doi: 10.1016/j.marchem.2019.03.012

Chanut, J.-P., & Poulet, S. A. (1979). Distribution des spectres de taille des particules en suspension dans le fjord du Saguenay. *Canadian Journal of Earth Sciences*, *16*, 240-249.

Chanut, J. P., & Poulet, S. A. (1982). Short-term variability of the size spectra of suspended particles in a rapidly changing environment. *Estuarine, Coastal and Shelf Science*, *15*, 497-513.

Ciotti, A. M., & Bricaud, A. (2006). Retrievals of a size parameter for phytoplankton and spectral light absorption by colored detrital matter from water-leaving radiances at SeaWiFS channels in a continental shelf region off Brazil. *Limnology and Oceanography : Methods*, *4*(7), 237-253. doi: 10.4319/lom.2006.4.237

Comiso, J. C., Meier, W. N., & Gersten, R. (2017). Variability in the Arctic Sea ice cover: Results from different techniques. *Journal of Geophysical Research Oceans*, *122*(8), 6883-6900. doi: 10.1002/2017JC012768

Coulombier, T., Neumeier, U., & Bernatchez, P. (2012). Sediment transport in a cold climate salt marsh (St. Lawrence Estuary, Canada), the importance of vegetation and waves. *Estuarine Coastal and Shelf Science*, *101*, 64-75.

D'Anglejan, B. F. (1970). Studies on particulate matter in the Gulf of St. Lawrence. McGill University, Manuscript report. 17, 0-31

D'Anglejan, B. F. (1990). Recent sediments and sediment transport processes in the St. Lawrence Estuary. Dans: M. I. El-Sabh, & N. Silverberg (eds.), *Oceanography of a Large-Scale Estuarine System. Coastal and Estuarine Studies* (Vol. 39, pp. 109-129). Springer, New York, NY.

D'Anglejan, B.F., & Ingram, R. G. (1976). Time-depth variations in tidal flux of suspended matter in the Saint Lawrence Estuary. *Estuarine and Coastal Marine Science*, *4*, 401-416.

D'Anglejan, B. F., & Smith, E. C. (1973). Distribution, transport, and composition of suspended matter in the St. Lawrence Estuary. *Canadian Journal of Earth Sciences*, *10*, 1380-1396.

Dahlke, H. E., Lyon, S. W., Stedinger, J. R., Rosqvist, G., & Jansson, P. (2012). Contrasting trends in floods for two sub-arctic catchments in northern Sweden – does glacier presence matter? *Hydrology and Earth System Sciences*, *16*, 2123-2141. doi: 10.5194/hess-16-2123-2012

Davies, E. J., Nimmo-Smith, W. A. M., Agrawal, Y. C., & Souza, A. J. (2012). LISST-100 response to large particles. *Marine Geology*, *307-310*, 117-122.

Deschamps, C.-E., Montero-Serrano, J.-C., & St-Onge, G. (2018). Sediment provenance changes in the western Arctic Ocean in response to ice rafting, sea level, and oceanic circulation variations since the last deglaciation. *Geochemistry, Geophysics, Geosystems*, *19*(7), 2147-2165.

Desiage, P.-A., Montero-Serrano, J.-C., St-Onge, G., Crespi-Abril, A., Giarratano, E., Gil, M., & Haller, M. (2018). Quantifying sources and transport pathways of surface sediments in the Gulf of San Jorge, Central Patagonia (Argentina). *Oceanography*, *31*(4), 92-103. doi: 10.5670/oceanog.2018.401

Devine, L., Scarratt, M., Plourde, S., Galbraith, P. S., Michaud, S., & Lehoux, C. (2017). Chemical and biological oceanographic conditions in the Estuary and Gulf of St. Lawrence during 2015. DFO Can. Sci. Advis. Sec. Res. Doc. 2017/034. v + 48 p.

Devlin, N. J., Barry, J., Mills, D. K., Gowen, R. J., Foden, J., Sivyer, D., & Tett, P. (2008). Relationships between suspended particulate material, light attenuation and Secchi depth in UK marine waters. *Estuarine, Coastal and Shelf Science*, *17*(3), 429-439. doi: 10.1016/j.ecss.2008.04.024

Devred, E., Sathyendranath, S., Stuart, V., Maass, H., Ulloa, O., & Platt, T. (2006). A two-component model of phytoplankton absorption in the open ocean: Theory and applications. *Journal of Geophysical Research*, *111*(C03011), 1-11. doi: 10.1029/2005jc002880

DFO. (2012). Development of a St. Lawrence Estuary marine protected areas ecological monitoring plan. DFO Can. Sci. Advis. Sec. Sci. Adv. Rep. 2012/039. 25 p.

DFO. (2020, June 13, 2020). Freshwater runoffs of the St. Lawrence at the height of Québec City. Repéré le June 21, 2020, à https://catalogue.ogsl.ca/en/dataset/84a17ffc-4898-4261-94de-4a5ea2a9258d

Dionne, J.-C. (1969). Erosion glacielle littorale, estuaire du Saint-Laurent. *Revue de Géographie de Montreal*, *23*(1), 5-20.

Dionne, J.-C. (1981). Données préliminaires sur la charge sédimentaire du couvert de glace dans la baie de Montmagny, Québec. *Géographie physique et Quaternaire*, *35*(2), 277-282. doi: 10.7202/1000445ar

Dionne, J.-C. (1984). An estimate of ice-drifted sediments based on the mud content of the ice cover at Montmagny, Middle St. Lawrence Estuary. *Marine Geology*, *57*(1-4), 149-166.

Dionne, J.-C. (2002). Sediment content of the ice-cover in muddy tidal areas of the turbidity zone of the St. Lawrence estuary and the problem of the sediment budget. Dans: T. Healy, Y. Wang, & J.-A. Healy (eds.), *Muddy Coasts of the World: Processes, Deposits and Function* (Vol. 4, pp. 463-478). Elsevier Science.

Dolgopolova, E. N., & Isupova, M. V. (2011). Water and sediment dynamics at Saint Lawrence River mouth. *Water Resources*, *38*(4), 453-469. doi: 10.1134/s009780781104004x

Doxaran, D., Froidefond, J. M., Lavender, S., & Castaing, P. (2002). Spectral signature of highly turbid waters - Application with SPOT data to quantify suspended particulate matter concentrations. *Remote Sensing of Environment*, *81*(1), 149-161.

Drapeau, G. (1990). Nearshore sediment dynamics in the St. Lawrence Estuary. Dans: M. I. El-Sabh, & N. Silverberg (eds.), *Oceanography of a Large-Scale Estuarine System. Coastal and Estuarine Studies* (Vol. 39, pp. 130-154). Springer, New York, NY.

Drapeau, G. (1992). Dynamique sédimentaire des littoraux de l'estuaire du Saint-Laurent. *Géographie physique et Quaternaire*, *46*(2), 233-242. doi: 10.7202/032907ar

Droppo, I. G., Jeffries, D., Jaskot, C., & Backus, S. (1998). The prevalence of freshwater flocculation in cold regions: A case study from the Mackenzie River Delta, Northwet Territories, Canada. *Arctic*, *51*(2), 155-164.

Dufour, R., Benoît, H., Castonguay, M., Chasse, J., Devine, L., Galbraith, P. S., Harvey, M., Larouche, P., Lessard, S., Petrie, B., Savard, L., Savenkoff, C., St-Armand, L., & Starr, M. (2010). Rapport sur le status et les tendances de l'écosystème : écozone de l'estuaire et du golfe du Saint-Laurent. MPO Sec. Can. Cons. Sci. Doc. Res. 2010/030. v + 187 p.

Dyer, K. R., & Manning, A. J. (1999). Observation of the size, settling velocity and effective density of flocs, and their fractal dimensions. *Journal of Sea Research*, *41*(1-2), 87-95.

Eberl, D. D. (2003). *User's Guide to RockJock - A program for determining quantitative mineralogy from X-ray diffraction data*. Open-File Report 03-78, U.S. Geological Survey, Boulder, CO. 47 p.

Eberl, D. D., & Smith, D. B. (2009). Mineralogy of soils from two continental-scale transects across the United States and Canada and its relation to soil geochemistry and climate. *Applied Geochemistry*, *24*(8), 1394-1404. doi: 10.1016/j.apgeochem.2009.04.010

Eisma, D. (1986). Flocculation and de-flocculation of suspended matter in estuaries. *Netherlands Journal of Sea Research*, *20*(2-3), 183-199.

Eisma, D., Schuhmacher, T., Boekel, H., Vanheerwaarden, J., Franken, H., Laan, M., Vaars, A., Eijgenraam, F., & Kalf, J. (1990). A camera and image-analysis system for *in situ* observation of flocs in natural waters. *Netherlands Journal of Sea Research*, *27*(1), 43-56.

El-Sabh, M. I. (1988). Physical oceanography of the St. Lawrence Estuary. Dans: B. Kjerfve (ed.), *Hydrodynamics of Estuaries: Volume II Estuarine Case Studies* (pp. 61-78). CRC Press, Boca Raton, Florida.

El-Sabh, M. I., Lie, H.-J., & Koutitonsky, V. (1982). Variability of the near-surface residual current in the lower St. Lawrence estuary. *Journal of Geophysical Research Oceans*, *87*(C12), 9589-9600.

El-Sabh, M. I., & Silverberg, N. (1990). The St. Lawrence Estuary : Introduction. Dans: M. I. El-Sabh, & N. Silverberg (eds.), *Oceanography of a Large-Scale Estuarine System. Coastal and Estuarine Studies* (Vol. 39, pp. 1-9). Springer, New York, NY.

Eleveld, M. A., van der Wal, D., & van Kessel, T. (2014). Estuarine suspended particulate matter concentrations from sun-synchronous satellite remote sensing: Tidal and meteorological effects and biases. *Remote Sensing of Environment*, *143*, 204-215.

Elson, J. A. (2010, March 4, 2015). St. Lawrence Lowland. Repéré le June 5, 2020, à https://thecanadianencyclopedia.ca/en/article/st-lawrence-lowland

Fauchot, J., Saucier, F. J., Levasseur, M., Roy, S., & Zakardjian, B. (2008). Wind-driven river plume dynamics and toxic Alexandrium tamarense blooms in the St. Lawrence

estuary (Canada): A modeling study. *Harmful Algae*, *7*(2), 214-227. doi: 10.1016/j.hal.2007.08.002

Gagné, H., Lageunesse, P., St-Onge, G., & Bolduc, A. (2009). Recent transfer of coastal sediments to the Laurentian Channel, Lower St. Lawrence Estuary (Eastern Canada), through submarine canyon and fan systems. *Geo-Marine Letters*, *29*, 191-200.

Gagnon, M., Bergeron, P., Leblanc, J., & Siron, R. (1997). *Synthèse des connaissances sur les aspects physiques et chimiques de l'eau et des sédiments du golfe du Saint-Laurent et de la baie des Chaleurs*. Ministère des Pêches et des Océans - Région Laurentienne. Division des sciences de l'environnement marin, Institut Maurice-Lamontagne et Environnement Canada - Région du Québec, Conservation de l'environnement, Centre Saint-Laurent. Rapport technique. Zones d'intervention prioritaire 19, 20 et 21. 191 p.

Galbraith, P. S., Bourgault, D., & Belzile, M. (2018). Circulation et renouvellement des masses d'eau du fjord du Saguenay. *Le Naturaliste canadien*, *142*(2), 36-46. doi: 10.7202/1047147ar

Galbraith, P. S., Chassé, J., Caverhill, C., Nicot, P., Gilbert, D., Lefaivre, D., & Lafleur, C. (2019). Physical oceanographic conditions in the Gulf of St. Lawrence during 2018. DFO Can. Sci. Advis. Sec. Res. Doc. 2019/046. iv + 79 p.

Galbraith, P. S., Chasse, J., Gilbert, D., Larouche, P., Brickman, D., Pettigrew, B., Devine, L., Gosselin, A., Pettipas, R. G., & Lafleur, C. (2011). Physical oceanographic conditions in the Gulf of St. Lawrence in 2010. DFO Can. Sci. Advis. Sec. Res. Doc. 2011/045. iv + 82 p.

Garrels, R. M., & Mackenzie, F. T. (1971). *Evolution of sedimentary rocks*. W. W. Norton & Company, Inc., New York, NY. xvi + 397 p.

Gearing, J. N., Tronczynski, J., & Macko, S. A. (1994). Particulate organic matter in the St. Lawrence Estuary: anthropogenic and natural sources. Dans: K. R. Dyer, & R. J. Orth (eds.), *Changes in Fluxes in Estuaries: Implications from Sciences to Management* (pp. 125-130). Olsen & Olsen, Fredensborg, Danemark.

Gilbert, D., & Pettigrew, B. (1997). Interannual variability (1948–1994) of the CIL core temperature in the Gulf of St. Lawrence. *Canadian Journal of Fisheries and Aquatic Sciences*, *54*, 57-67.

Gobeil, C. (2006). Biogeochemistry and chemical contamination in the St. Lawrence Estuary. Dans: P. J. Wangersky (ed.), *The Handbook of Environmental Chemistry* (Vol. 5H, pp. 121-147). Springer, Berlin, Heidelberg. doi: 10.1007/698_5_023

Gouvernement du Québec. (2012). The great geological domains of Québec. Repéré le June 5, 2020, à https://mern.gouv.qc.ca/wp-content/uploads/geological-domains-quebec.pdf

Harris, J. E. (1977). Characterization of suspended matter in the Gulf of Mexico—II particle size analysis of suspended matter from deep water. *Deep Sea Research*, *24*(11), 1055-1061.

Hart, B. T. (1982). Uptake of trace metals by sediments and suspended particulates: a review. *Hydrobiologia*, *91*, 299-313.

Herron, M. M. (1988). Geochemical classification of terrigenous sands and shales from core or log data. *Journal of Sedimentary Research*, *58*(5), 820-829.

Hirata, T., Aiken, J., Hardman-Mountford, N., Smyth, T. J., & Barlow, R. G. (2008). An absorption model to determine phytoplankton size classes from satellite ocean colour. *Remote Sensing of Environment*, *112*(6), 3153-3159. doi: 10.1016/j.rse.2008.03.011

Hirata, T., Hardman-Mountford, N. J., Brewin, R. J. W., Aiken, J., Barlow, R., Suzuki, K., Isada, T., Howell, E., Hashioka, T., Noguchi-Aita, M., & Yamanaka, Y. (2011). Synoptic relationships between surface Chlorophyll-*a* and diagnostic pigments specific to phytoplankton functional types. *Biogeosciences*, *8*(2), 311-327. doi: 10.5194/bg-8-311-2011

Huang, J., Chen, X., Jiang, T., Yang, F., Chen, L., & Yan, L. (2016). Variability of particle size distribution with respect to inherent optical properties in Poyang Lake, China. *Applied Optics*, *55*(22), 5821-5829. doi: 10.1364/AO.55.005821

Ingram, R. G., & El-Sabh, M. I. (1990). Fronts and mesoscale features in the St. Lawrence estuary. Dans: M. I. El-Sabh, & N. Silverberg (eds.), *Oceanography of a Large-Scale Estuarine System. Coastal and Estuarine Studies* (Vol. 39, pp. 71-93). Springer, New York, NY.

IOCCG. (2000). *Remote sensing of ocean colour in coastal, and other optically-complex, waters*. S. Sathyendranath (ed.), Reports of the International Ocean-Colour Coordinating Group, No. 3, IOCCG, Dartmouth, Canada.

IPCC. (2019). *Climate Change and Land: an IPCC special report on climate change, desertification, land degradation, sustainable land management, food security, and greenhouse gas fluxes in terrestrial ecosystems*. [P. R. Shukla, J. Skea, E. C. Buendia, V. Masson-Delmotte, H.-O. Pörtner, D. C. Roberts, P. Zhai, R. Slade, S. Connors, R. v. Diemen, M. Ferrat, E. Haughey, S. Luz, S. Neogi, M. Pathak, J.

Petzold, J. P. Pereira, P. Vyas, E. Huntley, K. Kissick, M. Belkacemi, & J. Malley, (eds.)]. In press.

Itamiya, H., Sugita, R., & Sugai, T. (2019). Analysis of the surface microtextures and morphologies of beach quartz grains in Japan and implications for provenance research. *Progress in Earth and Planetary Science*, *6*(43), 1-14. doi: 10.1186/s40645-019-0287-9

Jaegle, M. (2015). *Nature et origine des sédiments de surface de l'estuaire du Saint-Laurent*. (Mémoire). Université du Québec à Rimouski, Institut des sciences de la mer de Rimouski, Rimouski, Canada, 82 p.

Jaegler, T. (2014). *Variabilité spatiale et temporelle des propriétés optiques et chimiques de la matière organique dissoute dans les rivières de la Côte-Nord, Québec, Canada*. (Mémoire). Université du Québec à Rimouski, Rimouski, Québec, 181 p.

Jago, C. F., Jones, S. E., Sykes, P., & Rippeth, T. (2006). Temporal variation of suspended particulate matter and turbulence in a high energy, tide-stirred, coastal sea: Relative contributions of resuspension and disaggregation. *Continental Shelf Research*, *26*(17-18), 2019-2028.

Jonasz, M. (1983). Particle-size distributions in the Baltic. *Tellus B: Chemical and Physical Meteorology*, *35*(5), 346-358. doi: 10.3402/tellusb.v35i5.14624

Kemp, A. C., Wright, A. J., Edwards, R. J., Barnett, R. L., Brain, M. J., Kopp, R. E., Cahill, N., Hortons, B. P., Charman, D. J., Hawkes, A. D., Hilll, T. D., & van de Plassche, O. (2018). Relative sea-leve change in Newfoundland, Canada during the pas ~3000 years. *Quaternary Science Reviews*, *201*, 89-110. doi: 10.1016/j.quascirev.2018.10.012

Kostadinov, T. S., Siegel, D. A., & Maritorena, S. (2009). Retrieval of the particle size distribution from satellite ocean color observations. *Journal of Geophysical Research*, *114*(C9). doi: 10.1029/2009jc005303

Koutitonsky, V., & Bugden, G. L. (1991). The physical oceanography of the Gulf of St. Lawrence: a review with emphasis on the synoptic variability of the motion. Dans: J. C. Therriault (ed.), *The Gulf of St. Lawrence: small ocean or big estuary?* (pp. 57-90). Canadian Special Publication of Fisheries and Aquatic Sciences. 113, Mont-Joli, Quebec.

Kranck, K. (1979). Dynamics and distribution of suspended particulate matter in the St. Lawrence estuary. *Le Naturaliste canadien*, *106*(1), 163-173.

Kranck, K., & Milligan, T. G. (1991). Grain size in oceanography. Dans: J. P. M. Syvitsky (ed.), *Principles, methods, and application of particle size analysis* (pp. 332-345). Cambridge University Press, New York.

Laanen, M. L. (2007). *Yellow Matters: Improving the remote sensing of Coloured Dissolved Matter in inland freshwaters*. (Thesis). Vrike Unerversiteit Amsterdam, Amsterdam, Pays-Bas, 268 p.

Laliberté, J., Larouche, P., Devred, E., & Craig, S. (2018). Chlorophyll-a concentration retrieval in the optically complex waters of the St. Lawrence Estuary and Gulf using principal component analysis. *Remote Sensing*, *10*(265), 1-15. doi: 10.3390/rs10020265

Larouche, P., & Boyer-Villemaire, U. (2010). Suspended particulate matter in the St. Lawrence estuary and Gulf surface layer and development of a remote sensing algorithm. *Estuarine, Coastal and Shelf Science*, *90*(4), 241-249. doi: 10.1016/j.ecss.2010.09.005

Law, B. A., Hill, P. S., Maier, I., Milligan, T. G., & Page, F. (2014). Size, settling velocity and density of small suspended particles at an active salmon aquaculture site. *Aquaculture Environment Interactions*, *6*(1), 29-42. doi: 10.3354/aei00116

Leadprathom, N., Parkpian, P., Satayavivad, J., Delaune, R. D., & Jugsujinda, A. (2009). Transport and deposition of organochlorine pesticides from farmland to estuary under tropical regime and their potential risk to aquatic biota. *Journal of Environmental Science and Health, Part B*, *44*(3), 249-261. doi: 10.1080/03601230902728302

Lebeuf, M., Maltais, D., Larouche, P., Lavoie, D., Lefaivre, D., Starr, M., & Scarratt, M. (2019). Recent distribution, inventories and temporal trends of suspended particulate matter in the St. Lawrence Estuary, Canada. *Regional Studies in Marine Science*, *29*(100664), 1-13. doi: 10.1016/j.rsma.2019.100664

Lefort, S., Gratton, Y., Mucci, A., Dadou, I., & Gilbert, D. (2012). Hypoxia in the Lower St. Lawrence Estuary: How physics controls spatial patterns. *Journal of Geophysical Research Oceans*, *117*(C7).

Lei, S., Wu, D., Li, Y., Wang, Q., Huang, C., Liu, G., Zheng, Z., Du, C., Mu, M., Xu, J., & Lv, H. (2018). Remote sensing monitoring of the suspended particle size in Hongze Lake based on GF-1 data. *International Journal of Remote Sensing*, *40*(8), 3179-3203. doi: 10.1080/01431161.2018.1541109

Levasseur, M., Therriault, J.-C., & Legendre, L. (1984). Hierarchical control of phytoplankton succession by physical factors. *Marine Ecology Progress Series*, *19*, 211-222.

Li, X. Y., & Logan, B. E. (1995). Size distributions and fractal properties of particles during a simulated phytoplankton bloom in a mesocosm. *Deep Sea Research Part II: Topical Studies in Oceanography*, *42*(1), 125-138.

LISST-100X Particle Size Analyzer. (2015). *User's Manual Version 5.1*. Sequoia Scientific, Inc., Bellevue, WA. 144 p.

Locat, J., & Levesque, C. (2009). Le fjord du Saguenay: une physiographie et un registre exceptionnels. *Revue des sciences de l'eau*, *222*, 135-157.

Loisel, H., Nicolas, J.-M., Sciandra, A., Stramski, D., & Poteau, A. (2006). Spectral dependency of optical backscattering by marine particles from satellite remote sensing of the global ocean. *Journal of Geophysical Research*, *111*(C9), 1-14. doi: 10.1029/2005jc003367

Löptien, U., & Meier, H. E. M. (2011). The influence of increasing water turbidity on the sea surface temperature in the Baltic Sea: A model sensitivity study. *Journal of Marine Systems*, *88*(2), 323-331. doi: 10.1016/j.jmarsys.2011.06.001.

Loring, D. H., & Nota, D. J. G. (1973). *Morphology and sediments of the Gulf of St. Lawrence* (Vol. 182). Bulletin of the Fisheries Research Board of Canada, Ottawa, Ontario. 147 p.

Lucotte, M., & D'Anglejan, B. (1986). Seasonal control of the Saint-Lawrence maximum turbidity zone by tidal-flat sedimentation. *Estuaries*, *9*(2), 84-94.

Lyu, H., Wang, Y. N., Jin, Q., Li, X. J., Cao, K., Wang, Q. A., & Li, Y. M. (2017). A practical approach to retrieving the finer areas of algal bloom in inland lakes from coarse spatial resolution satellite data. *International Journal of Remote Sensing*, *38*(14), 4069-4085.

Ma, H., Kim, S. D., Allen, H. E., & Cha, D. K. (2002). Effect of copper binding by suspended particulate matter on toxicity. *Environmental Toxicology and Chemistry*, *21*(4), 710-714. doi: 10.1002/etc.5620210404

Mann, K. H., & Lazier, J. R. N. (2006). *Dynamics of marine ecosystems: Biological-physical interactions in the oceans* (3rd edition). Blackwell Publishing, Oxford, U.K. 503 p.

McLennan, S. M. (2001). Relationships between the trace element composition of sedimentary rocks and upper continental crust. *Geochemistry, Geophysics, Geosystems*, *2*(4), 2000GC000109.

Mélin, F., & Vantrepotte, V. (2015). How optically diverse is the coastal ocean? *Remote Sensing Environment*, *160*, 235-251. doi: 10.1016/j.rse.2015.01.023

Mertz, G., El-Sabh, M. I., & Koutitonsky, V. G. (1989). Low frequency variability in the lower St. Lawrence Estuary. *Journal of Marine Research*, *47*(2), 285-302. doi: 10.1357/002224089785076280

Mertz, G., & Gratton, Y. (1990). Topographic waves and topographically induced motions in the St. Lawrence Estuary. Dans: M. I. El-Sabh, & N. Silverberg (eds.), *Oceanography of a large-scale estuarine system. Coastal and Estuarine Studies* (Vol. 39, pp. 94-108). Springer, New York, NY.

Mikkelsen, O. A., Hill, P. S., & Milligan, T. G. (2006). Single-grain, microfloc and macrofloc volume variations observed with a LISST-100 and a digital floc camera. *Journal of Sea Research*, *55*(2), 87-102.

Mikkelsen, O. A., Milligan, T. G., Hill, P. S., Chant, R. J., Jago, C. F., Jones, S. E., Krivtsov, V., & Mitchelson-Jacob, G. (2008). The influence of schlieren on in situ optical measurements used for particle characterization. *Limnology and Oceanography : Methods*, *6*(3), 133-143.

Mikkelsen, O. A., & Pejrup, M. (2001). The use of a LISST-100 laser particle sizer for in-situ estimates of floc size, density and settling velocity. *Geo-Marine Letters*, *20*(4), 187-195. doi: 10.1007/s003670100064

Milligan, T. G., & Kranck, K. (1991). Electroresistance particle size analyzers. Dans: P. James, & M. Sybitsky (eds.), *Principle, Methods and Application of Particle Size Analyses* (pp. 109-118). Cambridge University Press. doi: https://doi.org/10.1017/CBO9780511626142.011

Ministère du Développement durable, de l'Environnement et de la Lutte contre les changements climatiques et Environnement et Changement climatique Canada. (2016). *Recommandations pour la gestion des matières en suspension (MES) lors des activités de dragage*. Québec. 64 p.

Mobley, C. D. (1994). *Light and water: Radiative transfer in natural waters*. Academic Press, San Diego, CA. 604 p.

Mohammadpour, G., Gagné, J.-P., Larouche, P., & Montes-Hugo, M. A. (2017). Optical properties of size fractions of suspended particulate matter in littoral waters of Québec. *Biogeosciences*, *14*(23), 5297-5312. doi: 10.5194/bg-14-5297-2017

Montero-Serrano, J.-C., Winkler, G., Boivin-Rioux, A., Hébert, A.-J., Cabrol, J., Bluteau, C., Chaillou, G., Tremblay, J. E., Gosselin, M., Bourgault, D., Dumont, D., Gélinas, Y., Galbraith, P. S., Xie, H., Rochon, A., Starr, M., St-Onge, G., Forest, A., & Fraboulet, E. (2018, 5-6 Novembre 2018). *Caractérisation des conditions océanographiques hivernales du Sain-Laurent - Synthèse des premiers résultats de la mission Odyssée Saint-Laurent*. Communication présentée à la Réunion Scientifique Annuelle de Québec-Océan, Rivière-du-Loup, Québec, Canada.

Montes-Hugo, M. A., & Mohammadpour, G. (2012). Biogeo-optical modeling of SPM in the St. Lawrence Estuary. *Canadian Journal of Remote Sensing*, *38*(2), 197-209.

Montes-Hugo, M. A., Roy, S., Gagné, J.-P., Demers, S., Çizmeli, S., & Mas, S. (2012). Ocean colour and distribution of suspended particulates in the St. Lawrence Estuary. *EARSel eProceedings*, *11*(1), 1-11. doi: 10.12760/01-2012-1-01

Morel, A., & Antoine, D. (1994). Heating rate within the upper ocean in relation to its bio-optical state. *Journal of Physical Oceanography*, *24*(7), 1652-1665.

MPO. (2007). Zones d'importance écologique et biologique (ZIEB) de l'estuaire et du golfe du Saint-Laurent : identification et caractérisation. DFO Can. Sci. Advis. Sec. Avis scientifique 2007/016. 15 p.

Neu, H. J. A. (1970). *A study on mixing and circulation in the St. Lawrence Estuary up to 1964*. Bedford Institute of Oceanography, Dartmouth, Canada. AOL Report 1970-9. 31 p.

Neukermans, G., Loisel, H., Mériaux, X., Astoreca, R., & McKee, D. (2012). In situ variability of mass-specific beam attenuation and backscattering of marine particles with respect to particle size, density, and composition. *Limnology and Oceanography*, *57*(1), 124-144. doi: 10.4319/lo.2011.57.1.0124

Neukermans, G., Reynolds, R. A., & Stramski, D. (2016). Optical classification and characterization of marine particle assemblages within the western Arctic Ocean. *Limnology and Oceanography*, *61*(4), 1472-1494. doi: 10.1002/lno.10316

Neumeier, U., & Cheng, C. (2015). *Hydrodynamics and sediment dynamics in an ice-covered tidal flat*. Communication présentée à la Coastal Sediments 2015, San Diego, California.

Nieke, B., Reuter, R., Heuermann, R., Wang, H., Babin, M., & Therriault, J. C. (1997). Light absorption and fluorescence properties of chromophoric dissolved organic matter (CDOM), in the St Lawrence Estuary (Case 2 waters). *Continental Shelf Research*, *17*(3), 235-252.

Organelli, E., Bricaud, A., Antoine, D., & Uitz, J. (2013). Multivariate approach for the retrieval of phytoplankton size structure from measured light absorption spectra in the Mediterranean Sea (BOUSSOLE site). *Applied Optics*, *52*(11), 2257-2273. doi: 10.1364/AO.52.002257

Park, Y. A., Choi, J. Y., & Gao, S. (2001). Spatial variation of suspended particulate matter in the Yellow Sea. *Geo-Marine Letters*, *20*(4), 196-200.

Parsons, T. R., Maita, Y., & Lalli, C. M. (1984). *A manual of chemical & biological methods for seawater analysis*. Pergamon Press, Oxford, UK. 184 p.

Pinet, N., Brake, V., Campbell, C., & Duchesne, M. (2011). Seafloor and shallow subsurface of the St. Lawrence River Estuary. *Geoscience Canada*, *38*(1), 31-40.

Plourde, S., Dodson, J. J., Runge, J. A., & Therriault, J. C. (2002). Spatial and temporal variations in copepod community structure in the lower St. Lawrence Estuary, Canada. *Marine Ecology Progress Series*, *230*, 211-224. doi: 10.3354/meps230211

Plourde, S., Starr, M., Devine, L., St-Pierre, J.-F., St-Armand, L., Joly, P., & Galbraith, P. S. (2014). Chemical and biological oceanographic conditions in the Estuary and Gulf of St. Lawrence during 2011 and 2012. DFO Can. Sci. Advis. Sec. Res. Doc. 2014/049. v + 46 p.

Poulet, S. A., Chanut, J.-P., & Morissette, M. (1986a). Étude des spectres de taille des particules en suspension dans l'estuaire et le golfe du Saint-Laurent. *Oceanologica*, *9*(2), 179-189.

Poulet, S. A., Cossa, D., & Marty, J.-C. (1986b). Combined analyses of the size spectra and biochemical composition of particles in the St. Lawrence estuary. *Marine Ecology Progress Series*, *30*, 205-214.

Prieur, L., & Sathyendranath, S. (1981). An optical classification of coastal and oceanic waters based on the specific spectral absorption curves of phytoplankton pigments, dissolved organic matter, and other particulate materials. *Limnology and Oceanography*, *26*(4), 671-689.

Pye, K., & Blott, S. J. (2004). Particle size analysis of sediments, soils and related particulate materials for forensic purposes using laser granulometry. *Forensic Science International*, *144*(1), 19-27. doi: 10.1016/j.forsciint.2004.02.028

Qiu, Z., Sun, D., Hu, C., Wang, S., Zheng, L., Huan, Y., & Peng, T. (2016). Variability of particle size distributions in the Bohai Sea and the Yellow Sea. *Remote Sensing*, *8*(11:949), 1-19. doi: 10.3390/rs8110949

Ralston, D. K., & Geyer, W. R. (2017). Sediment transport time scales and trapping efficiency in a tidal river. *Journal of Geophysical Research: Earth Surface*, *122*(11), 2042-2063.

Ramalhosa, E., Pereira, E., Vale, C., Valega, M., Monterroso, P., & Duarte, A. C. (2005). Mercury distribution in Douro estuary (Portugal). *Marine Pollution Bulletin*, *50*(1), 1218-1222. doi: 10.01016/j.marpolbul.2005.04.020

Ramesh, R., & D'Anglejan, B. (1995). Mineralogy, chemistry and particle size interrelationships in some post-glacial marine deposits of the St. Lawrence Lowlands. *Journal of Coastal Research*, *11*(4), 1167-1179.

Renosh, P. R., Schmitt, F. G., Loisel, H., Sentchev, A., & Meriaux, X. (2014). High frequency variability of particle size distribution and its dependency on turbulence over the sea bottom during re-suspension processes. *Continental Shelf Research*, *77*, 51-60.

Reynolds, R. A., Stramski, D., Wright, V. M., & Woźniak, S. B. (2008). *Particle size distributions of coastal waters measured with an in situ laser diffractometer*. Communication présentée à la Ocean Optics XIX, Castelvecchio Pascoli, Italy.

Reynolds, R. A., Stramski, D., Wright, V. M., & Woźniak, S. B. (2010). Measurements and characterization of particle size distributions in coastal waters. *Journal of Geophysical Research*, *115*(C08024), 1-19. doi: 10.1029/2009jc005930

Roy, S., Blouin, F., Jacques, A., & Therriault, J. C. (2008). Absorption properties of phytoplankton in the Lower Estuary and Gulf of St. Lawrence (Canada). *Canadian Journal of Fisheries and Aquatic Sciences*, *65*(8), 1721-1737.

Runyan, H., Reynolds, R. A., & Stramski, D. (2020). Evaluation of particle size distribution metrics to estimate the relative contributions of different size fractions based measurements in Arctic waters. *Journal of Geophysical Research Oceans*, *125*(6).

Saucier, F. J., & Chassé, J. (2000). Tidal circulation and buoyancy effects in the St. Lawrence Estuary. *Atmosphere-Ocean*, *38*(4), 505-556.

Saucier, F. J., Roy, F., Senneville, S., Smith, G., Lefaivre, D., Zakardjian, B., & Dumais, J.-F. (2009). Modélisation de la circulation dans l'estuaire et le golfe du Saint-Laurent

en réponse aux variations du débit d'eau douce et des vents. *Revue des sciences de l'eau*, *22*(2), 159-176. doi: 10.7202/037480ar

Sheldon, R. W., Prakash, A., & Jr., S. (1972). The size distribution of particle in the ocean. *Limnology and Oceanography*, *17*(3), 327-340.

Shi, K., Li, Y. M., Zhang, Y. L., Li, L., Lv, H., & Song, K. S. (2014). Classification of inland waters based on bio-optical properties. *IEEE Journal of Selected Topics in Applied Earth Observations and Remote Sensing*, *7*(2), 543-561.

Shi, W., & Wang, M. (2019). Characterization of suspended particle size distribution in global highly turbid waters from VIIRS measurements. *Journal of Geophysical Research: Oceans*, *124*, 3796-3817. doi: 10.1029/2018jc014793

Sholkovitz, E. R. (1976). Flocculation of dissolved organic and inorganic matter during the mixing of river water and seawater. *Geochimica et Cosmochimica Acta*, *40*(7), 831-845. doi: 10.1016/0016-7037(76)90035-1

Silverberg, N., & Sundby, B. (1978). Observations in the turbidity maximum of the St. Lawrence Estuary. *Canadian Journal of Earth Sciences*, *16*, 939-950.

Sinclair, M. (1978). Summer phytoplankton variability in the lower St. Lawrence Estuary. *Journal de l'Office des recherches sur les pêcheries du Canada*, *35*(9), 1171-1185. doi: 10.1139/f78-188

Slade, W. H., & Boss, E. S. (2006). Calibrated near-forward volume scattering function obtained from the LISST particle sizer. *Optics Express*, *14*(8), 3602-3615.

Slade, W. H., & Boss, E. S. (2015). Spectral attenuation and backscattering as indicators of average particle size. *Applied Optics*, *54*(24), 7264-7277. doi: 10.1364/AO.54.007264

Smith, J. N., & Schafer, C. T. (1999). Sedimentation, bioturbation, and Hg uptake in the sediments of the estuary and Gulf of St. Lawrence. *Limnology and Oceanography*, *44*(1), 207-219.

St. Lawrence Center. (1996). *State of the environment report on the St. Lawrence River. Volume 1: The St. Lawrence ecosystem*. Environment Canada – Quebec Region, Environmental Conservation, and Éditions MultiMondes, Montreal, Canada. « St. Lawrence UPDATE » series. 664 p.

Sun, D., Qiu, Z., Hu, C., Wang, S., Wang, L., Zheng, L., Peng, T., & He, Y. (2016). A hybrid method to estimate suspended particle sizes from satellite measurements

over Bohai Sea and Yellow Sea. *Journal of Geophysical Research: Oceans*, *121*(9), 6742-6761. doi: 10.1002/2016jc011949

Tao, J., Hill, P. S., Boss, E., & Milligan, T. G. (2018). Variability of suspended particle properties using optical measurements within the Columbia River Estuary. *Journal of Geophysical Research: Oceans*, *123*(9), 6296-6311.

Therriault, J. C., & Lacroix, G. (1976). Nutrients, chlorophyll, and internal tides in the St. Lawrence estuary. *Journal of the Fisheries Research Board of Canada*, *33*(12), 2747-2757.

Therriault, J. C., & Levasseur, M. (1985). Control of phytoplankton production in the lower St. Lawrence estuary: light and freshwater runoff. *Naturaliste Canadien*, *112*, 77-96.

Traykovski, P., Latter, R. J., & Irish, J. D. (1999). A laboratory evaluation of the laser in situ scattering and transmissometery instrument using natural sediments. *Marine Geology*, *159*(1-4), 355-367.

Tremblay, L., & Gagné, J.-P. (2009). Organic matter distribution and reactivity in the waters of a large estuarine system. *Marine Chemistry*, *116*(1-4), 1-12.

Troude, J.-P., & Sérodes, J.-B. (1990). Caractéristiques hydrodynamiques d'un estran à forte sédimentation. *Canadian Journal of Civil Engineering*, *17*, 148-155.

Uitz, J., Claustre, H., Gentili, B., & Stramski, D. (2010). Phytoplankton class-specific primary production in the world's oceans: Seasonal and interannual variability from satellite observations. *Global Biogeochemical Cycles*, *24*(3), 1-19. doi: 10.1029/2009gb003680

Uitz, J., Claustre, H., Morel, A., & Hooker, S. B. (2006). Vertical distribution of phytoplankton communities in open ocean: An assessment based on surface chlorophyll. *Journal of Geophysical Research*, *111*(C8), 1-23. doi: 10.1029/2005jc003207

USGS. (2006, May 1st, 2020). Wentworth grain size chart. *U.S. Geological Survey Open-File Report 2006-1195* Repéré le February 12, à http://pubs.usgs.gov/of/2006/1195/htmldocs/nomenclature.htm

Vidondo, B., Prairiej, Y. T., Blanco, M., & Duarte, C. M. (1997). Some aspects of the analysis of size spectra in aquatic ecology. *Limnology and Oceanography*, *42*, 182-192. doi: 10.4319/lo.1997.42.1.0184

Wang, G., Cao, W., Wang, G., & Zhou, W. (2013a). Phytoplankton size class derived from phytoplankton absorption and chlorophyll-a concentrations in the northern South China Sea. *Chinese Journal of Oceanology and Limnology*, *31*(4), 750-761. doi: 10.1007/s00343-013-2291-z

Wang, S., Huan, Y., Qiu, Z., Sun, D., Zhang, H., Zheng, L., & Xiao, C. (2016). Remote sensing of particle cross-sectional area in the Bohai Sea and Yellow Sea: Algorithm development and application implications. *Remote Sensing*, *8*(10). doi: 10.3390/rs8100841

Wang, Y. P., Voulgaris, G., Li, Y., Yang, Y., Gao, J., Chen, J., & Gao, S. (2013b). Sediment resuspension, flocculation, and settling in a macrotidal estuary. *Journal of Geophysical Research: Oceans*, *118*, 5591-5608.

Wollast, R. (1988). The Scheldt Estuary. Dans: W. Salomons, B. L. Bayne, E. K. Duursma, & U. Förstner (eds.), *Pollution of the north sea: an assessment* (pp. 183-193). Springer, Berlin.

Woodward, J. C., Porter, P. R., Lowe, A. T., Walling, D. E., & Evans, A. J. (2002). Composite suspended sediment particles and flocculation in glacial meltwaters: preliminary evidence from Alpine and Himalayan basins. *Hydrological Processes*, *16*, 1735-1744.

Xi, H., Larouche, P., Tang, S., & Michel, C. (2014). Characterization and variability of particle size distributions in Hudson Bay, Canada. *Journal of Geophysical Research Oceans*, *119*, 3392-3406. doi: 10.1002/ 2013JC009542.

Yayla, K. M. (2009). *An empirical approach to the remote sensing of the chlorophyll in the optically complex waters of the estuary and gulf of Saint. Lawrence*. Université de Sherbrooke, Sherbrooke, QC, 190 p.

Yentsch, C. M., Horan, P. K., Muirhead, K., Dortch, Q., Haugen, E., Legendre, L., Murphy, L. S., Perry, M. J., Phinney, D. A., Pomponi, S. A., Spinrad, R. W., Wood, M., Yentsch, C. S., & Zahuranec, B. J. (1983). Flow cytometry and cell sorting: A technique for analysis and sorting of aquatic particles. *Limnology and Oceanography*, *28*(6), 1275-1280.

Zakardjian, B. A., Gratton, Y., & Vézina, A. F. (2000). Late spring phytoplankton bloom in the Lower St. Lawrence Estuary: the flushing hypothesis revisited. *Marine Ecology Progress Series*, *192*, 31-48.

Zhou, W., & Cao, W. (2008). Modelling the influence of mineral particles and phytoplankton on chlorophyll estimation from ocean colour remote sensing. *International Journal of Remote Sensing*, *29*(21), 6237-6248.